LIGHT SCATTERING PROPERTIES OF SOLID AEROSOL PARTICLES OF NACL AND $(NH_4)_2SO_4$

by

Roger Jon Perry

A Thesis Submitted to the Faculty of the

DEPARTMENT OF PHYSICS

In Partial Fulfillment of the Requirements
For the Degree of

MASTER OF SCIENCE

In the Graduate College

THE UNIVERSITY OF ARIZONA

1 9 7 7

STATEMENT BY AUTHOR

This thesis has been submitted in partial fulfillment of requirements for an advanced degree at The University of Arizona and is deposited in the University Library to be made available to borrowers under rules of the Library.

Brief quotations from this thesis are allowable without special permission, provided that accurate acknowledgement of source is made. Requests for permission for extended quotation from or reproduction of this manuscript in whole or in part may be granted by the head of the major department or the Dean of the Graduate College when in his judgment the proposed use of the material is in the interests of scholarship. In all other instances, however, permission must be obtained from the author.

SIGNED: Roger J. Remy

APPROVAL BY THESIS DIRECTOR

This thesis has been approved on the date shown below:

Donald R. Huffman — March 28, 1977

D. R. Huffman
Professor of Physics

Date

TABLE OF CONTENTS

TABLE OF CONTENTS--Continued

LIST OF ILLUSTRATIONS

LIST OF TABLES

ABSTRACT

This thesis presents experimental measurements of the light scattering properties of nonspherical aerosol particles of sodium chloride and ammonium sulfate. A polarization modulated nephelometer was used to make sensitive measurements of the scattering matrix elements normalized to the total intensity and an ultrasonic nebulizer was used to produce aerosols with a variable mean radius and accurately determined size distribution. Scanning electron microscope photographs of the particles are presented along with measurements of the aerosol size distributions. The scattering measurements are presented in comparison with the Mie theory predictions for spheres and illustrate the scattering behavior of two distinct particle shapes--nonspherical but rounded and cubic. Measurements are given for all elements of the general scattering matrix for an aerosol of each salt having comparable mean radii to characterize the scattering properties of the two particle shapes. Additional measurements of selected matrix elements at two wavelengths are presented for five sizes of each salt to allow determination of the scattering properties of the aerosols as a function of mean particle size.

CHAPTER 1

INTRODUCTION

This work presents experimental measurements of the light scattering properties of well characterized solid aerosol particles as a function of mean particle size and compares the results to the equivalent predictions of the Mie theory for spheres (van de Hulst 1957). The particles were crystallized from aerosols made from aqueous solu- containing either sodium chloride (NaCl) or ammonium sulfate ($(NH_4)_2SO_4$). Sodium chloride was chosen because it crystallizes into cubes whereas the ammonium sulfate particles form more nearly spherical shapes. In addition the salts have indicies of refraction within 5% of each other. Hence, for aerosols of similar mean particle size, it is possible to directly compare their light scattering properties on the basis of particle shape.

The Mie theory of scattering has been widely used to describe the scattering properties of small particles in the earth's atmosphere, interstellar space,etc., but strictly applies only to spheres. In particular, almost all models of the earth's atmosphere are based on this assumption. It is the purpose of this work to supply experimental measurements on solid aerosol particles for direct use in atmospheric physics and to show to what extent predictions based on the Mie theory can be used to describe the scattering properties of aerosols with nonspherical particle shapes.

NaCl and $(NH_4)_2SO_4$ are of special interest because aerosols of each salt occur naturally in the atmosphere. In the troposphere 50% of all particles in the size range 0.28 μm to 0.55 μm and 100% of all particles in the range 0.18 μm to 0.26 μm contain sulfate primarily in the form of $(NH_4)_2SO_4$ (Georgii et al. 1971 cited in Junge 1972). Samples of the aerosol particulate taken from within 15 m of the ocean surface contained a large percentage of NaCl particles with a diameter range of 2.0 μm ± 1.8 μm (Frank, Lodge and Goetz 1972).

This work presents measurements of all elements of the general scattering matrix for an $(NH_4)_2SO_4$ aerosol with mean radius 0.64 μm ± 0.03 μm and a NaCl aerosol with mean radius 0.63 μm ± 0.03 μm. The measurements are used to characterize the light scattering properties of aerosols of each basic particle shape and are compared with the theoretical predictions for spheres. In addition, scattering measurements of several matrix elements at two wavelengths of light, λ 0.6328 μm and λ 0.3250 μm, are presented as a function of mean particle size for five sizes of each salt. The mean radius of the aerosol particulate ranges from 0.08 μm to 1.0 μm for the NaCl and from 0.3 μm to 0.7 μm for the $(NH_4)_2SO_4$. The scattering measurements for all sizes of both salts are compared to the theoretical predictions for a distribution of spheres with equivalent mean radius.

This work differs from earlier studies in two respects. First, the polar nephelometer used in the experiment allows simple and

accurate measurements of the elements of the general scattering matrix. Second, an ultrasonic nebulizer is used to produce aerosols with a narrow size distribution and a variable mean size. Thus it is possible to measure accurately the light scattering properties of aerosols of nonspherical particle shape as a function of mean particle size.

CHAPTER 2

THEORY OF SCATTERING

The theory presented in this section is divided into two parts: the theory of light scattering by an individual particle and the theory of light scattering by a large number of independent, randomly-oriented particles. This theory is based on the treatment given by van de Hulst (1957, Chapters 3-5).

Light Scattering by Individual Particles

The scattering of light by a single particle may be expressed in terms of the incident and scattered electric field vectors. These fields are defined with respect to the scattering plane formed by the incident and scattered beams. The components of the electric field parallel and perpendicular to the plane are given by E_ℓ and E_r, respectively, as shown in Fig. 1. The angle through which the light is

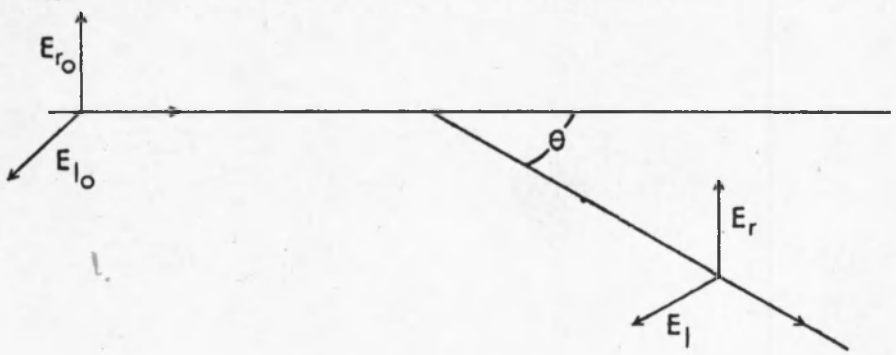

Fig. 1. Scattering Diagram for Electric Fields

deviated is called the scattering angle θ. The scattering problem may be represented by a complex 2 x 2 scattering-amplitude transformation matrix operating on a 1 x 2 electric field vector. Thus

$$\begin{bmatrix} E_{\ell} \\ E_r \end{bmatrix} = \begin{bmatrix} A_2 & A_3 \\ A_4 & A_1 \end{bmatrix} \begin{bmatrix} E_{\ell_o} \\ E_{r_o} \end{bmatrix},$$

where A_1, A_2, A_3, and A_4 are the transformation coefficients.

For a plane wave traveling in the z direction incident on an uncharged, isotropic, homogeneous sphere of radius a, the outgoing fields at a distance $r >> a$ become

$$\begin{bmatrix} E_{\ell} \\ E_r \end{bmatrix} = \begin{bmatrix} S_2 & 0 \\ 0 & S_1 \end{bmatrix} \frac{e^{ikz - ikr}}{ikr} \begin{bmatrix} E_{\ell_o} \\ E_{r_o} \end{bmatrix},$$

where $k = 2\pi/\lambda$, λ is the wavelength of incident light, and S_1 and S_2 are amplitude elements for a sphere. The Mie theory (Mie 1908) gives a Legendre polynomial expansion of S_1 and S_2 as functions of the scattering angle θ (van de Hulst 1957, p. 124). To specify the light scattering properties of a sphere, it is necessary to supply the particle radius, the complex index of refraction of the particle and the wavelength of the incident light. (For a detailed description of the Mie theory, see van de Hulst, Chapter 9.)

From the optical theorem for $\theta = 0$ and $S_1 = S_2 \equiv S(0)$, the amount of energy removed from the incident beam by the particle is determined by the coefficient of extinction

$$C_{ext} = \frac{4\pi}{k^2} \text{Re} \quad S(0) \ .$$

The scattering efficiency of the particle is defined as $Q_{ext} = (C_{ext}/G)$ where G is the geometrical area of the particle. For a sphere $Q_{ext} = (C_{ext}/\pi a^2)$.

To interpret the measurements of the scattered light, it is necessary to define the scattering process in terms of measurable intensities rather than amplitudes. The Stokes vector (Shurcliff 1962) may be used to completely describe the state of polarization of a beam of light. The four elements of the Stokes vector (I, Q, U, V) are defined in terms of the electric fields as

$$I = \langle E_\ell E_\ell^* + E_r E_r^* \rangle$$
$$Q = \langle E_\ell E_\ell^* - E_r E_r^* \rangle$$
$$U = \langle E_\ell E_r^* + E_r E_\ell^* \rangle$$
$$V = \langle i(E_\ell E_r^* - E_r E_\ell^*) \rangle .$$

The brackets refer to the time averages and the asterisks indicate complex conjugates. The physical meanings of the elements are as follows:

I is the intensity of the incident beam.

Q indicates the intensity of linearly polarized light at 0^o and 90^o, taking a value of +1 (-1) for complete horizontal (vertical) polarization.

U indicates the intensity of linear polarization at $\pm 45^{o}$, taking a value of +1 (-1) for complete polarization at $+45^{o}$ (-45^{o}).

V indicates the intensity of right or left circularly polarized light, taking a value +1 (-1) for complete right (left) circular polarization.

The Stokes vectors are transformed by a real 4 x 4 intensity matrix, referred to as the Mueller matrix for optical elements (Shurcliff 1962, Chapter 8).

The scattering process may also be expressed in terms of a 4 x 4 intensity scattering matrix relating the stokes vectors for the incident and scattered light intensities. For a single nonabsorbing particle, the sixteen elements are reduced to seven independent elements (van de Hulst 1957, p. 44). A sphere may be represented by three independent matrix elements.

Light Scattering for Many Particles

We now turn our attention to the light scattering problem for a large number of particles. The aerosols used in this experiment have low enough number densities that it may be assumed that the scattered light is only singly scattered before leaving the scattering volume. The particles are assumed to be randomly oriented and spaced so they may be treated as independent scatterers. This means that the light scattered

from a large number of particles may be expressed as the simple sum of the Stokes vectors for the light scattered by each particle.

The total intensity of the scattered beam is given by the sum of the intensities of light scattered from the single particles. Thus

$$I = \sum_{i=1}^{N} I'_i .$$

The scattering efficiency of the medium is given by the sum

$$Q_{ext} = \sum_{i=1}^{N} [Q'_{ext}]_i ,$$

which for a group of N identical particles gives

$$Q_{ext} = N\, Q'_{ext} .$$

Similarly, for identical spheres the sum of the scattered intensities is

$$I_{ext} = N I'_{ext} .$$

For a large number of particles with continuously distributed sizes, the sums are replaced by integrations.

Several assumptions may be used to simplify the general scattering matrix. A scattering region may be shown analytically to be isotropic for a large number of particles even though the particles themselves may be anisotropic (Perrin 1942). An equivalent statement given by van de Hulst (1957, p. 49) based on the analysis of Perrin

relates the isotropy of the scattering region of a large number of randomly oriented, asymmetric, identical particles. The scattering matrix simplifies to:

$$\begin{bmatrix} S_{11} & S_{12} & S_{13} & S_{14} \\ S_{12} & S_{22} & S_{23} & S_{24} \\ -S_{13} & -S_{23} & S_{33} & S_{34} \\ S_{14} & S_{24} & -S_{34} & S_{44} \end{bmatrix}$$

Matrix Type I

Perrin (1942) gives the same scattering matrix for a collection of randomly oriented identical particles with optical asymmetry or optical activity. Optical anisotropy may be present in the particle itself or may be introduced by the particle shape (van de Hulst 1957, p. 57).

A second general scattering matrix characterizing this experiment follows from the assumption that there are many randomly oriented identical particles which have an internal plane of symmetry (van de Hulst 1957, p. 50) or which display optical symmetry (Perrin 1942). Then the general scattering matrix reduces to

$$\begin{bmatrix} S_{11} & S_{12} & 0 & 0 \\ S_{12} & S_{22} & 0 & 0 \\ 0 & 0 & S_{33} & S_{34} \\ 0 & 0 & -S_{34} & S_{44} \end{bmatrix}$$

Matrix Type II

Finally, the scattering matrix for a distribution of spheres is (Perrin 1942)

$$\begin{bmatrix} S_{11} & S_{12} & 0 & 0 \\ S_{12} & S_{11} & 0 & 0 \\ 0 & 0 & S_{33} & S_{34} \\ 0 & 0 & -S_{34} & S_{33} \end{bmatrix}$$

Matrix Type III

Calculations using the Mie theory for single spheres were performed on a CDC 6400 computer with a subroutine developed by Dave (1968). Hunt (1974) developed a computer program which calculates the scattering matrix element S_{11} and the ratios S_{12}/S_{11}, S_{33}/S_{11}, and S_{34}/S_{11} for scattering angles 0^{o} to 180^{o} in 2^{o} steps, assuming a Gaussian distribution of mean radii. This program was used with the Dave subroutine.

CHAPTER 3

EXPERIMENT

The Polar Nephelometer

The scattering measurements in this experiment were made with a polar nephelometer designed by Hunt and Huffman (1973). A detailed description of this instrument may be found in Hunt (1974). A block diagram of the experiment is given in Fig. 2.

The collimated light from a laser was linearly polarized, then passed through a birefringence modulator before entering the scattering volume. The light scattered at an angle θ was detected by a photomultiplier tube mounted on a rotating arm. Provision was made to mount a variety of polarization elements in front of the photomultiplier, and a telescope was used to restrict the field of view of the photomultiplier to a narrow region in the center of the scattering volume. A birefringence modulator was used to produce a time-dependent retardation (see Fig. 3). It consisted of a piece of x-cut quartz crystal attached to a block of amorphous quartz. Both pieces were cut to have a natural resonant frequency of 50 kHz. The quartz crystal was driven piezoelectrically and the amplitude of its oscillation was adjusted by varying the ac voltage across it. The crystal in turn produced a periodic strain in the amorphous block. The resulting time-dependent retardation in the transmitted beam is $\delta = [(2\pi\ ds)/\lambda]\ \sin \omega t$ where d is the thickness of the amorphous block, λ the wavelength of the light

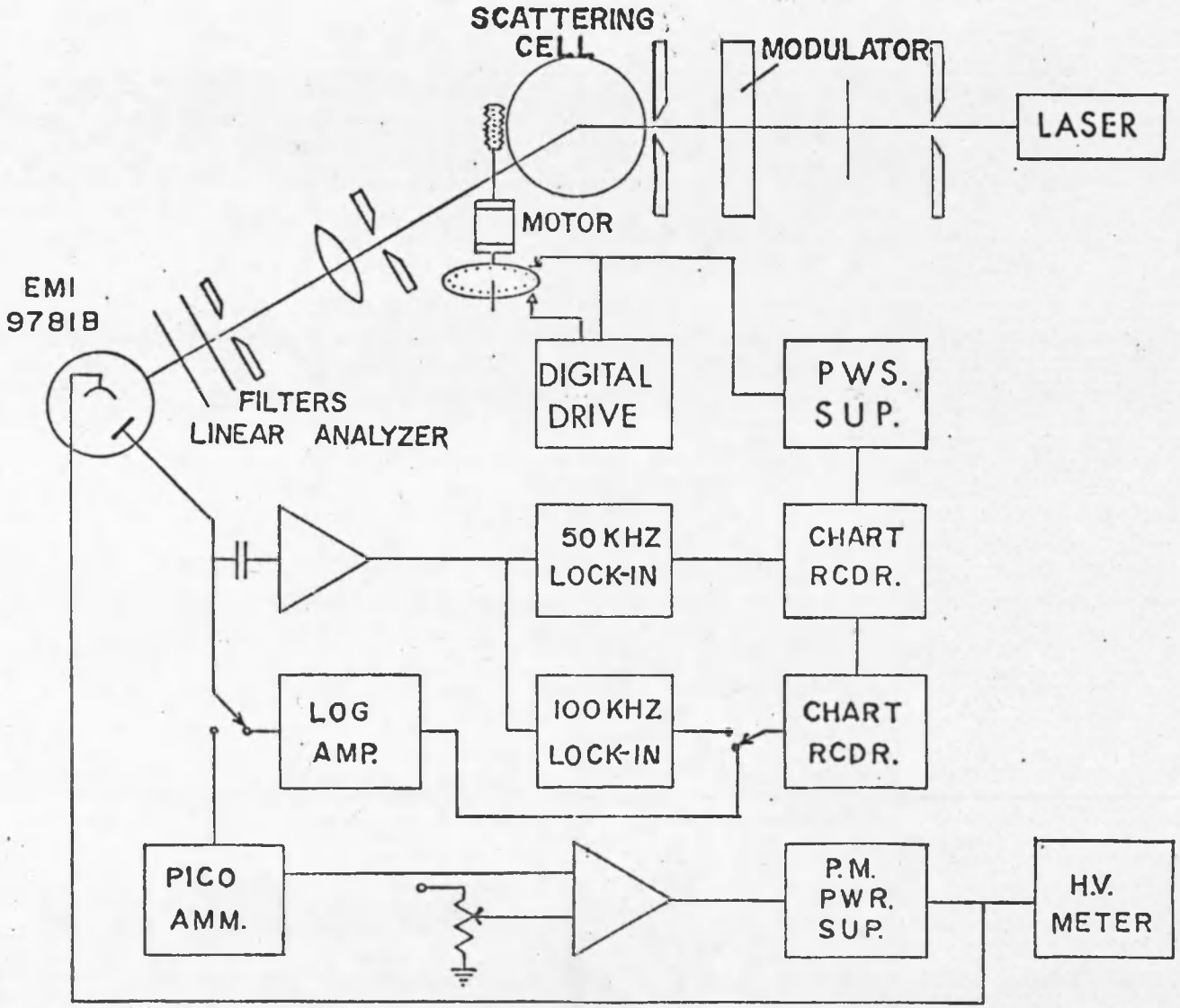

Fig. 2 Block Diagram of Experimental Apparatus (with permission A. Hunt 1974)

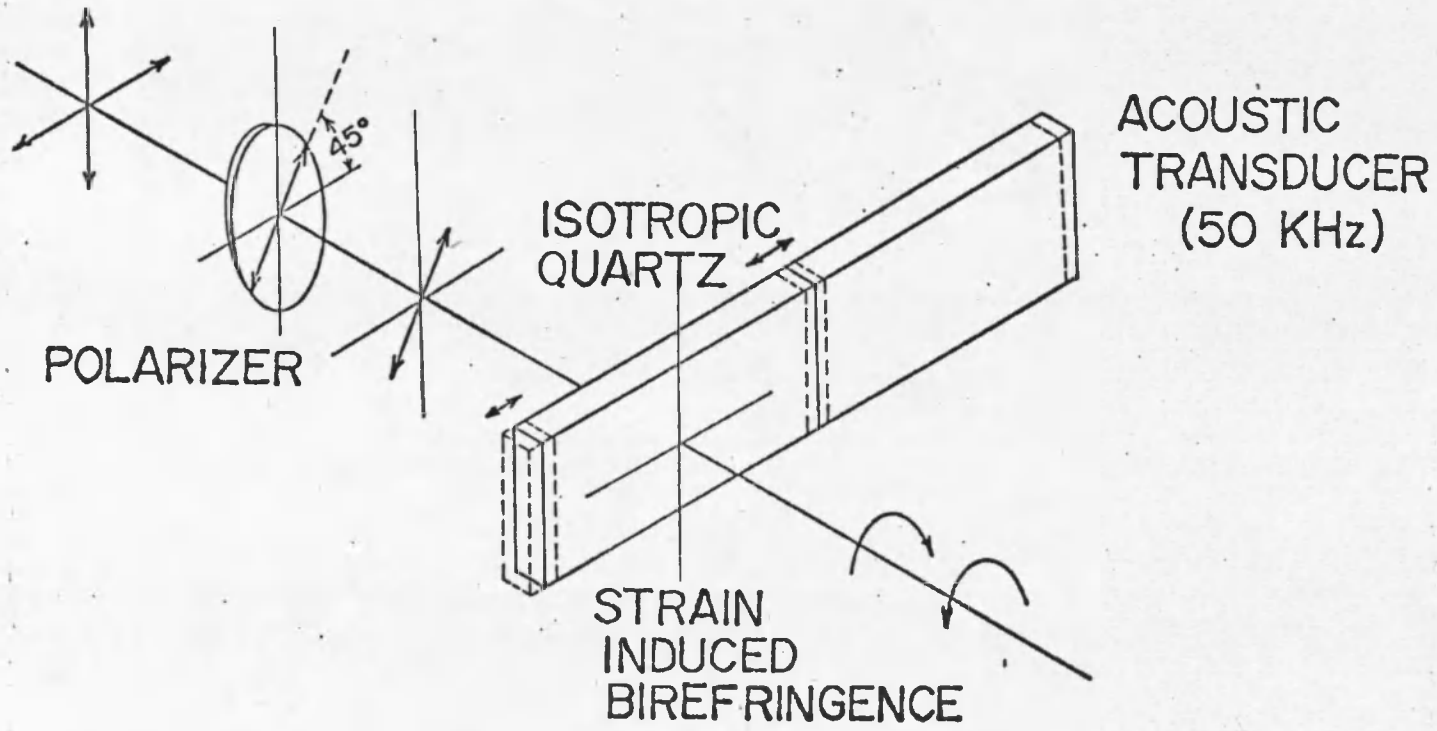

Fig. 3 Birefringence Modulator Element
(Used with permission of A. J. Hunt; from A. J. Hunt, Ph.D. Dissertation, University of Arizona, 1974)

being retarded, s the induced strain and sin (ωt) the time dependence (Hunt 1974).

In order to describe the scattering experiment, it is necessary to make use of Stokes vectors and Mueller notation (Shurcliff 1962). The Mueller representation of the retarder for arbitrary retardation δ at 0^o and 45^o relative to the scattering plane is given by (Hunt 1974).

For 0^o $\quad M =$

$$\begin{bmatrix} 1 & 0 & 0 & 0 \\ 0 & 1 & 0 & 0 \\ 0 & 0 & \cos\delta & \sin\delta \\ 0 & 0 & -\sin\delta & \cos\delta \end{bmatrix}$$

For 45^o $\quad M =$

$$\begin{bmatrix} 1 & 0 & 0 & 0 \\ 0 & \cos\delta & 0 & -\sin\delta \\ 0 & 0 & 1 & 0 \\ 0 & \sin\delta & 0 & \cos\delta \end{bmatrix}$$

The expansion of sin (δ) and cos (δ), where $\delta = A \sin(\omega t)$ and $A = (2\pi ds)/\lambda$, gives, in terms of Bessel functions of order i,

$$\sin(\delta) = 2J_1(A) \sin(\omega t) + 2J_3(A) \sin(3\omega t) + \ldots$$

and

$$\cos(\delta) = J_0(A) + 2J_2(A) \cos(2\omega t) + \ldots$$

By setting the amplitude of the oscillator so that $A = 2.40$, we insure $J_0(A) = 0$ (Abramowitz and Stegun 1972). This condition may be very accurately set in the experiment.

The entire scattering experiment may now be represented by a series of matrix transformations. As an example, if the modulator is oriented at 45^{o} and no final polarizer is used, we have:

$$[I_s] = 1/2 \quad [S] \quad [M] \quad [P] \quad [I_o].$$

Stokes Vector of Scattered Light | Scattering Matrix | Modulator | Linear Polarizer | Incoming Light Vector

$$\begin{bmatrix} I_s \\ Q_s \\ U_s \\ V_s \end{bmatrix} = 1/2 \begin{bmatrix} S_{11} & S_{12} & S_{13} & S_{14} \\ S_{21} & S_{22} & S_{23} & S_{24} \\ S_{31} & S_{32} & S_{33} & S_{34} \\ S_{41} & S_{42} & S_{43} & S_{44} \end{bmatrix} \begin{bmatrix} 1 & 0 & 0 & 0 \\ 0 & \cos\delta & 0 & -\sin\delta \\ 0 & 0 & 1 & 0 \\ 0 & \sin\delta & 0 & \cos\delta \end{bmatrix} \begin{bmatrix} 1 & 1 & 0 & 0 \\ 1 & 1 & 0 & 0 \\ 0 & 0 & 0 & 0 \\ 0 & 0 & 0 & 0 \end{bmatrix} \begin{bmatrix} 1 \\ 0 \\ 0 \\ 0 \end{bmatrix}$$

Since there are no additional polarizers in the light path, the photomultiplier will respond to the total intensity of the light given by the first element of the Stokes vector,

$$I_s = \frac{k}{2} \left[S_{11} + S_{12}\, 2J_2(A) \cos 2\omega t \right.$$

$$\left. + \; S_{14}\, 2J_1(A) \sin \omega t + \ldots \right] ,$$

where k is a sensitivity constant and A is determined so that $J_0(A) = 0$.

The signals measured at the lock-in amplifier were further modified by a constant current servo which normalized the ac signal to the dc total intensity. The resulting measurments in this example yeilded S_{12}/S_{11} at 2ω and S_{14}/S_{11} at ω. A listing of measurement methods for all elements of the scattering matrix is given in Appendix A.

The diagram of the constant current servo used in this experiment is given in Fig. 4. The constant current servo consisted of an operational amplifier which was used to control the dc high voltage to the photomultiplier. Any fluctuations in the total intensity below 20 cps resulted in a complementary shift in the phototube voltage thereby maintaining a constant current from the photomultiplier. This measurement technique is especially useful in dealing with aerosols when it is not possible to control fluctuations in the total intensity due to changes in the number of particles in the scattering volume.

In order to measure the total scattered intensity (S_{11}), the constant current servo was disabled and a logarithmic amplifier was used to measure the total dc photomultiplier current. The total intensity over four decades was displayed as a function of scattering angle on a chart recorder.

The Particle Production System

An ultrasonic nebulizer was used in this experiment because it produces liquid aerosols with a narrower size distribution than is found in pneumatic nebulization (Stupar and Dawson 1968) and a much narrower distribution than found in water clouds or solid atmospheric

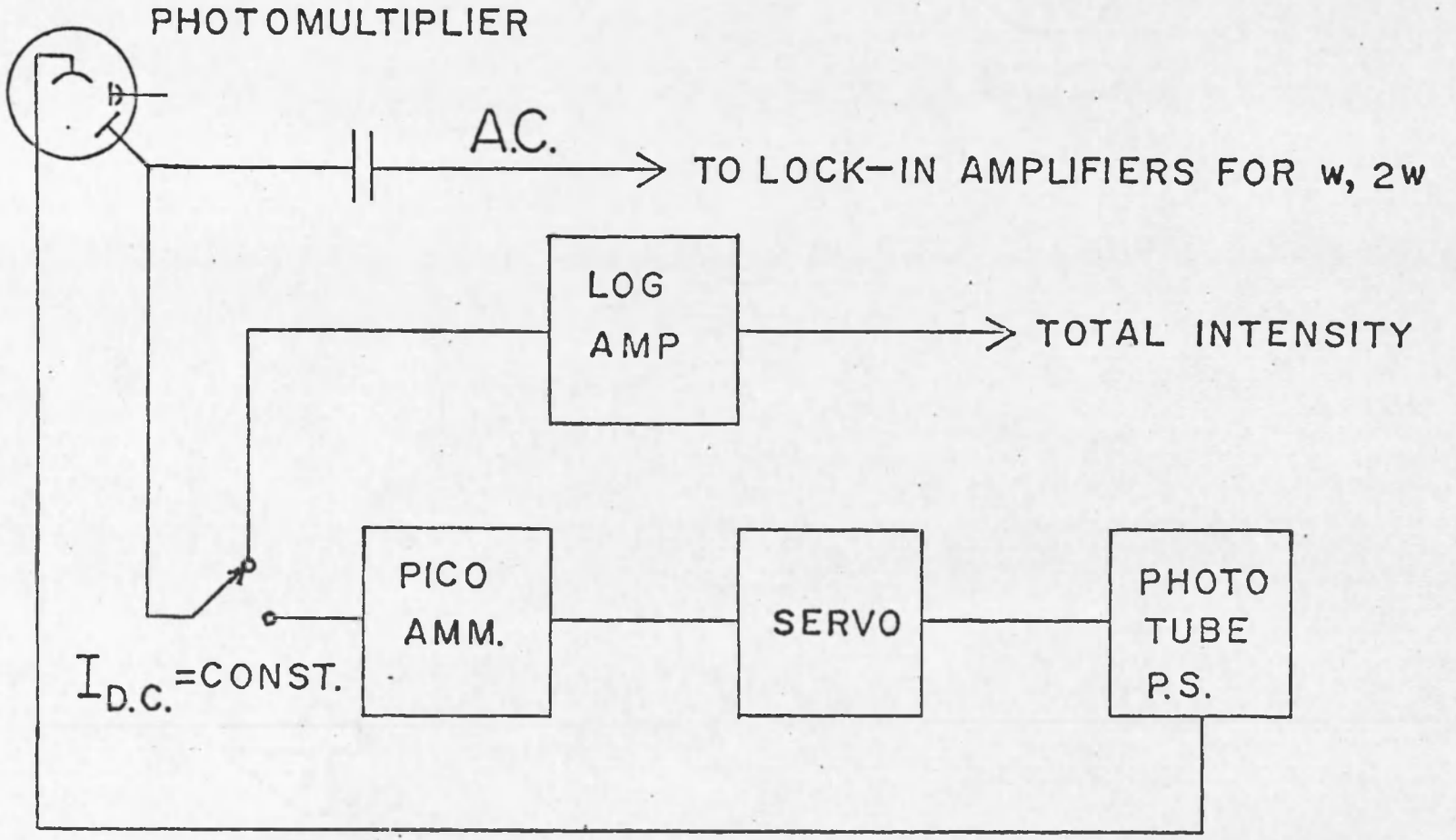

Fig. 4 A Block Diagram of Normalization Circuit.
(Used with permission of A. J. Hunt; from A. J. Hunt, Ph.D. Dissertation, University of Arizona, 1974)

aerosols (Junge 1972). In ultrasonic mebulization capillary waves are formed on the surface of the liquid. If the waves are driven to sufficient amplituce, a small spherical droplet separates from the crest leaving a lower amplitude wave behind (Lobdell 1968). The size distribution of the aerosol is determined by the uniformity of the surface waves and the dynamics of the droplet formation (Lang 1962). The following empirical formula (Lobdell 1968) gives the mean diameter of the droplets,

$$D = 0.34\ (8\pi\ \tau/\rho F^2)^{1/3},$$

where F is the driving frequency, τ the surface tension of the liquid and ρ its density.

A piezoceramic transducer driven by a radio frequency source produced the mapillary waves. The radio frequency source used in this experiment is described by Denton and Swartz (1974). Fig. 5 is a block diagram of the nebulizer assembly and sample cell. The sample cell used in this experiment was a modified version of the one given by Denton and Swartz (1974). The height of the transducer assembly was reduced and a thin-walled pyrex tubing of larger diameter was used. These modifications allowed optical measurements of the mean droplet radius using the sample chamber as a scattering cell.

The piezoceramic transducer was made of a disk of C600 barium titanate (Channel Industries) and had a natural resonant frequency of 1.29 MHz ± 0.03 MHz. When the radio frequency source was tuned to the

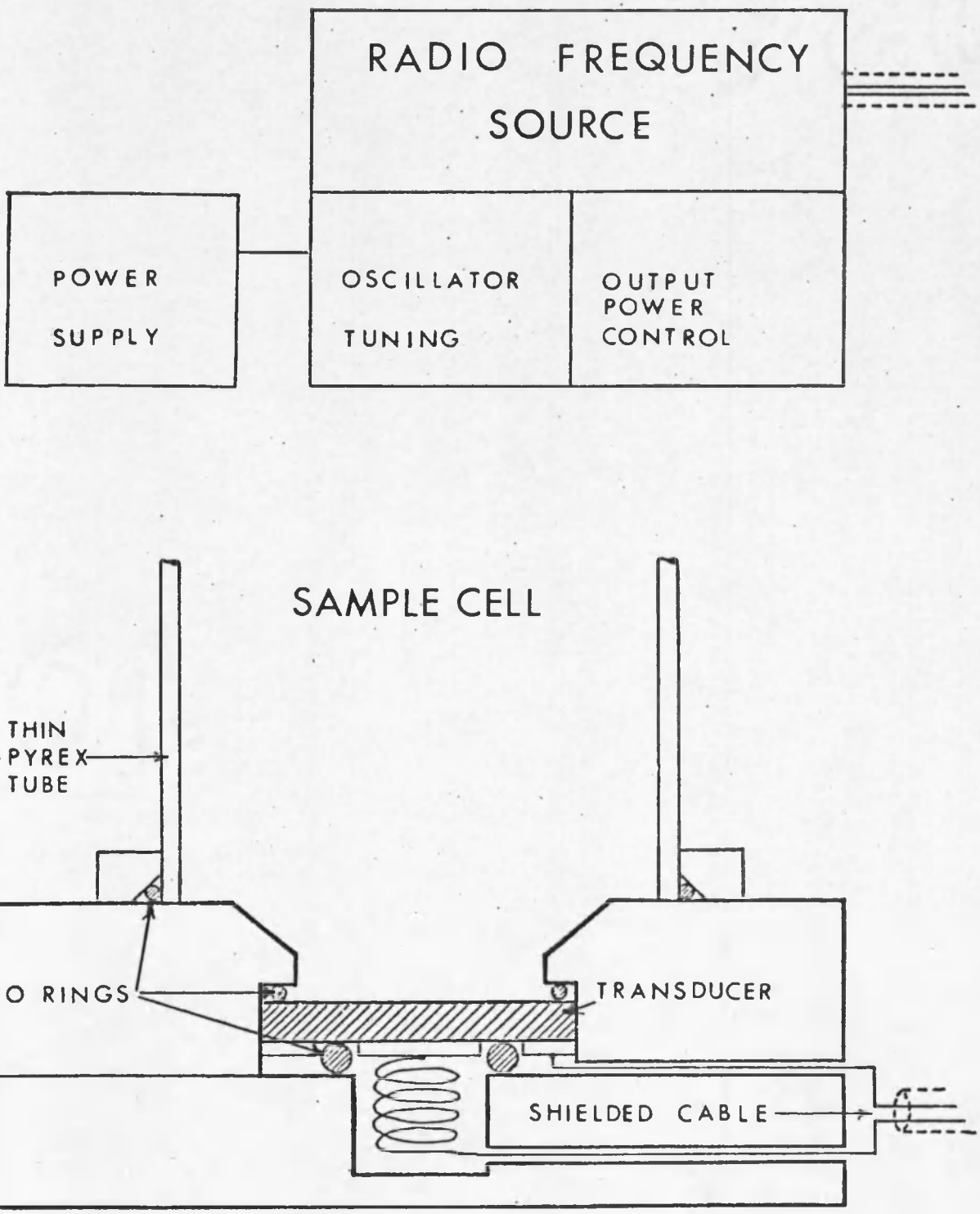

Fig. 5 Ultrasonic Nebulizer Assembly

resonant frequency of the transducer, a liquid jet formed directly over the transducer. Dense liquid aerosols were produced in the vicinity of the jet. Higher rates of atomization produced too large particles (Lang 1962). This happens because the larger capillary oscillations produce inherently large droplets, and through collisions these tend to coalesce to form still larger droplets. To avoid large particles and to produce a more uniform size distribution the nebulizer was run at low power (30 watts). Variations in the depth of the liquid in the sample cell did not substantially alter the rate of nebulization or particle size. The nebulizer could be used continuously for periods up to 40 minutes without noticeable decrease in the rate of nebulization. There was a definite maximum and minimum liquid level outside of which there was a rapid reduction in the nebulization rate.

The aerosols produced from aqueous solutions with different salt concentrations were carried from the sample cell by a steady flow of dry nitrogen through a 3-ft section of horizontal pipe to the scattering region. The droplets were dried by heating the section of pipe to a temperature of 210^{o}C and excess water vapor was removed from the aerosol by a layer of drying compound in the bottom of the pipe near the scattering region. To get reproducible measurements, it was necessary to change the drying compound, $CaSO_4$ (Dreirite) frequently. Finally, the solid aerosol passed vertically through a 5-mm diameter orifice into the scattering volume.

Solid aerosols with different mean sizes were produced by varying the salt concentration of the solution in the nebulizer. Five solutions with different concentrations were prepared for each salt. The ammonium sulfate solutions in grams per liter of H_2O were 5.0, 10.0, 20.2, 51.4, and 78.2. The NaCl concentrations were 1.25, 4.22, 10.0, 80.2, and 320.

Particle Sizing with the Electron Microscope

The particles were collected for microscopic examination by placing a vacuum trap directly over the scattering volume. The particles were collected on the surface of a Nuclepore filter with a pore size 0.2 μm.

Applied Research Laboratories Scanning Electron Microprobe Quantometer (S.E.M.) was used to make photographs of the particles. The samples were prepared for microscopy by mounting pieces of the Nuclepore filters on aluminum sample stools. The sample was then electrically connected to the stool with conducting paint after which carbon and gold were vacuum evaporated onto the sample. The conducting paint was necessary to prevent the sample from accumulating a charge in the electron beam. Samples were stored in a vacuum desiccator prior to measurement. Typical particle photographs are shown in Fig. 6.

Values for the mean particle size and standard deviation for use in the Mie theory calculations were measured from enlarged images of the S.E.M. photographs. The size distribution of the ammonium sulfate particles was easily measured since their shapes were basically

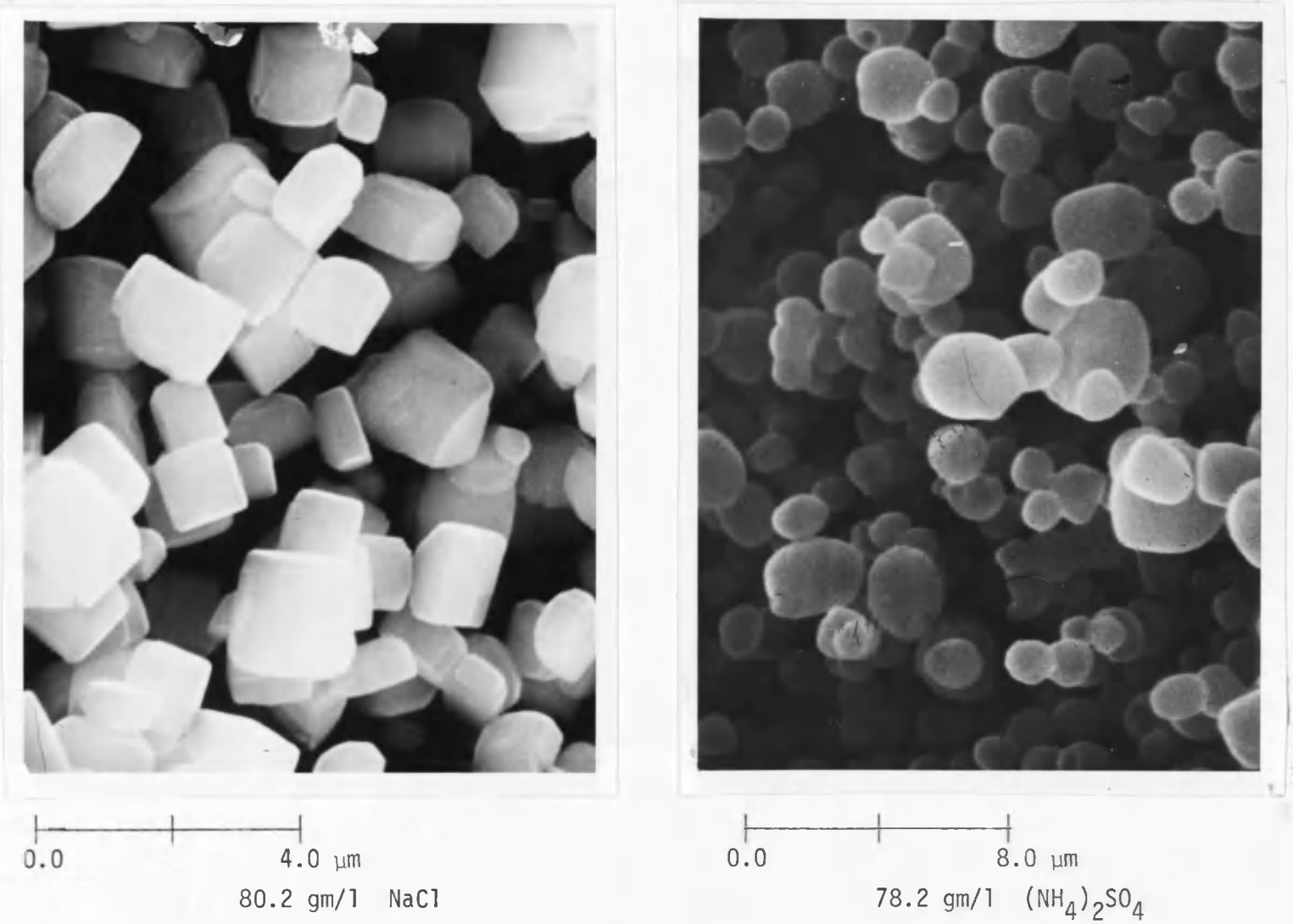

Fig. 6 Photographs of Solid Aerosol Particles

spherical. On the other hand, the sodium chloride particles were imperfect cubes (cf. Fig. 6). Consequently, the measurement of the cubic images on the photographs required further interpretation.

For either salt, all images measured on a given negative were analyzed as spheres or as cubes. For the case in which the particles were treated as spheres, a single number d, an effective diameter, was determined so that $\pi d^2/4$ would be an accurate estimate of the image area. For irregular images, d was obtained as the geometric mean of two linear measurements across the image, while for circular images d was measured directly. For the case in which the particles were treated as cubes, a single number ℓ, an effective side length, was determined so that ℓ^2 would be an accurate measure of the image area. As in the case for spheres, the geometric mean of two lengths was used to determine ℓ for irregular (non-square) images.

For both spherical and cubical particles, an average error of 3.2% in the mean size in microns was calculated. It was determined that two independent sources existed, measurement error and magnification error. These were computed separately and recombined using the normal propagation of errors to yield the total error. The average measurement error was calculated as follows. The mean size of the measured images was 17.5 mm, with a standard deviation of ± 4.7 mm. Measurements of the image were accurate to ± 0.5 mm. Dividing the measurement accuracy by the mean image size gave a measurement accuracy factor of 2.9%.

The second source of possible error was magnification. The field of view of the S.E.M. at 500X was measured by moving the image across the viewing screen and recording the distance traveled with a micrometer attached to the sample stage. It was necessary to increase the dimensions of the particles photographed by a factor of 1.016 ± 0.015 to give the correct magnification. This correction therefore introduced an additional error of 1.5% in the measurements. It was not necessary to make further measurements to calibrate the S.E.M. because the network of precision resistors which controls the magnification of the S.E.M. introduces the same percentage error at every power.

In order to compare the scattering measurements with the Mie theory predictions a mean radius was chosen for a sphere that had a volume equal to the mean volume of the aerosol particles. There are two methods for converting the mean size taken from the photograph to an equivalent mean radius. The particles in the photographs may be treated as a group of randomly oriented spheres or cubes using the method developed by Vouk (1948), or the mean size may be treated as a direct measure of the diameter of a sphere or the side of a cube.

According to Vouk (1948), the mean area of a collection of photographic images of randomly oriented identical objects without re-entrant sides (i.e., any line intersects the object no more than twice), is one-fourth the surface area of the object photographed.

In the case of spherical particles, an equivalent mean sphere was obtained whose radius was

$$r = \frac{1}{N} \sum_{i=1}^{N} \frac{1}{2} d_i = \frac{\bar{d}}{2}$$

with a variance given by

$$\sigma^2 = \frac{1}{N^2} \left[\Sigma d_i^2 - (\Sigma d_i)^2 \right].$$

For cubic particles a mean cube with side dimension s was calculated from

$$\frac{6 s^2}{4} = \left[\frac{1}{N} \sum_{i=1}^{N} \ell_i \right]^2$$

or

$$s = \sqrt{\frac{2}{3}} \frac{1}{N} \sum_{i=1}^{N} \ell_i = \sqrt{\frac{2}{3}} \bar{\ell},$$

and the resulting mean radius of the equivalent sphere would be

$$r = \sqrt{\frac{2}{3}} \left(\frac{3}{4\pi}\right)^{1/3} \bar{\ell}.$$

The variance parameter in this case would be

$$\sigma^2 = \left(\frac{3\pi}{4}\right)^{2/3} \cdot \frac{2}{3} \cdot \frac{1}{N^2}\left[\sum_{i=1}^{N} \ell_i^2 - \sum_{i=1}^{N} \ell_i\right].$$

Under the assumption that the mean size was a direct measure of the diameter of a sphere, then the two methods yield the same result wherein the mean radius of the equivalent mean sphere was $r = \frac{1}{2}\bar{d}$.

If it is assumed that the mean size, $\bar{\ell}$, was a direct measure of the side of the cube, then the mean radius would be

$$r = \sqrt[3]{\frac{3}{4\pi}} \frac{1}{N} \sum_{i=1}^{N} \ell_i = \sqrt[3]{\frac{3}{4\pi}}\ \bar{\ell}$$

with a variance given by

$$\sigma^2 = \left(\frac{3}{4\pi}\right)^{2/3} \frac{1}{N^2}\left[\sum_{i=1}^{N} \ell_i^2 - \left(\sum_{i=1}^{N} \ell_i\right)^2\right].$$

It was not possible to determine a priori which method gave the proper relationship for the conversion of the mean size of the cube to an equivalent mean radius. The mean radii given for the three highest concentrations of the NaCl were calculated using the assumption that the mean size, $\bar{\ell}$, was a direct measure of the side of a cube. This correction was necessary because it was found that the mean radii obtained from Vouk's (1948) method did not properly account for the size of the aerosol particles.

Due to the difficulties encountered in determining an equivalent mean radius for the non-spherical NaCl particles from photographs and scattering measurements, an alternate method was developed which allowed sizing of the solid particles from the initial concentration and the mean droplet radius of the liquid aerosols. The mean radius of the solid aerosol particles is given by

$$r_i = R_i\left(1 + \frac{\rho x 10^3}{y_i}\right)^{-\frac{1}{3}},$$

where R_i is the mean droplet radius, y_i is the solution concentration in grams per liter and ρ is the density of the salt (2.165 gm/cm^3 for NaCl and 1.769 gm/cm^3 for $(NH_4)_2SO_4$ Handbook of Chemistry and Physics, Weast 1970, pages B-137, and B-68 respectively). The expression was obtained by equating the volume of the solid particles to the volume of salt contained in a liquid droplet for a given concentration.

The mean radii found for the solid aerosol were used to calculate a mean droplet radius, R_i, for each concentration. These mean droplet radii were weighted by the total number of particles counted for each concentration, n_i, and used to determine a weighted mean droplet radius

$$R = \sum_{i=1}^{10} n_i R_i \div \sum_{i=1}^{10} n_i.$$

In this method either the weighted mean droplet radius or an independent measurement of the mean radius of the liquid aerosol may be

used to calculate an average mean radius for the solid aerosols directly from the initial solution concentration.

Summary of Particle Sizing from Theoretical Predictions

In order to size the aerosols from the scattering measurements by comparison with the theoretical predictions it is necessary to supply the mean radius, distribution width, indices of refraction of the salts and wavelength of the scattered light. Initially the mean radius and distribution width of the aerosols were taken from the S.E.M. measurements. Where possible, subsequent variations were made in the mean radius to obtain a closer comparison between the predictions and the scattering measurements. A Gaussian distribution based on the mean radius and variance of the particle size distribution were used in the computer program. The distribution was sampled by the Mie theory program at the mean radius and at 40 radii evenly distributed about the mean, covering the sample distribution range of about 3σ.

The two Metrologic lasers used in this experiment had wavelengths of λ 0.3250 μm and λ 0.6328 μm. The indices of refraction of $(NH_4)_2SO_4$ and NaCl for these wavelengths are

NaCl	1.591 at λ 0.3250 μm
	1.538 at λ 0.6328 μm

and

$(NH_4)_2SO_4$	1.540 at λ 0.3250 μm
	1.516 at λ 0.6328 μm.

The index of refraction for NaCl was obtained from the American Institute of Physics Handbook (Gray 1972). The index of refraction for the $(NH_4)_2SO_4$ was measured by the method of minimum defiation for the 60^o crystal face of the ammonium sulfate. Crystal ammonimu sulfate has an anisotropic index of refraction and for the sodium doublet it has principle indices of refraction 1.521, 1.523, and 1.533. In the Mie calculations, average values of index of refraction of 1.52 at λ 0.6328 μm and 1.54 at λ 0.3250 μm were used. The imaginary indices of both salts were 3 to 4 orders of magnitude smaller than the real indices of refraction and were ignored in the calculations.

CHAPTER 4

RESULTS

The primary experimental results to be presented in this paper are angulardependences of various scattering matrix elements found in Figs. 7-14 and in Appendix B, and particle sizes in Appendix C.

The Complete Scattering Matrix for a Single Size

Measurements of all elements of the general scattering matrix for 80.2 gm/l NaCl and 78.2 gm/l $(NH_4)_2SO_4$ are presented in Figs. 7 to 10, and 11 to 14 respectively. The measurements are used to characterize the light scattering properties of aerosols of nonspherical particles of the types shown in Fig. 6. The scattering measurement (solid line) used to determine each matrix element is presented graphically in the relative position on the page it would occupy in the general scattering matrix. The scattering matrix for each salt, S, is presented by 2 x 2 submatrices; A, B, C and D, respectively, where $S = \begin{bmatrix} AB \\ CD \end{bmatrix}$. The scattering measurements in the A and D submatrices are traced over the theoretical prediction for spheres (symboled line).

The Mie theory predictions for the rounded $(NH_4)_2SO_4$ particles (Figs. 11 to 14) match the scattering measurements in the angular position of features and overall amplitude. Thus it appears that slightly nonspherical but rounded particles are well described by the Mie theory. The predictions for the NaCl (Figs. 7 to 10) do not match the measurements for $\theta \geq 90^{o}$ and show large differences in

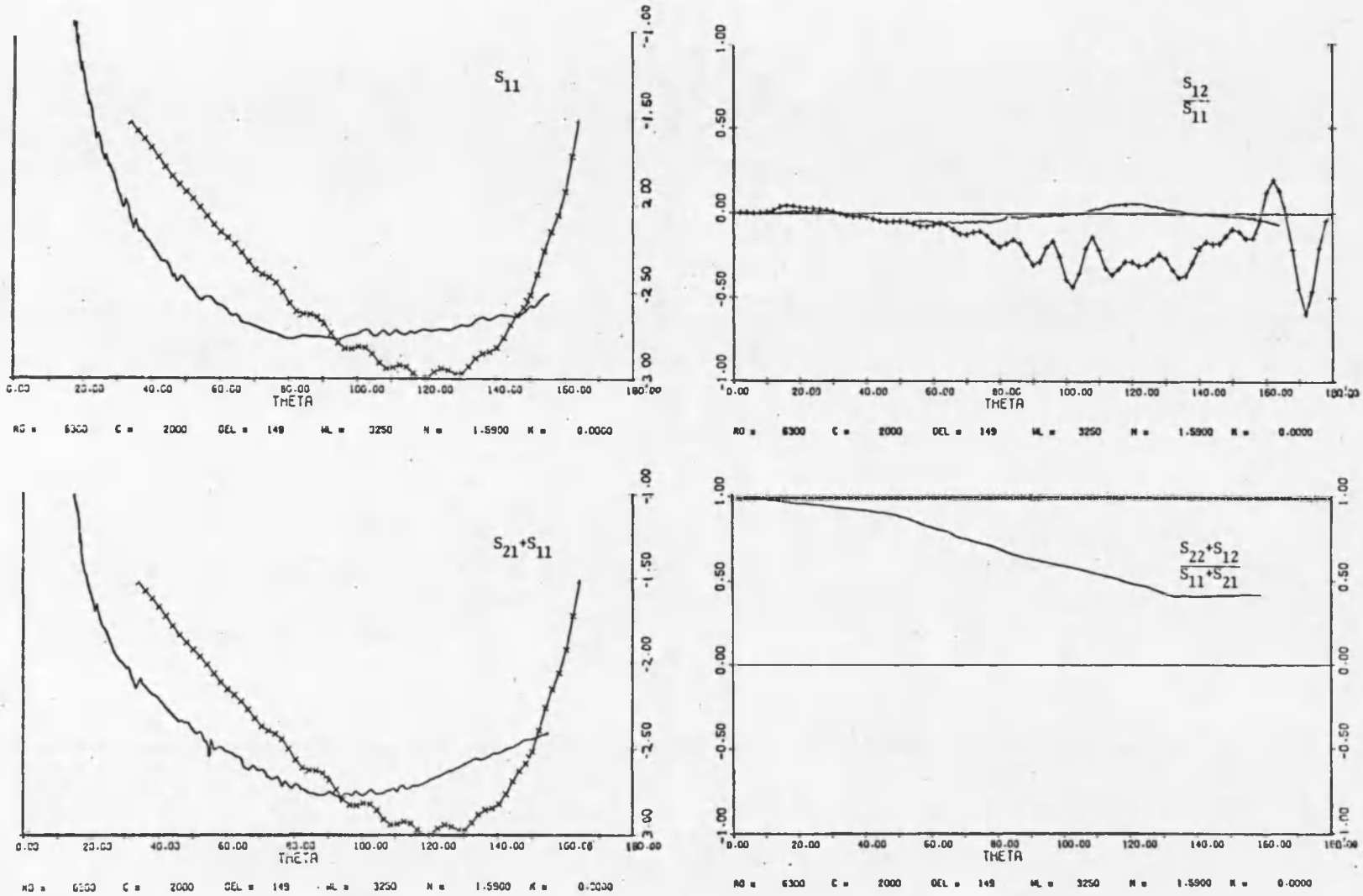

Fig. 7 Submatrix A NaCl 80.2 gm/l

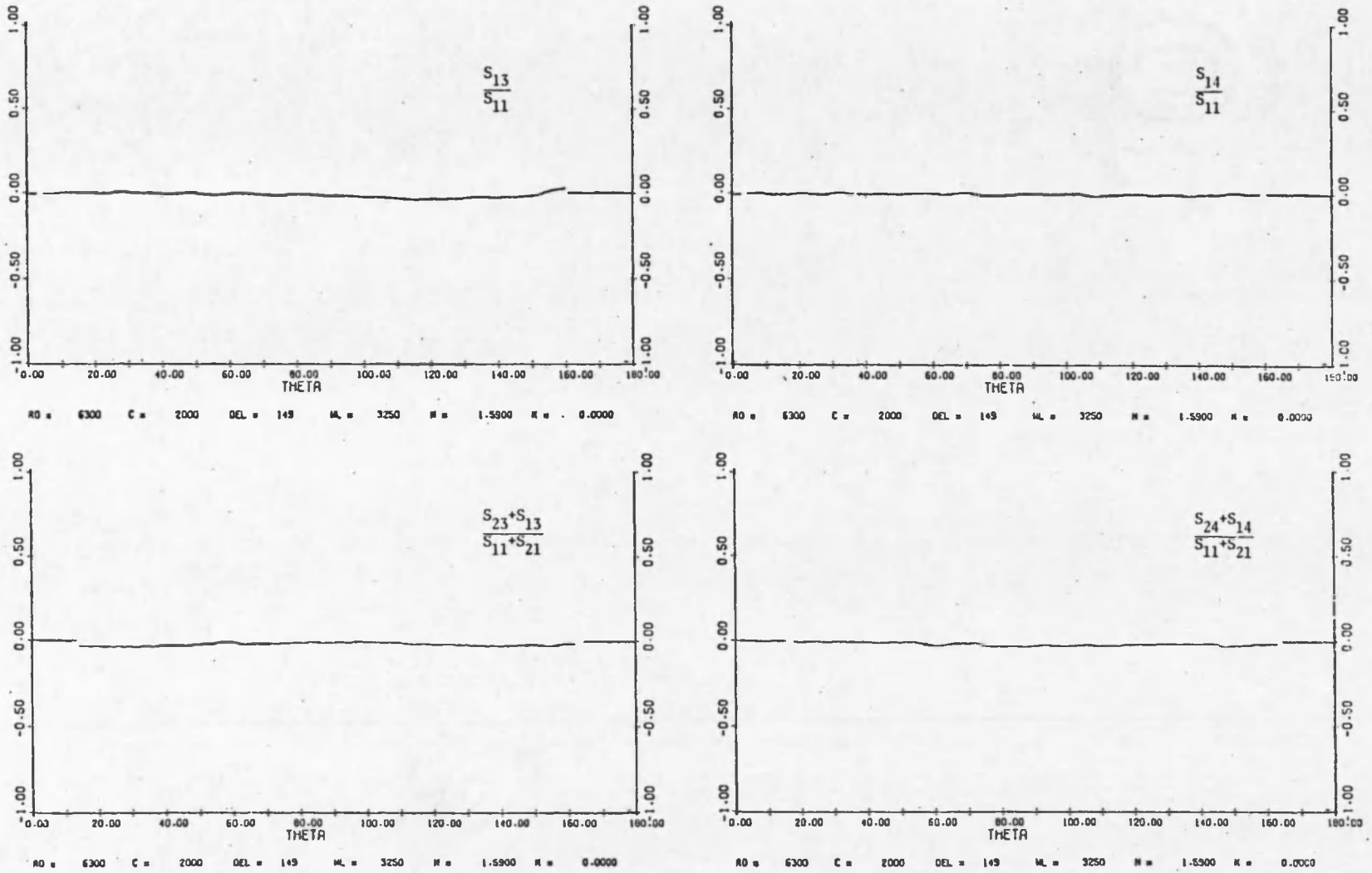

Fig. 8 Submatrix B NaCl 80.2 gm/l

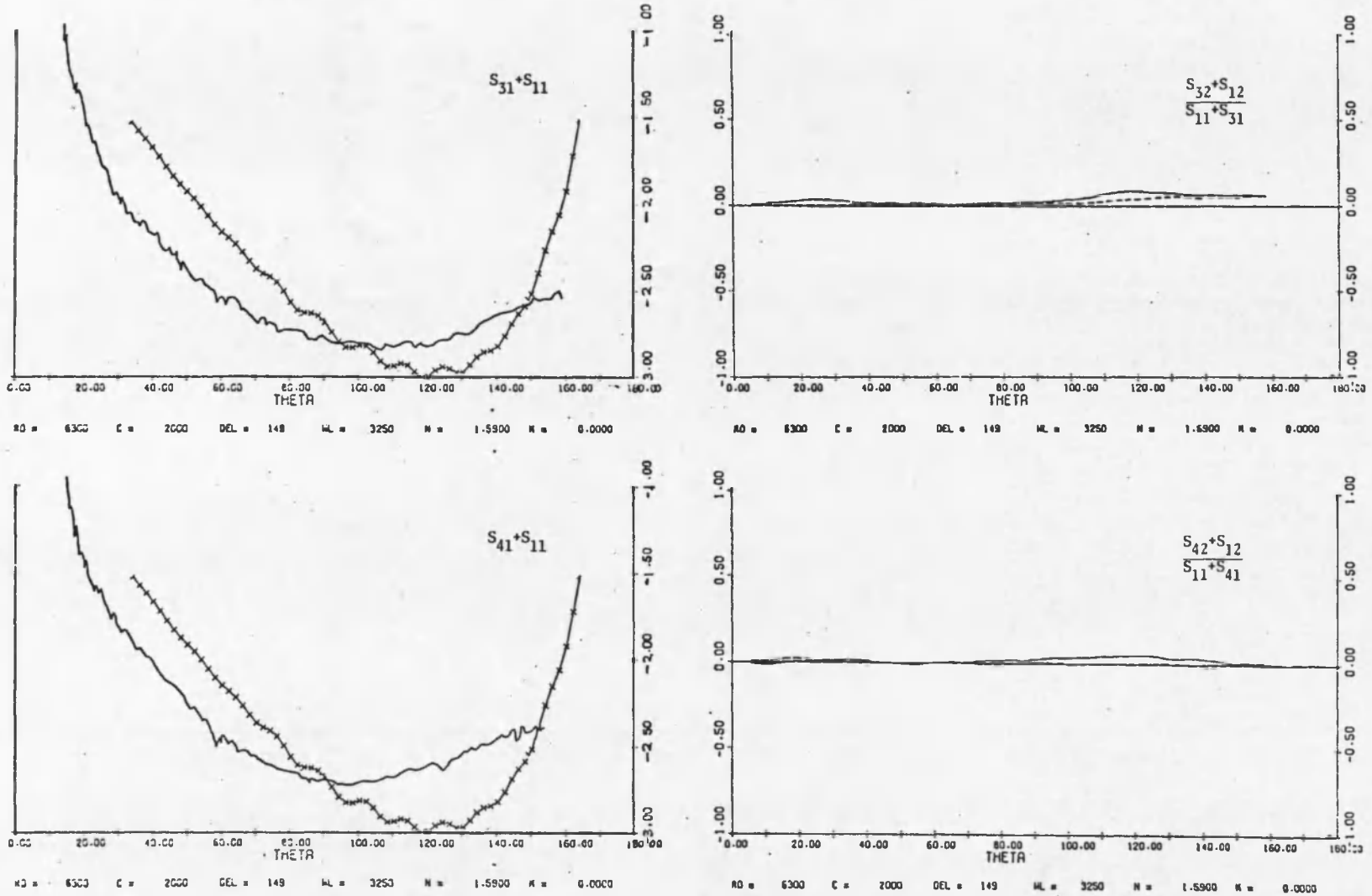

Fig. 9 Submatrix C NaCl 80.2 gm/l

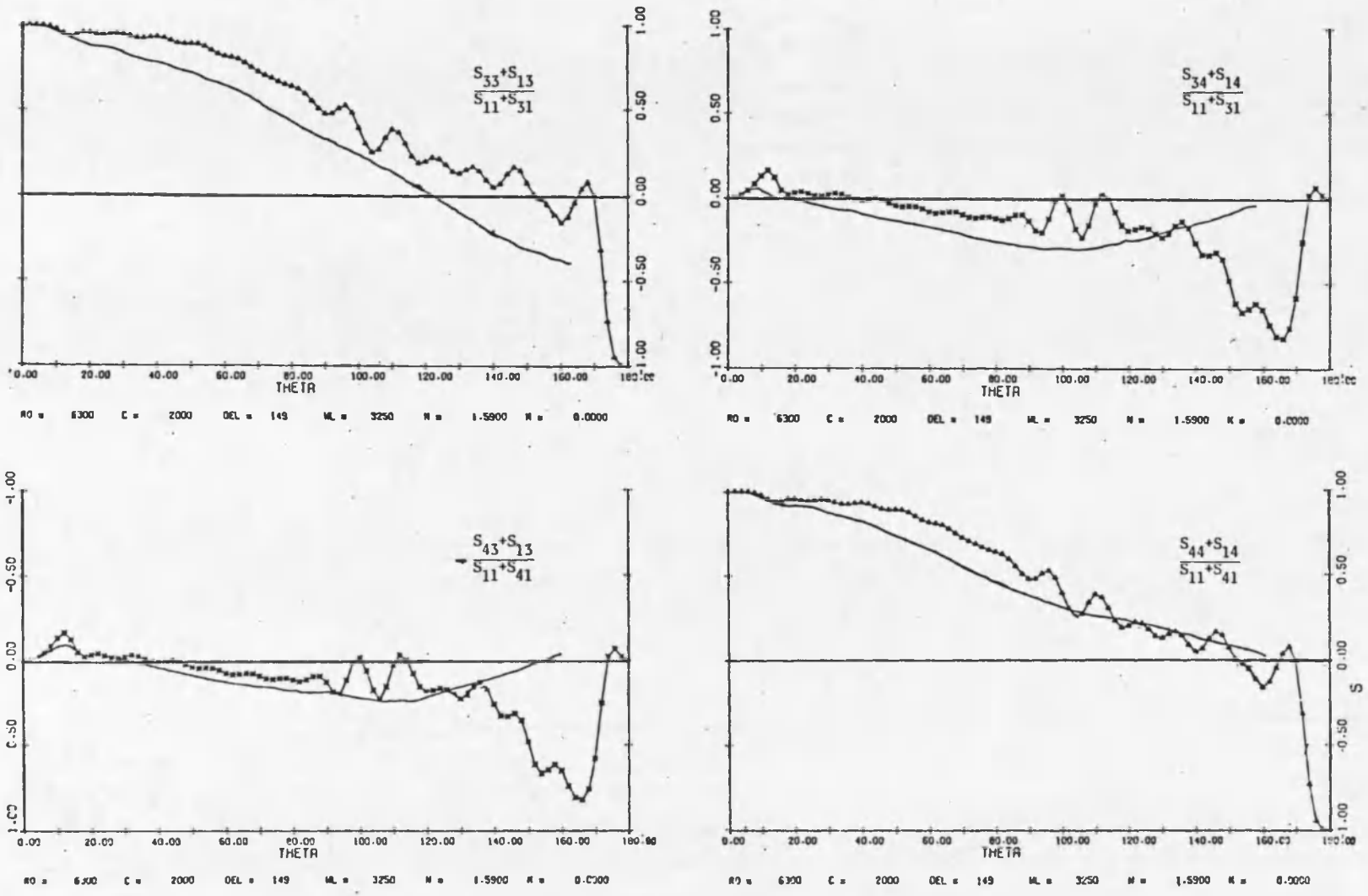

Fig. 10 Submatrix D NaCl 80.2 gm/l

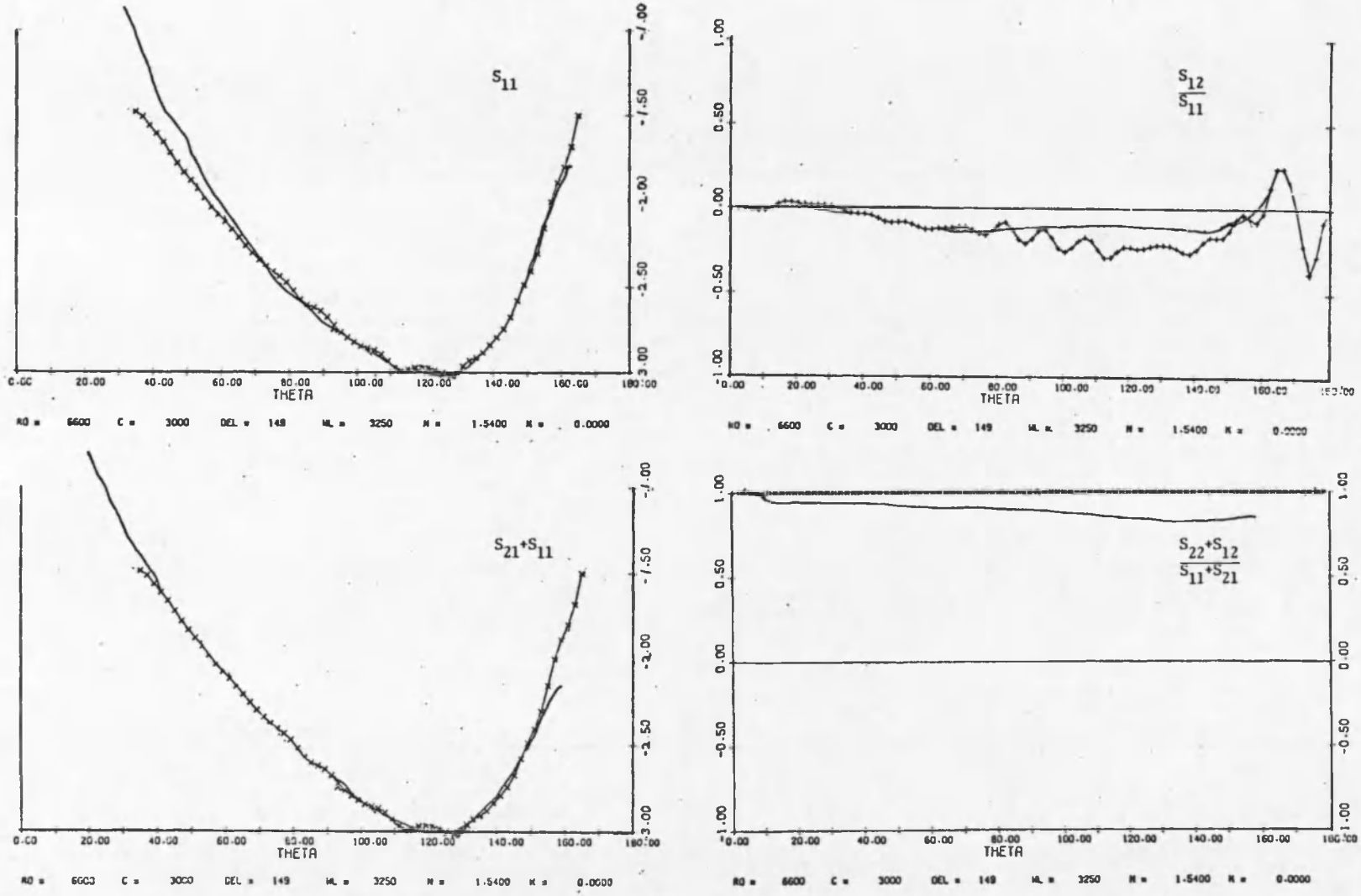

Fig. 11 Submatrix A $(NH_4)_2SO_4$ 78.2 gm/l

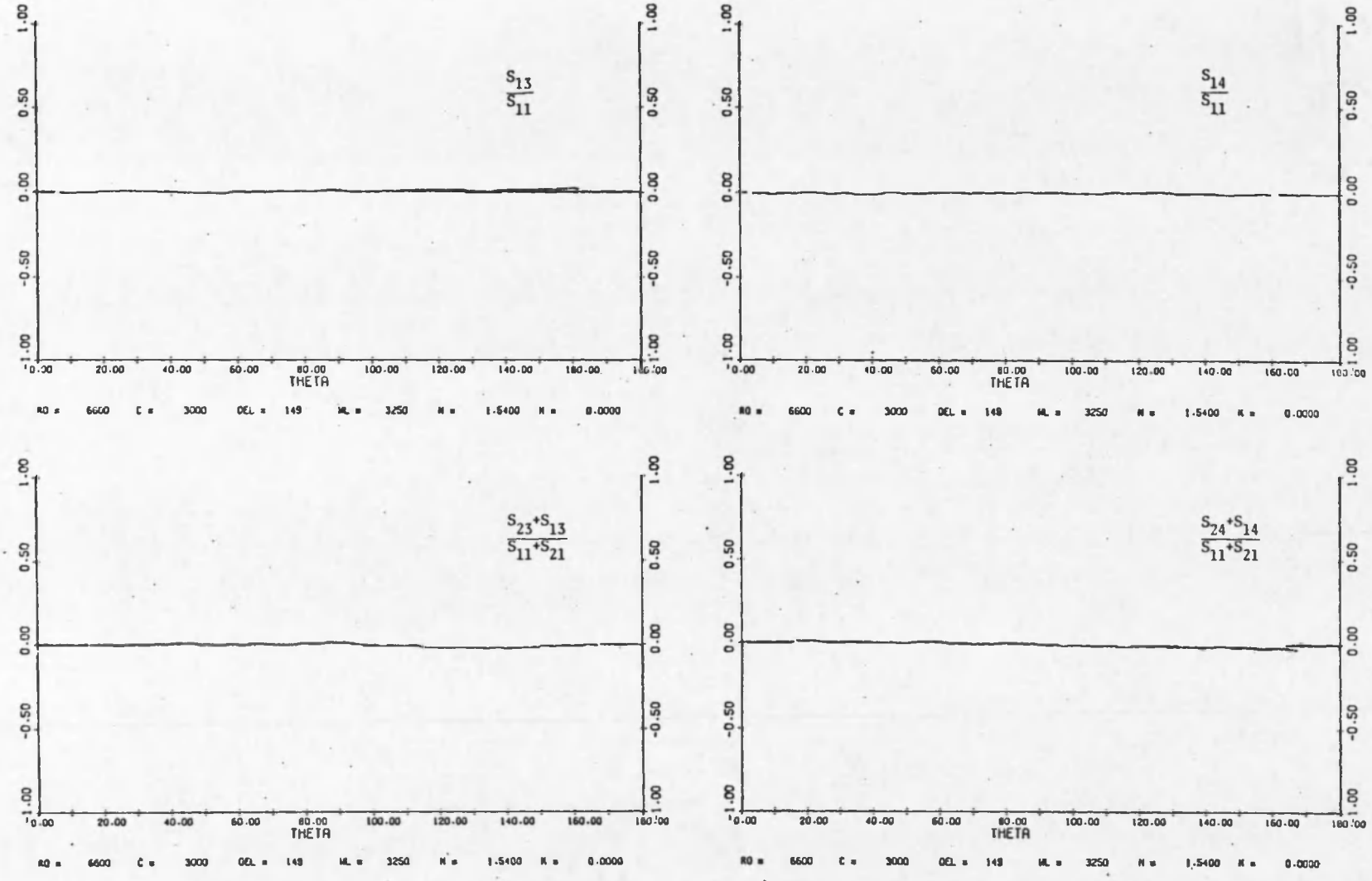

Fig. 12 Submatrix B $(NH_4)_2SO_4$ 78.2 gm/l

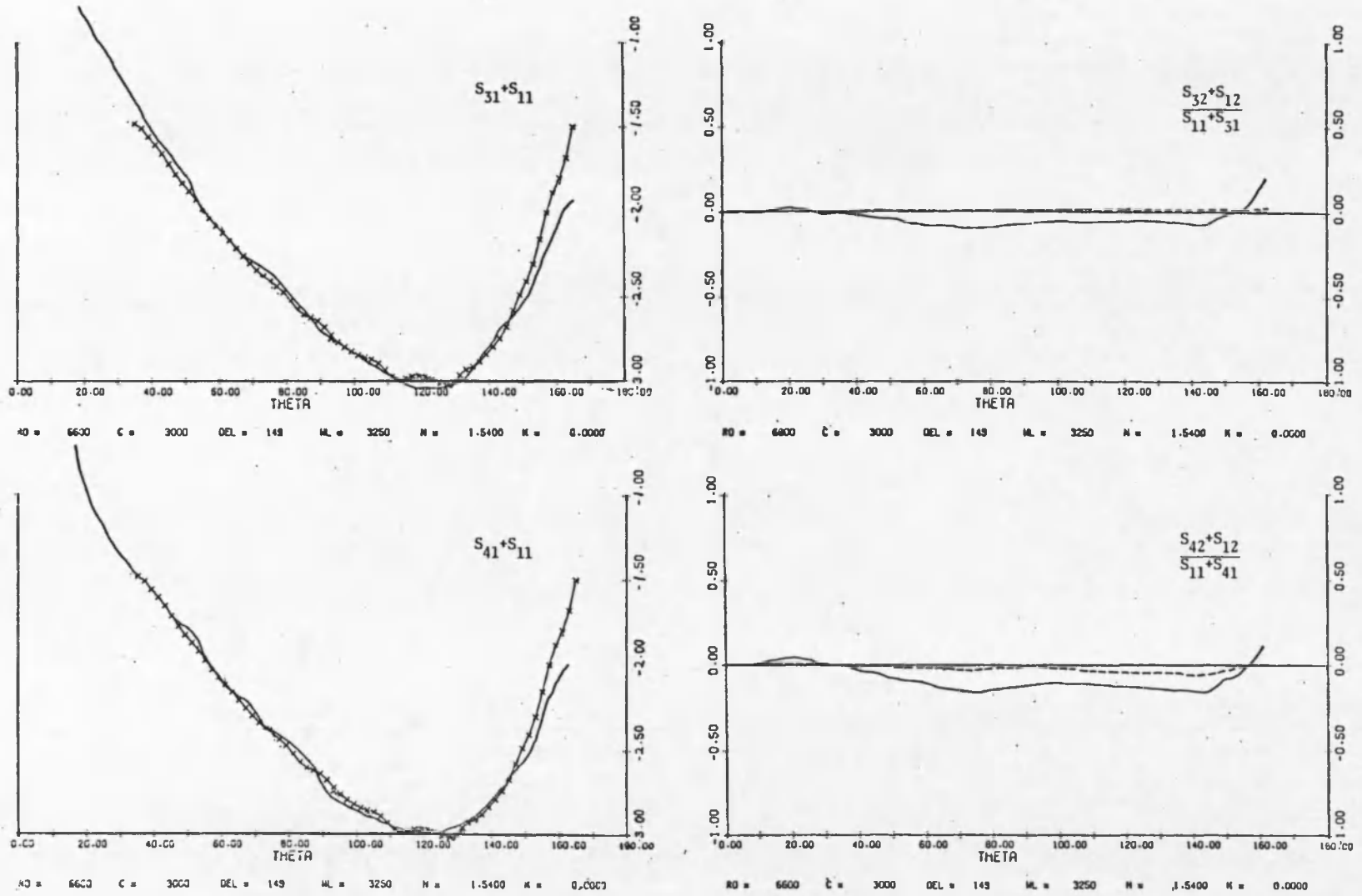

Fig. 13 Submatrix C $(NH_4)_2SO_4$ 78.2 gm/l

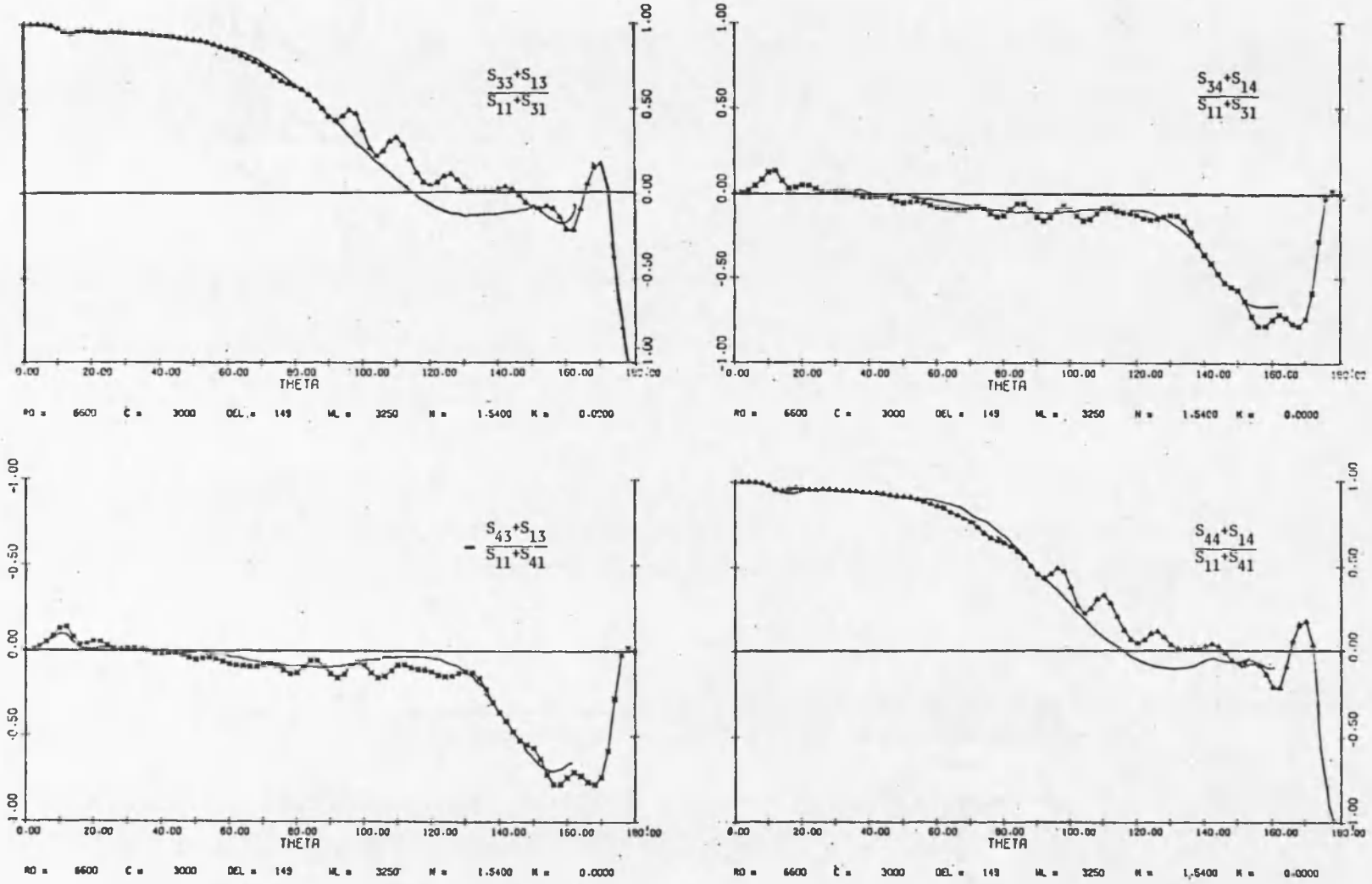

Fig. 14 Submatrix D $(NH_4)_2SO_4$ 78.2 gm/l

angular position of scattering features and amplitude. These differences are an indication of the effects of angular particles on the measurements. The scattering measurements in the B and C submatrices are a measure of the optical activity of the aerosols. The theoretical predictions for all elements in these matrices are zero.

The method for obtaining each matrix element is outlined in Appendix A. Measurements in the first column of the general scattering matrix are total intensity measurements and are presented on a four decade logarithmic scale. The matrix elements in the first row are measured directly. The remaining matrix elements are measured in combination with elements in the first row. In most measurements the additional elements are zero; in others it was possible to subtract the additional matrix elements to obtain the normalized matrix elements. Elements determined in this manner are indicated by a dashed line.

Selected Matrix Elements vs. Size

In Appendix B scattering measurements are presented for five concentrations of both salts. The measurements allow further analysis of the scattering properties of solid aerosols as a function of mean particle size. The measurements are traced over theoretical predictions for spheres of comparable mean radius and size distribution.

The differences between the measurements and the calculations for all concentrations of the NaCl aerosols suggest that the spherical particle theory is a poor approximation for such angular particles. The good agreement between measurements and calculations for the

rounded $(NH_4)_2SO_4$ particles indicate the relative success of the spherical particle theory for such particles. The differences evident in the scattering measurements for the two largest particle sizes of both salts appear to indicate the larger particles are more irregular in shape.

All measurements of a given concentration are presented together to allow an accurate sizing of the aerosol by the Mie theory prediction. Scattering measurements at two wavelengths of light: λ 0.6328 μm and λ 0.3250 μm are presented for the S_{11}, S_{12}/S_{11} and S_{33}/S_{11} matrix elements for each concentration. All scattering measurements for a given concentration are referred to in the text by an Appendix B figure number with B1 to B5 [B6 to B10] denoting the NaCl $[(NH_4)_2SO_4]$ measurements in order of increasing concentration. In addition, a lower case letter is used to distinguish between the different pages of scattering measurements presented for each concentration. (An index of the scattering measurements by mean radius and Mie coefficient is given in Table III.)

Sizing Results

The mean radius and size distribution of the aerosol particles for each concentration of both salts were obtained from photographs taken with a scanning electron microscope. Where possible, the aerosols were also sized by comparison of the theoretical predictions to the scattering measurements.

The statistical results obtained from S.E.M. photographs of all concentrations of both salts are given in Appendix C. The information

presented was calculated using the mathematical formulae found on page 928 of the Handbook of Mathematical Functions (Abramowitz and Stegun 1972). All measurements presented are of mean particle size in microns and require further interpretation of particle shape to determine mean particle radius (see Table I and Fig. 16). A histogram of percent frequency versus mean size is given for each concentration allowing a direct inspection of the particle size distributions for the aerosols.

Table I lists the mean radius and standard deviation found for each aerosol. The mean radii were calculated from the mean size, using the assumption that the mean size is a direct measure of the side of a cube or diameter of a sphere. The mean size, fractional deviation, basic shape of the particles, and number of particles counted for each concentration are also listed. The total number of particles counted for each salt and the weighted mean fractional deviation for the aerosol distributions are given at the bottom of the table.

In Table II, the mean particle radii from Table I are used to calculate the mean droplet radii, R_i , of the liquid aerosol formed from each concentration. The droplet radii are of use in sizing the liquid aerosol produced by ultrasonic nebulization. The mean droplet radii for the NaCl are compared to droplet radii calculated from the empirical formula given in Chap. 3 (page 27). The calculated droplet radii are used to estimate what effects variations of the surface tension and density for the different solutions have on the mean droplet radius. The approximate values for the surface tension and density

TABLE I

Mean Radius and Size Distribution for NaCl and $(NH_4)_2SO_4$ Aerosols Determined from S.E.M. Photographs

Concentration (gm/l)	Mean Radius (μm)	Standard Deviation (μm)	Mean Size (μm)	Fractional Deviation	Shape C = cube S = sphere	Total # Counted
NaCl						
1.25	0.150 ± 0.005	0.035	0.300 ± 0.010	0.237	S	249
4.22	0.231 ± 0.006	0.058	0.456 ± 0.011	0.252	S	119
10.0	0.317 ± 0.017	0.093	0.511 ± 0.018	0.294	C	402
80.2	0.628 ± 0.034	0.200	1.012 ± 0.037	0.318	C	414
320	1.030 ± 0.042	0.270	1.661 ± 0.043	0.263	C	132
					Total	1316
$(NH_4)_2SO_4$						
5.00	0.256 ± 0.009	0.075	0.515 ± 0.018	0.291	S	329
10.0	0.347 ± 0.010	0.104	0.694 ± 0.019	0.302	S	167
20.2	0.430 ± 0.018	0.143	0.860 ± 0.035	0.333	S	392
51.4	0.574 ± 0.019	0.178	1.150 ± 0.037	0.310	S	295
78.2	0.640 ± 0.025	0.210	1.280 ± 0.049	0.329	S	183
					Total	1366
					Total Both	2682

Weighted Mean Fractional Deviation

NaCl 0.284 ± 0.031 (11%)
$(NH_4)_2SO_4$ 0.314 ± 0.017 (5%)

Both 0.299 ± 0.029 (10%)

TABLE II

Mean Droplet Radii and Calculated Mean Radii for Each Concentration

Concentration (gm/l)	Calculated Mean Radius r' (μm)	Mean Radius r (μm)	Mean Droplet Radius R	Calculated Mean Droplet Radius R'	Solution* Density (gm/cm^3)	Surface* Tension (cp)
NaCl						
1.25	0.157	0.150	1.80	1.75	1.00	72.51
4.22	0.236	0.231	1.85	1.75	1.00	72.62
10.0	0.314	0.317	1.91	1.75	1.01	72.83
80.2	0.622	0.628	1.91	1.74	1.05	75.32
320	0.954	1.030	2.04	1.72	1.20	82.45
Weighted mean droplet radius NaCl			1.90 ± 0.06 (3.4%)			
Calculated mean droplet radius			1.74 ± 0.01 (1.0%)			
$(NH_4)_2SO_4$						
5.00	0.267	0.256	1.81			
10.0	0.336	0.347	1.95			
20.2	0.424	0.430	1.92			
51.4	0.575	0.574	1.89			
78.2	0.659	0.640	1.84			
Weighted mean droplet radius $(NH_4)_2SO_4$			1.87 ± 0.05 (2.8%)			
Weighted mean droplet radius Both			1.88 ± 0.06 (3.2%)			

*Values for surface tension and density from CRC Handbook, 51st. ed., pages F-28 and D-207

used in the calculations are based on information given of pages F-28 and D-207, respectively, of the Handbook of Chemistry and Physics (Weast 1970). The weighted mean droplet radii for the salt solutions are given at the bottom of the table. The mean droplet radii and the initial concentration are used to determine an average particle radius, r', for each concentration. The weighted mean droplet radii found for both salts are comparable in size with the mean droplet radius determined form light scattering measurements of a liquid aerosol (Fig. 15). The mean droplet radius of Fig. 15 was determined by comparison of the S_{12}/S_{11} predictions with measurements.

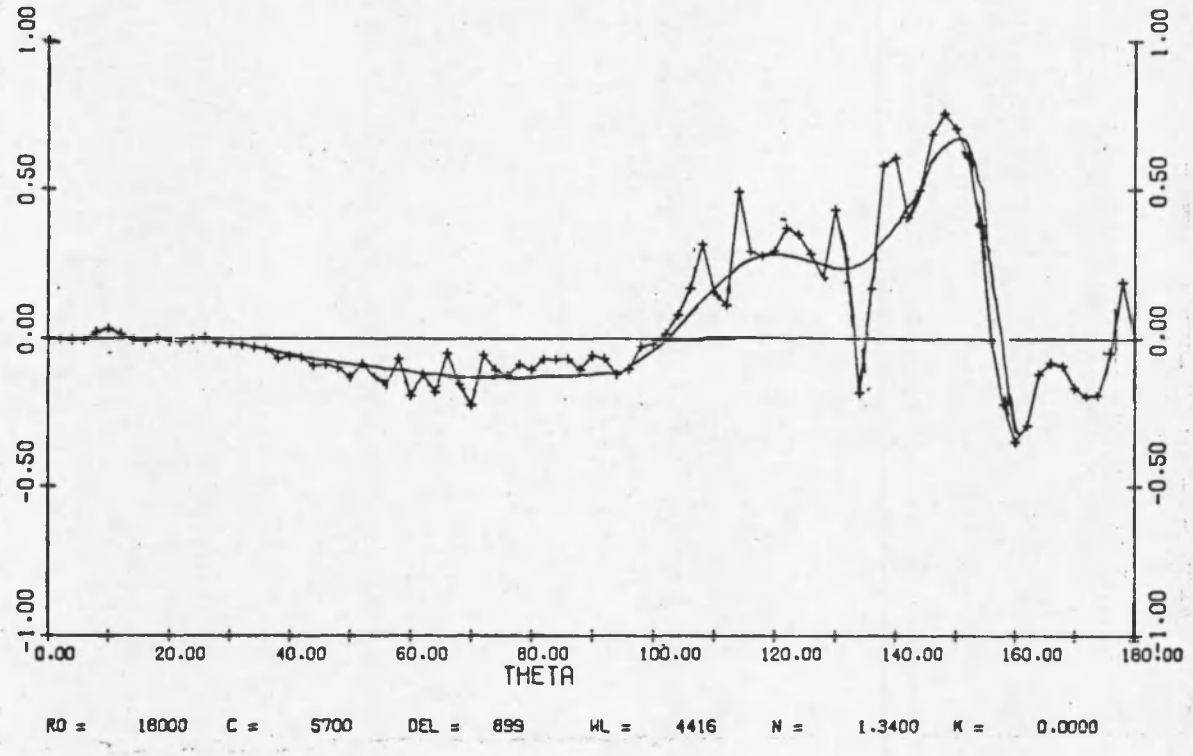

Fig. 15 S_{12}/S_{11} Scattering Measurement for H_2O Aerosol

Table III lists the mean particle radii determined from direct comparison of the theoretical predictions with the scattering measurements. The mean radii from Table I are used to determine Mie coefficients, $x = \frac{2\pi r}{\lambda}$, for $\lambda = 0.6329$ μm and $\lambda = 0.3250$ μm. Comparison of the theoretical predictions with the scattering measurements of the NaCl aerosols was greatly restricted due to the nonspherical particle shapes, and did not allow an accurate sizing of these aerosols. Comparison of the predictions to the $(NH_4)_2SO_4$ scattering measurements was not restricted by the effects of particle shape and could be used to size the aerosols. Of special interest are Figs. B7b and B7c for the 20.0 gm/l $(NH_4)_2SO_4$ showing how variation of the mean radius used in the prediction affects the comparison with the scattering measurements. The same set of experimental measurements is presented on both pages.

Figure 16 is a logarithmic graph of mean particle size versus concentration. The solid lines are the best logarithmic fit for the data using $\log_{10}(y) = a + b[\log_{10}(x)]$. Error bars show one fractional deviation of particle size about the mean size and indicate the amount of overlap between particle size distribution. The solid line for the $(NH_4)_2SO_4$ has a slope of 0.335 ± 0.009, the line for the three largest particle sizes of the NaCl, has a slope of 0.336 ± 0.007. The slopes of the lines for both salts indicate that the mean size of the aerosols are directly proportional to the cube root of the concentration. The graph also reveals a net shift in particle sizes for the higher

TABLE III

Mean Radius from Scattering Measurements

Index of Appendix B Measurements

Concentration (gm/l)	Mean Radius Scattering Measurements λ0.6328 (μm)	λ0.3250 (μm)	Mean Radius Table I		Appendix B Fig. Number λ0.6328	λ0.3250	Mie Coefficient $x = 2\pi r/\lambda$ λ0.6328	λ0.3250
NaCl								
1.25	0.15	0.15	0.150	B1	a	b	1.5	2.9
4.22	0.20	0.20	0.231	B2	a	b	2.3	4.5
10.0	0.26	0.26	0.317	B3	a	b	3.1	6.1
80.2	0.52	0.63	0.628	B4	a	b	6.2	12.1
320	1.03	1.03	1.030	B5	a	b	10.2	19.9
$(NH_4)_2SO_4$								
5.0	0.25	0.23	0.256	B6	a	b	2.5	4.9
10.0	0.32	0.26, 0.32	0.347	B7	a	b, c	3.4	6.7
20.2	0.38	0.38	0.430	B8	a	b	4.3	8.3
51.4	0.50	0.50	0.574	B9	a	b	5.7	11.1
78.2	0.60	0.66	0.640	B10	a	b	6.4	12.4

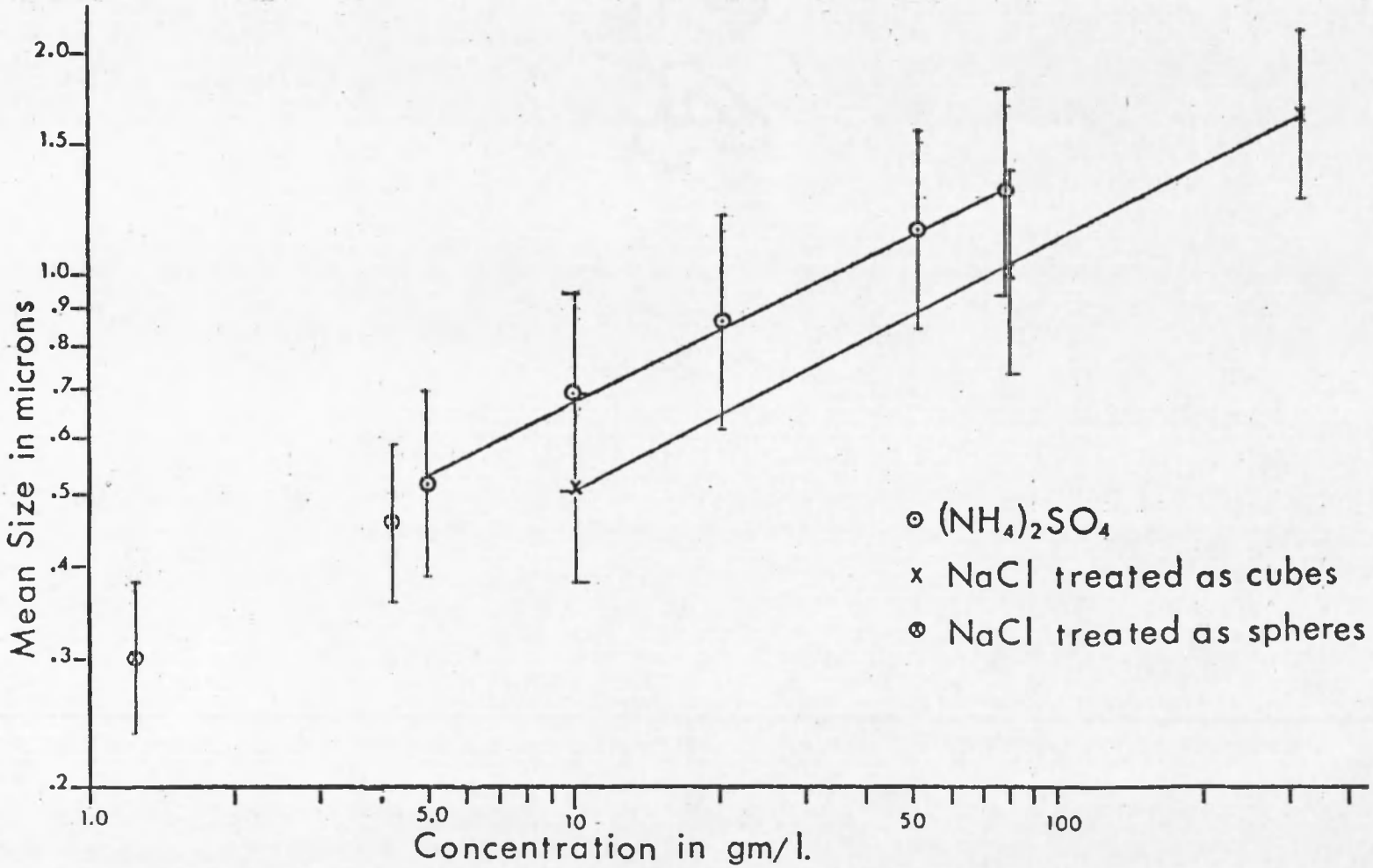

Fig. 16 Mean Particle Size versus Solution Concentration

concentrations of NaCl that is consistent with the assumption that the mean particle size is a direct measure of the side of a cube. The linear relationship for the $(NH_4)_2SO_4$ indicates that variations in the mean droplet radius due to changes in the properties of the solutions with concentration are of secondary importance and do not have a substantial effect on mean particle sizes.

CHAPTER 5

DISCUSSION OF THE RESULTS

The discussion of the experimental results found in this work is limited to observations concerning the light scattering properties of the NaCl and $(NH_4)_2SO_4$ particles and the methods used to determine the size and distribution of the aerosols. First, differences in the scattering properties of the aerosols most likely due to non-spherical particle shapes are discussed for one mean particle size of each salt. Then the above differences are discussed as a function of Mie coefficient for various mean particle sizes. Next, the methods used to size the aerosols and the effects of particle shape on the accuracy of the measurements are discussed. Finally, the particle size distributions are analyzed to determine the basic distribution type and are compared with the size distribution found for other artificial and natural aerosols.

The Complete Scattering Matrix

Measurements containing all elements of the general scattering matrix are presented in Figs. 7 to 10 for the 80.2 gm/l NaCl and 11 to 14 for the 78.2 gm/l $(NH_4)_2SO_4$ aerosols. These measurements are used to characterize the light scattering properties of solid aerosols of each salt.

The form of the desired scattering matrix when each element (except S_{11}) is normalized by dividing by S_{11} is

$$\left[\begin{array}{cc|cc} S_{11} & S_{12}/S_{11} & S_{13}/S_{11} & S_{14}/S_{11} \\ \multicolumn{2}{c|}{(A)} & \multicolumn{2}{c}{(B)} \\ S_{21}/S_{11} & S_{22}/S_{11} & S_{23}/S_{11} & S_{24}/S_{11} \\ \hline S_{31}/S_{11} & S_{32}/S_{11} & S_{33}/S_{11} & S_{34}/S_{11} \\ \multicolumn{2}{c|}{(C)} & \multicolumn{2}{c}{(D)} \\ S_{41}/S_{11} & S_{42}/S_{11} & S_{43}/S_{11} & S_{44}/S_{11} \end{array}\right]$$

The matrix elements actually measured by the instrument are given by

$$\left[\begin{array}{cc|cc} S_{11} & S_{12}/S_{11} & \dfrac{S_{13}}{S_{11}} & \dfrac{S_{14}}{S_{11}} \\ \multicolumn{2}{c|}{(A)} & \multicolumn{2}{c}{(B)} \\ S_{21} + S_{11} & \dfrac{S_{22} + S_{12}}{S_{11} + S_{21}} & \dfrac{S_{23} + S_{13}}{S_{11} + S_{21}} & \dfrac{S_{24} + S_{14}}{S_{11} + S_{21}} \\ \hline S_{31} + S_{11} & \dfrac{S_{32} + S_{12}}{S_{11} + S_{31}} & \dfrac{S_{33} + S_{12}}{S_{11} + S_{31}} & \dfrac{S_{34} + S_{14}}{S_{11} + S_{31}} \\ \multicolumn{2}{c|}{(C)} & \multicolumn{2}{c}{(D)} \\ S_{41} + S_{11} & \dfrac{S_{42} + S_{12}}{S_{11} + S_{41}} & \dfrac{S_{43} + S_{13}}{S_{11} + S_{41}} & \dfrac{S_{44} + S_{14}}{S_{11} + S_{41}} \end{array}\right]$$

where A, B, C and D indicate the relative positions of the 2 x 2 submatrices given in Figs. 7 to 10 and 11 to 14. Measurements of matrix elements normalized to the total intensity in columns 2, 3, and 4 are accurate to ± 3% and ± 1.5° (Hunt 1974). The total intensity measurements in column 1 are presented on a logrithmic scale are are accurate to ± 0.05 decade and ± 3°.

In many cases the additional matrix elements measured with a given element are found to be zero (S_{13} and S_{14}) or << S_{11} (S_{12}, S_{21}, S_{31} and S_{41}), and the resulting measurement is of the desired matrix element. In the cases where there are additional non-zero terms with the desired matrix element, it is necessary to further consider the theoretical relationships between matrix elements found for the type I and II scattering matrices. In particular, the relationships $S_{ij} = |S_{ji}|$, $i \neq j$ for i and j = 1, 2, 3, 4 for the type I and II matrices appear to be experimentally varified for $S_{23}/S_{11} = S_{32}/S_{11}$, $S_{24}/S_{11} = S_{42}/S_{11}$ and $S_{34}/S_{11} = -S_{43}/S_{11}$ measurements (Figs. 8 to 10 for the NaCl and 12 to 14 for the $(NH_4)_2SO_4$) within ± 3%. The above theoretical relationships follow directly from the assumption that the aerosol particles are randomly oriented (van de Hulst 1957, p. 50) and can be expected to hold for the measurements of both salts.

The measurements of particular importance are the S_{13}/S_{11} (= S_{31}/S_{11}) and S_{14}/S_{11} (= S_{41}/S_{11}) in Figs. 8 and 11. These measurements are equal to 0.00 ± 3% for all scattering angles and may be eliminated from all measurements in the third and fourth row and column. As a consequence, all measurements in Figs. 10 and 14 can be looked upon as a direct measure of the desired matrix elements S_{33}/S_{11}, S_{34}/S_{11}, $-S_{43}/S_{11}$ and S_{44}/S_{11}. By subtracting the S_{12}/S_{11} matrix element from the measurements in the second column (Figs. 9 and 13) it was possible to obtain the S_{32}/S_{11} and S_{42}/S_{11} matrix elements (dashed line) within a ± 4% accuracy. The presence of the $S_{12}/S_{11} = S_{21}/S_{11}$ matrix elements in the S_{22}/S_{11} measurement results in an additional term

proportional to $(S_{12}/S_{11})^2$ which is less than 2% for all scattering angles and may be ignored in the present discussion. Upon implementing the above results, the general scattering matrix reduces to

$$\left[\begin{array}{cc:cc} S_{11}\ (.05) & \frac{S_{12}}{S_{11}}\ (3\%) & \frac{S_{13}}{S_{14}}\ (3\%) & \frac{S_{14}}{S_{11}}\ (3\%) \\ & (A) & & (B) \\ \frac{S_{12}}{S_{11}}\ (3\%) & \frac{S_{22}}{S_{11}}\ (4\%) & \frac{S_{23}}{S_{11}}\ (3\%) & \frac{S_{24}}{S_{11}}\ (3\%) \\ \hdashline \frac{S_{13}}{S_{11}}\ (3\%) & \frac{S_{32}}{S_{11}}\ (4\%) & \frac{S_{33}}{S_{11}}\ (3\%) & \frac{S_{34}}{S_{11}}\ (3\%) \\ & (C) & & (D) \\ \frac{S_{14}}{S_{11}}\ (3\%) & \frac{S_{42}}{S_{11}}\ (4\%) & \frac{S_{43}}{S_{11}}\ (3\%) & \frac{S_{44}}{S_{11}}\ (3\%) \end{array}\right]$$

where the given percentages indicate the relative accuracy of the measurements.

B and C Submatrices

The scattering measurements in the B and C submatrices are used to determine the general matrix type for the aerosols of both salts. Inspection of the S_{23}/S_{11} and S_{24}/S_{11} measurements (Figs. 8, 12) and the S_{32}/S_{11} and S_{42}/S_{11} (dashed lines) (Figs. 9, 13) show these elements to be zero ± 3% and ± 4% respectively. With S_{13}/S_{11} $(= S_{31}/S_{11})$ and $S_{14}/S_{11} = (S_{41}/S_{11})$ also equal to zero ± 3% (Figs. 8, 12) the measurements of all elements in the B and C submatrices are found to be zero and as a result the aerosols of both salts have the scattering properties of a type II general scattering matrix.

A and D Submatrices

Since the elements of submatrices B and C have been shown to be zero, the scattering measurements in the A and D submatrices contain all the information necessary to characterize the light scattering properties of aerosols of both salts. For a distribution of spheres the diagonal matrix elements are related with $S_{11} = S_{22}$ and $S_{33} = S_{44}$. The degree to which these relationships hold as a function of the scattering angle is a direct measure of the nonspherical nature of the aerosol particulate. In regions where the measurements of the diagonal matrix elements are found to be equal, the theoretical predictions for spheres may be used to size the aerosol particulate.

The total intensity peak in the forward angles for the S_{11} and $S_{11} + S_{21}$ measurements is due to light diffracted around the aerosol particulate. For spherical particles the width of the intensity peak is dependent on the mean particle radius (van de Hulst, 1957, p. 391). The measurements for both salts do not show any noticeable dependence on particle shape for $\theta < 60^{o}$ and it is evident that the width of the scattered intensity peak depends primarily on the mean particle size (cf. Holland and Gagne, 1971).

For $(NH_4)_2SO_4$ (Fig. 11) the close fit of the S_{11} prediction to the S_{11} and $S_{11} + S_{21}$ ($S_{11} >> S_{21}$) measurements indicates the mean radius and distribution used in the calculation is a reasonable approximation to the size parameters of the aerosols. Comparison of the prediction to the measurements shows no effects of particle shape for large scattering angles and indicates a spherical particle shape.

It is not possible to judge the accuracy of the mean radius used in the predictions for NaCl from the S_{11} and $S_{11} + S_{21}$ measurements due to the limited match between the two. The NaCl measurements could have been placed about 0.4 decade higher for proper comparison to the prediction in the forward angles. For NaCl (Fig. 7) comparison of the prediction to the measurements beyond 60^{o} shows large differences due to nonspherical particle shape. Around 90^{o} there is a net increase of scattered light relative to the prediction and for $\theta > 120^{o}$ there is a distinct decrease in the back scattered intensity. These scattering features are a common characteristic of aerosols with nonspherical particle shapes (cf. Holland and Gagne, 1970, Huffman and Thursby, 1969). For spherical particles the increase in scattered intensity for large scattering angles is a cooperative effect where light is internally scattered once by the aerosol particles. The amount of light back scattered by the aerosol is decreased by nonspherical shapes (Hanson and Hovenier 1974, p. 19) because irregular particle shapes distribute the back scattered light more uniformly through all scattering angles. For 20-μm ice particles, Huffman and Thursby (1969) attributed the additional scattered intensity at 90^{o} to the presence of multiple facets on the aerosol particulate that internally scatter light through larger angles than is possible for a sphere.

The S_{22}/S_{11} measurement is ideally suited to the determination of the effects of nonspherical particle shape in the scattering measurements. The theoretical prediction, $S_{22}/S_{11} = 1$ is independent of

mean radius and distribution of the aerosol and allows comparison of the scattering measurements for any aerosol to be made on the basis of particle shape. Regions where the S_{22}/S_{11} measurements $\approx$ 1 shows that the effects of particle shapes are of minor importance. For $(NH_4)_2SO_4$ (Fig. 11) the measurement shows $S_{22}/S_{11} \geq 0.9$ for $\theta < 90^o$ and declines steadily from 1.0 at 5^o to 0.84 at 160^o. In contrast, for NaCl (Fig. 7) $S_{22}/S_{11} \geq 0.9$ for $\theta < 50^o$ and declines to 0.42 at 160^o. For $\theta > 100^o$ the S_{22}/S_{11} measurement may be used as a quantitative estimate of the relative sphericity of the aerosol particulate. The S_{22}/S_{11} measurement clearly shows the $(NH_4)_2SO_4$ particulate to be more rounded than the NaCl and the factor of two difference in their scattering properties at 160^o indicates a large difference in their relative sphericity. The measurements of Holland and Gagne (1970) show that $S_{22}/S_{11} = 0.32$ at 160^o, indicating, as is the case, that the silicate particles used in their experiment were more irregular in shape than the NaCl particulate. Further measurements of nonspherical aerosol particulates are necessary to determine how to use the S_{22}/S_{11} measurement to determine the relative sphericity of aerosol particulates.

The S_{22}/S_{11} measurements are an explicit representation of the ideas presented by Holland and Gagne (1970) and clearly demonstrate that for aerosols with nonspherical particle shapes the theoretical predictions should be aligned with the scattering measurements in forward angles. The steady decline of the measurements for both salts with increasing scattering angle show the effects of particle shape to be of importance for large scattering angles. Comparison of the predictions

to the scattering measurements in these regions as suggested by Plass and Kattawar (1971) cannot be expected to give an accurate sizing of the aerosol particulate without further consideration of particle shape.

In submatrix D the S_{33}/S_{11} prediction for the diagonal matrix elements shows greater sensitivity to variations in mean radius for large scattering angles than the S_{11} prediction, and may be used to size aerosols with nearly spherical particle shapes. In Fig. 14 the S_{33}/S_{11} and S_{44}/S_{11} measurements for the $(NH_4)_2SO_4$ are equal for all scattering angles. The slightly nonspherical particle shapes do not result in any noticeable differences between the two measurements. The S_{33}/S_{11} prediction fits the measurements over most of the scattering range and indicates a rounded particle shape. For $\theta > 90^{o}$ there are differences between the prediction and scattering measurements that are perhaps caused by irregularities in the particle shapes. It is possible to obtain a closer fit for the scattering measurements in this region by increasing the mean particle radius used in the predictions, but this results in a larger mean radius than is indicated by the other measurements and is not justified because of the effects of nonspherical particle shape in the back scattering angles. The differences between the prediction and the S_{33}/S_{11} and S_{44}/S_{11} measurements in Fig. 14 are a conservative indication of the effects of particle shape for large scattering angles

In Fig. 10 the inequality of the S_{33}/S_{11} and S_{44}/S_{11} measurements for the NaCl shows the aerosol particulate to be nonspherical.

The measurements are equal out to 100^{o} and then diverge showing a 0.45 difference at 160^{o}. The separation between the measurements is less than that found in the S_{22}/S_{11} measurement and it would appear that the S_{33} and S_{44} matrix elements are less effected by irregularities in the particle shape. The down shift of the S_{33}/S_{11} scattering measurement relative to the theory clearly indicates the nonspherical particle shape to be of importance for large scattering angles. The S_{44}/S_{11} measurement is of interest because it is the only case where the prediction is found to match a NaCl measurement beyond 120^{o}. The S_{33}/S_{11} prediction for both measurements shows a closer match with the scattering measurements for all angles than is found of the S_{11} and S_{22}/S_{11} predictions, and suggests a decrease in the effects of particle shape in the measurements.

The remaining off diagonal matrix elements S_{12}/S_{11}, S_{34}/S_{11} and S_{43}/S_{11} are of particular interest. The theoretical predictions for these matrix elements are sensitive to variations in mean radius and distribution in the forward scattering angles allowing a more meaningful comparison to the scattering measurements in regions where the particle shape is not an important factor. Comparison of the predictions to the scattering measurements for large scattering angles, $\theta > 90^{o}$, also allows further distinctions to be made on the basis of particle shape.

In Figs. 10 and 14, the S_{34}/S_{11} and S_{43}/S_{11} measurements for each salt are found to be equal for all scattering angles. The measurements experimentally verify the theoretical relationships between off diagonal elements and show them to be independent of particle shape. For both salts the close fit of the S_{34}/S_{11} prediction to the scattering measurements is of direct use in sizing the aerosols. Of the measurements presented, the S_{34}/S_{11} and S_{43}/S_{11} matrix elements allow the most accurate sizing of the nonspherical aerosol particulate.

In Fig. 14 for $(NH_4)_2SO_4$ the S_{34}/S_{11} prediction for the S_{34}/S_{11} and S_{43}/S_{11} measurements is an excellent approximation to the measurements and shows the mean radius and distribution used in the calculations to be substantially correct. The prediction also shows that irregularities in the particle shape have a negligible effect on the scattering measurement.

In Fig. 10 for the NaCl comparison of the S_{34}/S_{11} prediction to the S_{43}/S_{11} scattering measurement in the forward angles shows a slight difference in amplitude and indicates that the distribution used in the prediction was too narrow. The amplitude differences noted for the S_{34}/S_{11} measurement are caused by a non-zero dc offset in the lock-in amplifier which was not corrected for in the placement of the measurement relative to the prediction. The distinct bend in the S_{34}/S_{11} and S_{43}/S_{11} measurements at 110^{o} and the subsequent decline in the signal shows a large dependence on the nonspherical particle shape relative to the prediction. The abrupt change in measurement at 110^{o} seems to be a characteristic scattering feature of the NaCl particulate (also see

Fig. B5b) and may be caused by the regularity of the cubic particle shape.

The S_{12}/S_{11} prediction displays a strong angular dependence of scattering features on mean radius and index of refraction with the amplitude being dependent on distribution width (Hanson and Hovenier 1974). The S_{12}/S_{11} measurements for both salts tend to be shallower than the S_{34}/S_{11} measurements and show a larger dependence on the shape of the aerosol particles. For large scattering angles the vertical shift of the S_{12}/S_{11} measurements for both salts and loss of character or averaging of scattering features is a common scattering feature of nonspherical particle shapes (Holland and Gagne, 1970).

The S_{12}/S_{11} prediction for the $(NH_4)_2SO_4$ measurement (Fig. 11) shows coincidence in the angular location of scattering features indicating the mean radius used in the prediction is accurate to within ± 10%. The difference in signal amplitude between the prediction and measurement is probably due to nonspherical particle shape. The difference may be reduced by broadening the distribution used in the prediction, but it is not likely that this would represent a more accurate sizing of the aerosol.

For NaCl the S_{12}/S_{11} measurement (Fig. 7) clearly shows that the NaCl aerosol has scattering properties fundamentally different than the theoretical prediction for spheres. The positive polarization feature at 120^{o} may be characteristic of the cubical shape of the NaCl particulate. Other aerosols with regular nonspherical particle shapes have been found to have comparable scattering features at

different angles (cf. Huffman and Thursby, 1969). For $\theta < 50^{o}$ the rough angular agreement between the prediction and the scattering features for the NaCl measurement suggests the mean radius used in the calculation is acceptable, although the comparison is quite limited. The comparison for $\theta < 50^{o}$ shows some difference in amplitude, indicating the distribution width used in the calculation is too narrow. For $\theta > 50^{o}$ the prediction shows up to 35% difference between the predicted and measured polarizations. An increase of the distribution width would result in a smaller difference of about 25%. Comparison of the S_{12}/S_{11} signal amplitudes for the two salts shows a 20% difference in polarization at 120^{o} and indicates a larger dependence on particle shape for the NaCl measurement. The S_{12}/S_{11} prediction cannot be manipulated to give positive polarization around 120^{o} without a substantial decrease in the mean radius used in the calculation.

The measurements in the A and D submatrices show the nonspherical particle shapes can substantially alter the scattering properties of aerosols. The scattering properties of aerosols show the largest dependence on particle shape for $\theta > 90^{o}$. When compared with the theoretical predictions the measurements in the D submatrix appear to be effected less by particle shape than the measurements in the A submatrix. In the forward scattering angles, the scattering properties of both salts appear to depend only on the mean particle radius and wavelength. In this region the theoretical predictions for spheres may be used to accurately size the aerosol particles.

Selected Matrix Elements vs. Size Parameter

In Appendix B scattering measurements at two wavelengths are presented that allow a comprehensive study of the scattering properties of aerosols of both salts as a function of mean particle size. Differences between the theoretical predictions and the measurements allow further analysis of the light scattering properties of aerosols with nonspherical particle shapes. The measurements presented clearly show limitations in the applicability of the theoretical predictions and indicate in what range of particular sizes and scattering angles the theory may be used to accurately size the aerosols.

The scattering measurements and predictions for both salts may be compared by Mie coefficient $x = \frac{2\pi r}{\lambda}$, since the bulk optical properties of the salts at $\lambda 0.6328$ μm and $\lambda 0.3250$ μm are nearly equal. This is useful for determining similarities and differences between measurements made for both salts. For aerosols with rounded particle shapes comparison by x is used to check the accuracy of the mean radius for each concentration and consistency of the measurements. For aerosols with irregular particle shapes, changes in the basic particle shape with mean size may be determined from comparison of the measurements.

NaCl Particles

Inspection of Figs. B1-B5 shows large differences in the scattering properties of the NaCl aerosols due to the cubic shapes of the particles. All the measurements show some effects due to nonspherical

particle shapes ranging from the B1a measurements, that show minor differences when compared with the prediction, to the B4 and B5 measurements that have little in common with the predictions. In the forward scattering angles the measurements have features similar to the predictions that vary with Mie coefficient. The measurements show progressively larger differences due to particle shape with increasing x and for the higher concentrations show scattering features that do not vary with mean size or wavelength and depend only on the regularity of the particle shape.

The total intensity measurements for all concentrations of the NaCl are shallower functions of the scattering angle than the predictions. The S_{11} measurements show the nonspherical particle shape to be an important factor for $\theta > 90^{o}$ where the back scattered light is as much as a decade less than predicted. The S_{11} predictions for the lower concentrations (B1-B3) are a closer approximation to the measurements indicating that the aerosol particles have a more rounded shape. The particle radius for $r \leq 0.32$ μm determines the basic scattering properties and differences due to nonspherical particle shape are of importance only beyond 120^{o}. The B4 and B5 measurements for $r > 0.6$ μm show the largest differences due to the shape of the aerosol particles. The form of the S_{11} measurements for $x > 6$ remains the same at both wavelengths and does not show any dependence on the mean radius of the aerosols. The similarity of the measurements indicates that the basic particle shape is the same for both concentrations and comparison with

prediction shows that the cubic forms dominates the scattering properties of the aerosols.

Changes in the S_{33}/S_{11} measurements due to nonspherical particle shapes are evident as a decrease in the slope of the measurement relative to the prediction. For the smaller mean radii, $r \leq 0.25$ μm, measurements with $x < 4$ are a shallower function of the scattering angle than the prediction and have a slope equal to the average slope of the prediction. The measurements show features similar to those found in the prediction and have the same horizontal intercept demonstrating most of the size dependence expected for spherical particulates. For mean radii $0.3\ \mu m \leq r \leq 0.6\ \mu m$ the slope of the measurements with $4 < x < 6$ are more negative than predicted, and as a result there are large differences in signal amplitude and horizontal intercept. The measurements still show some amplitude and angular dependence predicted for spheres but are displaced downward up to 0.50 at 160^{o}.

The overall differences between predictions and measurements are less pronounced for aerosols with mean radii $r > 0.6$ μm. For $x > 9$ both the prediction and measurements have nearly constant slopes. The B4b, B5a and B5b scattering measurements have the same basic shape and appear to lack any pronounced scattering features. The measurements do not show any angular dependence that might be considered to be a characteristic of the cubic particle shape, but do show a substantial averaging of scattering features due to nonspherical particle shape. The close comparison between the S_{33}/S_{11} prediction and the

B5a measurement is inconsistent with the comparisons found for the B4b, B5b measurements and is not understood.

The S_{12}/S_{11} measurement in Fig. B1a with $r = 0.15$ μm and $x = 1.5$ does not show any effects of a nonspherical particle shape. This measurement sets an approximate upper limit for the range of measurements where the Mie theory can be expected to apply rigorously. The S_{12}/S_{11} measurements with $x > 2$ show a definite "half and half" character due to the nonspherical particle shapes. For $\theta < 60^{o}$ the predictions fit the measurements for all particle sizes showing a simple dependence on Mie coefficient. Beyond 90^{o} the measurements are shifted vertically relative to the prediction and show up to 50% difference in polarization due to the nonspherical particle shapes. The scattering measurements with $2 < x < 6$ for aerosols with $r \leq 0.26$ μm (Figs. B1-B3) show progressively larger shifts in polarization with increasing Mie coefficient. Comparison of the B1b and B3a measurements by Mie coefficient indicate that there is some change in the shape of the aerosol particle with increasing mean radius. Comparison of the S.E.M. photographs for these samples showed that the particle shape went from being nearly spherical for mean radius $r = 0.15$ μm to being an imperfect cube for $r \geq 0.32$ μm. The change in the shape of the aerosol particulate accounts for the increase in differences found between the measurements and prediction with x.

The measurements of particular interest for NaCl are for aerosols with mean radii $r > 0.6$ μm (Figs. B4, B5). These measurements show a stable scattering feature around 120^{o} that depends on the cubic

particle shape and does not vary with increasing Mie coefficient. The small positive polarization feature found at both wavelengths has an amplitude of 4.5% ± 0.6%. The angular position of the maximum is shown in the table:

Solution Concentration	λ0.6328 μm	λ0.4416 μm	λ0.3250 μm
80.2 gm/l	$128^{o} \pm 1^{o}$	$128^{o} \pm 1^{o}$	$121^{o} \pm 2^{o}$
320 gm/l	122^{o}	---	$117^{o} \pm 2^{o}$

Further measurements and analysis are necessary to determine the angular dependence of this peak on index of refraction and particle shape.

The S_{12}/S_{11} measurements in Figs. B2a and B3a with λ0.6328 μm show a similar polarization feature at $121^{o} \pm 3^{o}$ and $122^{o} \pm 2^{o}$ respectively that has a maximum amplitude of 9%. The S_{12}/S_{11} measurements with λ0.3250 μm (B2b, B3b) for these concentrations do not show a positive polarization feature in this region. The apparent anomaly in the sensitivity of the scattering measurements to particle shape is easily explained. The state of polarization of the prediction for the smaller Mie coefficients, $x < 2.5$, is nearly zero around 120^{o} and as a result a small difference in the shape of the aerosol particulate will result in a measureable positive polarization feature that will not be evident at shorter wavelengths.

The S_{34}/S_{11} measurement presented in figs. B4b and B5b also show a stable shape dependent scattering feature. The distinct bend in the scattering measurement around 110^{o} was noted in measurements for

aerosols with mean radii $r \geq 0.3$ μm and appeared regularly for Mie coefficients $x \geq 4$. The feature was found to have an angular position between 120^{o} and 130^{o} for $\lambda 0.4416$ μm and from 100^{o} - 110^{o} for $\lambda 0.3250$ μm.

$(NH_4)_2SO_4$ Particles

In Figs. B6 to B10 the theoretical predictions are found to be a reasonable approximation to the scattering measurements at both wavelengths. Comparison of the predictions and measurements indicates that the aerosol particulate for all concentrations of $(NH_4)_2SO_4$ have rounded particle shapes. The nonspherical shape of the particulate does not cause a substantial change in the scattering properties of the aerosols. The measurements show scattering features at all angles that allow the aerosols to be accurately sized by the predictions despite some reduction in signal amplitudes for measurements with $x > 8$ due to irregular particle shapes. Comparison of the measurements by Mie coefficient shows a slight increase in the effects of particle shape with mean radius. S.E.M. photographs of the aerosols show that the larger particles tended to be more deformed but the change in shape was not enough to allow the photographs for different concentrations to be distinguished on the basis of particle shape. The scattering measurements for $(NH_4)_2SO_4$ show differences that depend on the size of the particle irregularities relative to the wavelength of the scattered light and indicate that measurements with the shorter wavelength are more sensitive to the nonspherical shape of the aerosol particulate.

The total intensity measurements for $(NH_4)_2SO_4$ are the least effected by the shape of the aerosol particulate. The S_{11} measurements for all concentrations show a substantial increase in back scattered light that is a characteristic of a spherical particle. The predictions are a close approximation to the measurements at both wavelengths and it is apparent that the mean radius and distribution used in the calculations are substantially correct. The minor differences found between the prediction and the measurements with $2.5 < x < 12.4$ indicate that the S_{11} scattering properties of the $(NH_4)_2SO_4$ aerosols with mean radii $0.26\ \mu m < r < 0.64\ \mu m$ are equivalent to that of a distribution of spheres. Beyond 140^o there are up to 0.25 decade differences between the measurement and prediction that depend on several factors. There is a 0.1 - 0.2 decade decrease in the intensity due to irregular particle shapes, but it is of minor importance compared to the 1 - 2 decade increase in back scattered light that depends on a nearly spherical shape. All the $\lambda 0.6328$-μm measurements are shallower than the predictions due to a decrease in the sensitivity of the photo multiplier to the longer wavelength. The resulting differences in amplitude at the extremes of the $\lambda 0.6328$ measurements are larger than the differences due to the irregular particle shape. The amplitude of the S_{11} prediction for $\theta > 120^o$ increases with x for $x < 7$. As a result a 5-10% error in the mean radius used in the calculation will be evident as a difference between measurement and prediction comparable to the effects of nonspherical particle in the measurements.

Comparison of the S_{33}/S_{11} predictions with the measurements shows much larger differences for $\theta > 90^{o}$ than are evident in the other measurements. Most of the difference depends on the choice of the parameters used in the calculation and does not reflect any increase in the sensitivity of the S_{33}/S_{11} measurement to the non-spherical shape of the aerosol particle. Differences that do depend on the shape of the aerosol particulate are evident for $\theta > 90^{o}$ as a down shift of the S_{33}/S_{11} measurements relative to the prediction. The measurements with $x < 8$ and $r \leq 0.64$ μm show progressively larger differences in position with mean radius but do not show any averaging effects due to irregular particle shapes. Comparison of these measurements by Mie coefficient reveals differences of up to 0.20 between measurements and shows that the aerosols with larger mean radius are more irregular in shape. For $x > 8$ the differences between the predictions and measurements are smaller. The effects of nonspherical particle shape are evident as a downshift of 0.25 relative to the prediction and a decrease in the angular and amplitude dependence of the measurements beyond 90^{o}.

It is possible to obtain a closer match between the S_{33}/S_{11} prediction and the measurements by increasing the mean radius used in the calculation. The mean radius found to give best fit for the S_{33}/S_{11} measurement for large angles is 10-15% larger than the mean radius found for the S_{12}/S_{11} and S_{11} matrix elements. (See Figs. B7b and B7c.) Since the nonspherical particle shape of the aerosols also produces a similar shift in the S_{33}/S_{11} measurement, increasing the

mean radius used in the calculation does not represent an accurate sizing of the aerosol. The S_{33}/S_{11} predictions also show a definite interdependence of mean radius and distribution for large angles, making it likely that part of the differences found are the result of, or the oversimplification of, the distribution used in the calculations or an error in the distribution width. Further predictions with a systematic choice of size parameters and more exacting choices of distribution are necessary to accurately determine the effects of the nonspherical particle shape in the S_{33}/S_{11} measurements.

The S_{12}/S_{11} predictions are a close approximation to the scattering measurements for $x < 8$ (Figs. B(6 to 10)a, B (6 and 7)b) and an acceptable estimate for $8 < x < 12.5$ (Figs. B(8 to 10)b). These predictions allow the most accurate sizing of the aerosols and can be used to determine the mean radius of the aerosols within ± 10% (Hunt 1974). The measurements with $x < 5$ and $r \leq 0.45$ μm show no effects due to irregular particle shapes and only minor differences relative to the prediction due to a few percent error in the mean radius used in the calculations. For $5 < x < 8$ the measurements decrease in amplitude beyond 120^{o} and show that the negative polarization feature or glory phenomena (Hanson and Hovenier 1974, p. 16) evident in the prediction for $2 < x < 9$ is very sensitive to particle shape. The measurements with $x > 8$ and $r \geq 0.45$ μm show the largest averaging effects due to nonspherical particle shape. The measurements retain features similar to the predictions but decrease in amplitude beyond 80^{o} showing

up to 30% shift in polarization for large angles. The S_{12}/S_{11} measurements show a uniform increase in the effects of irregular particle shape with Mie coefficient. Comparison of the measurements by x does not reveal any measureable increase in the irregularity of the particle shape with mean radius and indicates that increased effects of particle shape result primarily from a decrease in the wavelength of the scattered light.

Discussion of Sizing Results

From Theoretical Predictions

The predictions for the S_{11}, S_{12}/S_{11}, S_{33}/S_{11} and S_{34}/S_{11} matrix elements may be used to determine the mean size and distribution for an aerosol. The accuracy of the sizing is not the same for each because the matrix elements do now show equal sensitivity to variations in x, distribution width and dependence on particle shape.

The S_{12}/S_{11} and S_{34}/S_{11} predictions are ideally suited for sizing aerosols with nonspherical particles. Both show features in the forward scattering angles that allow an accurate sizing of an aerosol and allow an unambiguous determination of the effects of particle shape for large scattering angles. The S_{12}/S_{11} prediction is commonly used to size particles in aerosols (Hunt and Huffman 1973, Hanson and Hovenier 1974) and colloidal suspensions (Hunt 1974). The S_{12}/S_{11} prediction was used extensively in this work (Fig. 15, B1a and Figs. B6 to B10) to obtain mean radii for the aerosols with about a ± 10% accuracy (Hunt and Huffman 1973). Hanson and Hovenier (1974) present a series

of topographical maps of the S_{12}/S_{11} prediction with contour lines in a constant percent polarization for $0 \leq x \leq 40$ and $0 \leq \theta \leq 180^{o}$ for several values of n and distribution width. Their presentation allows a direct inspection of the essential properties of the S_{12}/S_{11} matrix element and show that the predictions have a strong angular dependence on x and n and an amplitude dependence inversely proportional to the width of the size distribution.

In appendix B the S_{34}/S_{11} predictions show angular dependence on x and n and an amplitude dependence on distribution width similar to those found in the S_{12}/S_{11} predictions. Survey measurements started for the NaCl indicate that the S_{34}/S_{11} measurement is ideally suited for sizing nonspherical aerosols and give a closer agreement with the predictions over a larger range of the scattering angles than the S_{12}/S_{11} measurements. The S_{34}/S_{11} matrix element is not commonly measured or discussed in the literature and should prove a fruitful area for further studies of aerosols.

A lack of sensitivity to variations in x in the forward scattering angles and measurements effects due to nonspherical particle shape beyond 90^{o} limit the use of the S_{11} and S_{33}/S_{11} predictions in sizing aerosols with nonspherical particle shapes. The S_{33}/S_{11} predictions given in this work show both angular and amplitude dependence on mean radius and distribution beyond 90^{o} and do not allow an unambiguous determination of the size parameters for aerosols. The only feature in the S_{33}/S_{11} predictions in the forward scattering region that

is suitable for sizing purposes is a small indent around 20^{o} occurring for $x > 6$. This feature is noticeably lacking in the measurements. The S_{33}/S_{11} prediction may be used to size aerosols with nearly spherical particles but requires special consideration because irregularities in the particle shape were found to produce changes in the measurements that result in an overestimate of the mean particle radius when compared with the predictions.

The total intensity of the scattered light is discussed extensively in the literature and is the most commonly measured of the matrix elements (Hunt 1974, Holland and Gagne 1970). The S_{11} predictions in this work do not allow an accurate sizing of the aerosols. The predictions with $x < 6$ may be used to size aerosols but require a close comparison with the measurements beyond 90^{o}. For $x > 6$ the S_{11} predictions are relatively insensitive to variations in x and lack features that can be used to size the aerosols. Total intensity measurements are of particular use in determining extrinsic properties of the aerosols like the total number of scatterers and extinction coefficient (van der Hulst 1957, p. 388; Deirmendjian 1964) but require placement of the measurement on an absolute scale.

It was not possible with the present experimental system to accurately position the S_{11} measurements on an absolute scale or place them relative to the predictions. The measurements were positioned to give a reasonable fit for all angles, for the $(NH_4)_2SO_4$ aerosols the position of the measurements is substantially correct and the predictions can be used to size the aerosols. The computer plots of the

S_{11} predictions did not extend far enough into the forward scattering angles to allow proper placement of the NaCl measurements for sizing purposes and the comparison is only useful in determining the effects of nonspherical particle shapes. It will be necessary to modify the S_{11} predictions and the total intensity measurement system and to use calibration methods such as those given by Pritchard and Elliott (1960) to achieve an accuracy comparable to the standards present in the literature. Neither modification would substantially alter the shape of the total intensity measurements presented in this work but would have allowed a more meaningful comparison between the measurements and predictions.

An example of how the S_{11}, S_{12}/S_{11} and S_{33}/S_{11} predictions were used to size the aerosols is given in Figs. B7b and B7c where predictions with two different mean radii are compared to the same set of scattering measurements. Ideally the comparison between the predictions and scattering measurements would indicate the same mean radius and distribution for all matrix elements at both wavelengths. In Figs. B7b and B7c it is evident that the mean radius that gives the best fit for the S_{12}/S_{11} and S_{11} measurements (B7b) is smaller by 20% than the mean radius found to match the S_{33}/S_{11} measurement (B7c). The mismatch between the S_{12}/S_{11} measurement and the prediction, Fig. B7c, due to the shift in mean radius shows the forward scattering angles of the S_{12}/S_{11} prediction is a very sensitive region for sizing purposes. Further differences between the mean radii found to give the best fits at each wavelength (see Figs. B6a, B6b) result from an

increase in the effects of particle shape for the shorter wavelength and a few percent error in the indices of refraction used in the predictions. In practice it was not possible to accurately size aerosols with non-spherical particles by comparison of the predictions with the scattering measurements due to the large differences in the scattering properties of the aerosols. For the NaCl aerosols the comparison was very approximate for $\theta < 60^{o}$ and futile beyond 90^{o}. The $(NH_4)_2SO_4$ aerosols could be sized by the predictions but required the complete set of measurements of both wavelengths to determine the accuracy and consistency of the mean radius found for each concentration.

In Fig. 15, the mean radius of a H_2O aerosol produced by the ultrasonic nebulizer is determined by comparison of the S_{12}/S_{11} measurement with the theoretical prediction giving $r = 1.80\ \mu$ ($\pm$ 10%). The weighed mean fractional deviation, 0.30 ± 0.03, found in Table I was used to determine the distribution width. In comparison, the weighted mean droplet radius for the liquid aerosols in Table II is 1.88 ± 0.06. There is a 4% difference between mean radii for the liquid aerosols obtained from the two methods.

Use of predicted scattering patterns from Mie theory provides a fast and accurate way to determine the mean radius for aerosols with a highly spherical particle shape like the H_2O. Since the measurement shows little or no differences due to irregularities in particle shape, it is possible to directly size the aerosols using a computer. By digitizing the measurements, and using a variational method to determine the mean radius and distribution of the aerosol (Kerker 1972, p. 8) it

would be possible to substantially decrease the error in the sizings obtained for both liquid aerosols and solid aerosols in this work.

From Mean Particle Size

The mean difficulty encountered in calculating the mean radii of the aerosols from the mean size is in determining the accuracy of the mean radii found for the cubically shaped aerosols. Since neither of the methods discussed in Chapter 3 have provisions that allow direct determination of the accuracy of the conversion, it is necessary to develop an alternate means of obtaining the conversion factor and its error from the measurements.

It is possible to determine the relationship between the mean size and mean radius for the cubic particles by fitting the data in figure 16 with a generalized form of the logarithm of the expression $r = R\,(1 + \frac{\rho \times 10^3}{y})^{-1/3}$ relating the mean radius, r, of solid aerosols to the mean droplet radius, R. The particular logarithmic curve used to fit the data is $\log(m) = a + b \log\,(1 + \frac{\rho \times 10^3}{y})$ where m is the mean size, y the solution concentration and ρ the density of the salt. In the case of the spherically shaped particles, the antilog of the parameter a_s is a direct measure of the mean diameter, D, of the liquid aerosols, i.e., $D = 10^{a_s}$. For the cubically shaped particles, the mean diameter found, $L = 10^{a_c}$ is a direct measure of the mean size of a droplet with an equivalent cubic shape. Assuming that the mean diameter of the liquid aerosols is the same for all concentrations of both salts, the conversion factor relating the mean radius to the mean

size of a cube is $k = \frac{D}{2L}$. The values found for a and b are

	a	b
spheres	0.578 ± 0.009	-0.346 ± 0.004
cubes	0.516 ± 0.004	-0.347 ± 0.007

and as a consequence, D = 3.97 μm ± 0.09 μm and L = 3.28 μm ± 0.11 μm. Combining the above values for D and L to determine the conversion factor for the mean radius of a cube gives k = 0.605 ± 0.023. In comparison, the conversion factor k = 0.62 obtained by assuming the mean size is a direct measure of the side of a cube is nearly equal to (2.5%) the above value for k and justifies the use of this assumption in calculating the mean radii for the cubic particles. The error in k determined from the measurements results from assuming an error in the mean size of the aerosols of the form $\sigma/\sqrt{n}$, and indicates an additional 3.9% error in the mean radii found for the cubically shaped particles. The assumed error in the mean size is analogous to the standard deviation of the mean, $\sigma/\sqrt{n}$ where σ is the standard deviation, and n is the number of particles measured and is intended to reflect the precision of the mean size found for the aerosols. The 3.9% error found from the measurements is a conservative estimate of accuracy of the conversion of mean size to mean radius and, when combined with an average 3.2% measurement error, indicates an overall error of 5.0% in the mean radii for the cubic shaped particles.

Dependence of the mean radius on concentration. In Table II, the emperical formula $R' = 0.17\ (8\ \pi\tau/\rho F^2)^{1/3}$ found by Lang (1962) was

used to calculate the mean droplet radii, R', for the NaCl solutions. the radii R' were used to determine the effects of variation of the surface tension τ and solution density ρ on the mean droplet radius. The calculated droplet radii show a slight decrease with concentration and resulted in a 1% variation in the calculated mean droplet radius $\overline{R'}$ = 1.74 μm ± 0.01μm indicating that changes in the concentration of the NaCl solutions have a negligible effect on the mean radii of the aerosols. In comparison, the mean droplet radius, $\overline{R}$, calculated from the mean radii of the solid aerosols using the expression $R = r\left(1 + \frac{\rho x\ 10^3}{y}\right)^{1/3}$ are

NaCl	1.90 μm ± 0.60 μm (3.4%)
$(NH_4)_2SO_4$	1.87 μm ± 0.05 μm (2.8%)
Both	1.88 μm ± 0.06 μm (3.2%)

The percent variation in the above values is relatively small and it does not appear that the mean radius of the liquid aerosols are effected to any great extent by variations in the solution concentration.

Indirect sizing of the solid aerosols. Since the mean droplet radii of the liquid aerosol do not show a large dependence on the solution concentration, the use of the mean radius $\overline{R}$ = 1.88 μm to calculate an average particle radius

$$r' = 1.88\ \mu m\ \left(1 + \frac{\rho\ x\ 10^3}{y}\right)^{-1/3}$$

from the concetration y and the density ρ (Table II) is

justifiable. Comparison of r' with the mean radius, r, determined from the S.E.M. photographs (Table II) shows that it is possible to indirectly size the solid aerosols with a reasonable degree of accuracy using the above expression and measurements of the mean droplet radius. Further experimental varification of the dependence of the mean particle size, m, on concentration, y, is evident in Fig. 16 where the slope, b, of the best logarithmic fit for the measurements ($\log m = a + b \log (y)$) are 0.335 ± 0.009 for spheres and 0.336 ± 0.007 for cubes. The values are seen to be very nearly equal to the theoretical value of 1/3. The mean droplet radius R = 1.86 μm ± 0.05 μm, calculated from the horizontal intercept of the $(NH_4)_2SO_4$ measurements, is within 1.1% of the mean droplet radius, $\overline{R}$ = 1.88 μm ± 0.06 μm used in the above expression. In the present work, Fig. 16 represents the easiest way to indirectly size the solid aerosols of either salt from the solution concentration. The relationship $r = R(1 + \frac{\rho \times 10^3}{y})^{-1/3}$ (R = 1.88 μm) is more general in nature and may be used to indirectly size aerosols of other materials allowing for greater flexibility in the use of the ultrasonic nebulizer as a source of solid aerosols.

Particle Size Distributions

The non-zero values found for the skewness, γ_1, and excess, γ_2, in Appendix C are an indication that the particle size distributions are non-Gaussian. The use of a Gaussian distribution in the theoretical predictions is justified because the Gaussian is a close approximation to the aerosol distribution over a range of about two standard deviations of particle sizes centered about the mean. It is also apparent

from the close comparison found between the predictions and the measurements for the spherically shaped aerosols that a Gaussian approximation based on the first two moments of the particle size distributions is substantially correct and gives all the salient features of the scattering measurements.

Fractional deviation of the particle distributions. It is possible to make a direct comparison of the aerosol size distributions independent of the mean particle size by combining the first two moments of the distributions to determine the fractional deviation. This is evident in Fig. 16 where the error bars in the mean size are a direct measure of the fractional defiation of the aerosols. It would appear from the consistency in the range of particle sizes indicated by the error bars that the fractional defiation is a constant independent of the mean size and shape of the aerosols. The mean fractional deviation of the aerosols given in Table I are

NaCl	0.284 ± 0.031	(11%)
$(NH_4)_2SO_4$	0.314 ± 0.017	(5%)
Both	0.299 ± 0.029	(10%)

It would appear from the relatively small variations in the mean fractional deviation found for the solid aerosols that the ultrasonic nebulizer produces aerosols with a fairly stable size distribution and as such, is ideally suited for studies of the scattering properties of aerosols.

The fractional deviation for several other natural and artificial aerosols found in the literature are given below:

Vibrating orifice	0.05 to 0.10	(Pinnick, Carrol and Hofmann 1976)
Sinclair-LaMer	0.07 to 0.10	(Kerker 1972)
Ultrasonic nebulizer (1.3MHz)	0.30 ± 0.03	
Venus clouds (theoretical)	0.31	(Hanson and Hovenier 1974)
Silicate particles	0.43	(Holland and Gagne 1970)
Natural NaCl aerosols	0.90	(Frank et al. 1972)

From this comparison, it can be seen that the fractional deviation of the aerosols studied in this work are in the middle of the range of values found for the artificial aerosols and is much smaller than the value found for the naturally occurring NaCl aerosol. The close comparison between the fractional deviation found in this work and the theoretical value found by Hanson and Hovenier (1974) for the Venus clouds is particularly interesting and suggests the possiblity of experimental varification of their results.

By taking into account the skewness, γ_1, and excess, γ_2, of the particle size distribution, it is possible to determine a theoretical expression for the aerosol size distribution that would cover a broader range of particle sizes than a Gaussian distribution. The skewness and excess found for the speherically shaped $(NH_4)_2SO_4$ particles increases with the mean size of the particles and in the case of

the NaCl aerosols shows some additional variation with shape that appears to be an artifact of the measurement process. Further analysis would be necessary if these parameters are to be related to the distribution of the liquid aerosols. The mean values of the skewness and excess in Appendix C are

	γ_1	γ_2
NaCl	0.305 ± 0.286	0.363 ± 0.624
$(NH_4)_2SO_4$	0.953 ± 0.144	1.078 ± 0.577

By using the above values for γ_1 and γ_2 to calculate the parameters $B_1 = \gamma_1^2$ and $B_2 = \gamma_2 + 3$, the Pearson system for frequency curves (Elderton 1917) may be used to predict an analytic form for the particle size distributions by comparing B_1 and B_2 to the range of values found to be within the confines of a basic distribution type. The results for both salts were combined to give $B_1 = 0.522 \pm 0.470$ and $B_2 = 3.73 \pm 0.86$. These values indicate that the most common distribution is a type I (Elderton 1917, p. 53) although the range of parameters also encompasses the type III and type IV distributions. Of the distributions found, the type III is the most physically meaningful and has been commonly used in the literature to describe particle size distributions of other aerosols (Deirmendjian 1964, Hanson and Hovenier 1974). The type III distribution is a gamma distribution of the form $n(x) = k(1 + x/a)^{\gamma a} e^{-\gamma x}$ (Elderton 1917, p. 65), where k is a normalization constant, a is the mode of the distribution and γ the width of the distribution. The main advantage in using the type III distribution for the aerosols is that

it is compatible with other distributions used in the literature and may be used to allow a more direct comparison of the experimental measurements in this work with other studies.

CHAPTER 6

SUGGESTIONS FOR FUTURE WORK

The suggestions for future work presented in this work were chosen because they would expand the capabilites of the experimental system and would be of immediate use in future studies. The suggestions made concern the develope ment of a light scattering standard and modifications of the present experimental system that would improve the accuracy of the total intensity measurements and increase the number of matrix elements directly measured by the polar nephelometer. For suggestions concerning further practical applications of the present experimental apparatus, Hunt (1974) may be referred to.

Light Scattering Standards

The development of a light scattering standard would be of immediate use in the calibration of the present experimental system, and would help expedite comparison of the experimental results obtained from different experimental systems. One possibility for a light scattering standard might consist of an aqueous solution of polysteyrene spheres in a sealed sample cell. The scattering properties of the polysteyrene spheres have been thoroughly studied and are well characterized by the Mie theory for spheres (Hunt 1974; Hunt and Huffman 1973; Kerker 1965, p. 81; Pinnick et al. 1976). The main advantages of such a scattering standard are: It can be prepared with known number density, it would provide a direct and sensitive means for

determining the alignment accuracy of the system for all scattering angles and it would allow the use of the Mie theory prediction in calibration of the experimental apparatus. Further, the optical quality of the scattering standard could be enhanced and carefully controlled by the use of a system similar to those presently employed for the sorting of biological cells (Herzenburg, Sweet and Herzenberg 1976). The main difficulties in making such a scattering standard is in obtaining an inexpensive sample cell of high optical quality, and controlling the quality and stability of the aqueous solution of polystyrene spheres for long periods of time.

Modifications

The two suggested modifications of the experimental equipment are: to add a second photo-multiplier tube at a fixed angle to monitor the total scattered intensity, and to redesign the equipment to allow placement of the modulator head on the scanning arm. By monitoring the total intensity at a fixed angle, it would be possible to actively normalize the total intensity scattering measurements to eliminate variations in the total intensity due to fluctuations in the number of particles in the scattering volume. This would substantially reduce the signal to the noise ratio of the total intensity measurements and allow accurate placement of the scattering measurements on a logarithmic scale. By placing the modulator head on the pickup arm it is theoretically possible to obtain direct measurements of the normalized matrix elements S_{21}/S_{11}, S_{31}/S_{11}, S_{41}/S_{11} and improve the accuracy of the

measurements for the S_{32}/S_{11} and S_{42}/S_{11} matrix elements. One important consequence of placing the modulator head in the pick-up arm is that it opens the possibility of making *in situ* measurements of atmospheric aerosols using the present experimental apparatus.

CHAPTER 7

CONCLUSION

A summary of the major conclusions of this work are as follows.

1. Scattering measurements for nonspherical but rounded particle shapes are closely approximated by the Mie theory for spheres.
2. The cubic particle shapes of the NaCl dominated the back scattering properties of the aerosols resulting in stable scattering features that appeared to be a characteristic of the cubic shape and did not vary with the mean size of the aerosol.
3. Except for a limited region in the forward scattering direction, the theoretical predictions for spheres are a poor approximation to the scattering measurements for the cubic particles.
4. An approximate upper limit for the applicability of the Mie theory to measurements at all scattering angles was found to be $r \leq 0.15$ μm, $x \leq 1.5$ for the NaCl and $r \leq 0.45$ μm, $x < 5$ for the $(NH_4)_2SO_4$ aerosols. Beyond these limits the nonspherical nature of the particles will have some effect on the accuracy of the sizing determined from comparison with the predictions.
5. The S_{12}/S_{11} and S_{34}/S_{11} matrix elements allow the most accurate sizing of nonspherical aerosols. Of the two, the S_{34}/S_{11} measurements are the best suited for sizing purposes because they show less dependence on the nonspherical particle shapes.
6. Aerosols with either round or cubic particle shapes were found to have type II scattering matrices where in the measurements,

obeyed the relationships $S_{ij} = |S_{ji}|$, $i \neq j$ and all measurements in the B and C submatrices were equal to zero.

7. Measurements in the D submatrix were found to be less sensitive to the shape of the aerosols than measurements in the A submatrix.
8. The S_{22}/S_{11} matrix element was found to be ideally suited for determining the relative spherocity of the particles and allowed direct comparison of the aerosols on the basis of particle shape independent of the mean size and distribution of the particles.
9. Comparison of the measurements by Mie coefficient indicated that the effects of a nonspherical particle shape depend on the absolute size of the particle irregularities relative to the wave length of the scattered light and increase with Mie coefficient.
10. The technique of drying nebulized aerosols to produce solid particles has proven to be ideally suited to the study of nonspherical aerosols, and may be used to produce aerosols with accurately predicted mean radius and distribution independent of the shape of the aerosol particles for a wide variety of materials.

APPENDIX A

INSTRUMENT CONFIGURATION FOR GENERAL SCATTERING MATRIX

(Used with permission of A. J. Hunt; from A. J. Hunt, Ph.D. Dissertation, University of Arizona, 1974)

LP (α), Linear Polarizer at angle α: (λ/4)(α), Quarter wave plate with the fast axis at angle α.

Element measured	Element obtained simultaneously	Modulator angle	Final filter	Data frequency	Calibration	Quantity measured
s_{11}	-	0°, 45°	none	dc	set to zero at reference angle	s_{11} (SUM)'
s_{12}	s_{14}	45°	none	2ω	LP(0°)	$\frac{s_{12}}{s_{11}}$ (POL)
s_{13}	$-s_{14}$	0°	none	2ω	LP(45°)	s_{13}/s_{11}
s_{14}	s_{12}	45°	none	ω	(λ/4)(0°)+LP(45°)	s_{14}/s_{11}
s_{21}	-	0°, 45°	LP(0°)	dc	same as s_{11}	$s_{11} + s_{21}$
s_{22}	-	45°	LP(0°)	2ω	set to 1.0	$\sigma = \frac{s_{12}+s_{22}}{s_{11}+s_{21}}$
s_{23}	$s_{24} + s_{14}$	0°	LP(0°)	2ω	-	$\frac{s_{23}+s_{13}}{s_{11}+s_{21}}$
s_{24}	$s_{13} + s_{23}$	0°, 45°	LP(0°)	ω	(λ/4)(45°)	$\frac{s_{24}+s_{14}}{s_{11}+s_{21}}$
s_{31}	-	0°, 45°	LP(45°)	dc	same as s_{11}	$s_{11}+s_{31}$
s_{32}	$s_{34} + s_{14}$	45°	LP(45°)	2ω	-	$\frac{s_{32}+s_{12}}{s_{11}+s_{31}}$

Element measured	Element obtained simultaneously	Modulator angle	Final filter	Data frequency	Calibration	Quantity measured
s_{33}	$s_{34} + s_{14}$	0°	LP(45°)	2ω	set to 1.0	$\frac{s_{33}+s_{13}}{s_{11}+s_{31}}$
s_{34}	$s_{13} + s_{33}$	0°, 45°	LP(45°)	ω	(λ/4)(0°)	$\frac{s_{34}+s_{14}}{s_{11}+s_{31}}$
s_{41}	-	0°, 45°	(λ/4)(0°)+LP(45°)	dc	same as s_{11}	$s_{11}+s_{41}$
s_{42}	$s_{14} + s_{44}$	45°	(λ/4)(0°)+LP(45°)	2ω	(λ/4)(45°)	$\frac{s_{42}+s_{12}}{s_{11}+s_{41}}$
s_{43}	$s_{14} + s_{44}$	0°	(λ/4)(0°)+LP(45°)	2ω	(λ/4)(90°)	$\frac{s_{43}+s_{13}}{s_{11}+s_{41}}$
s_{44}	-	0°	(λ/4)(0°)+LP(45°)	ω	set to 1.0	$\frac{s_{44}+s_{14}}{s_{11}+s_{41}}$

APPENDIX B

LIGHT SCATTERING MEASUREMENTS FOR AEROSOL PARTICLES OF NaCl AND $(NH_4)_2SO_4$

Definition of Symbols in Appendix B

Vertical Axis; top to bottom

Matrix Element	Prediction as Plotted	Description
S_{33}/S_{11}		Amount of 45^{o} polarized scattered light with S_{33}/S_{11} = +1 (-1) at θ = 0^{o} (180^{o})
S_{12}/S_{11}		Amount of linearly polarized light with S_{12}/S_{11} = +1 (-1) for 90^{o} (0^{o}) polarized light.
$S_{11} \equiv \log(S_{11}/S_{10})$		Logarithm of total intensity normalized to total intensity at θ = 10^{o} with 1 decade = 1 integer division.
S_{34}/S_{11}		Amount of circularly polarized scattered light $S_{34}/S_{11} \equiv 0$ at θ = 0^{o}

Note the experimental measurements (solid line) for the above matrix elements are traced over the computer plots for direct comparison.

Horizontal Axis; left to right

Symbol	Description
THETA	Scattering angle 0 to 180^{o}
RO	Mean radius
C	Standard deviation
DEL	Step size between successive radii used in calculation
WL	Wavelength of scattered light
N	Real index of refraction particles
K	Imaginary index of refraction

All these values are in Angstroms.

For convenience, the Mie coefficient, $x = \frac{RO}{2\pi WL}$, for the computer prediction is given along with the sample and concentration in the figure heading at the bottom of the page.

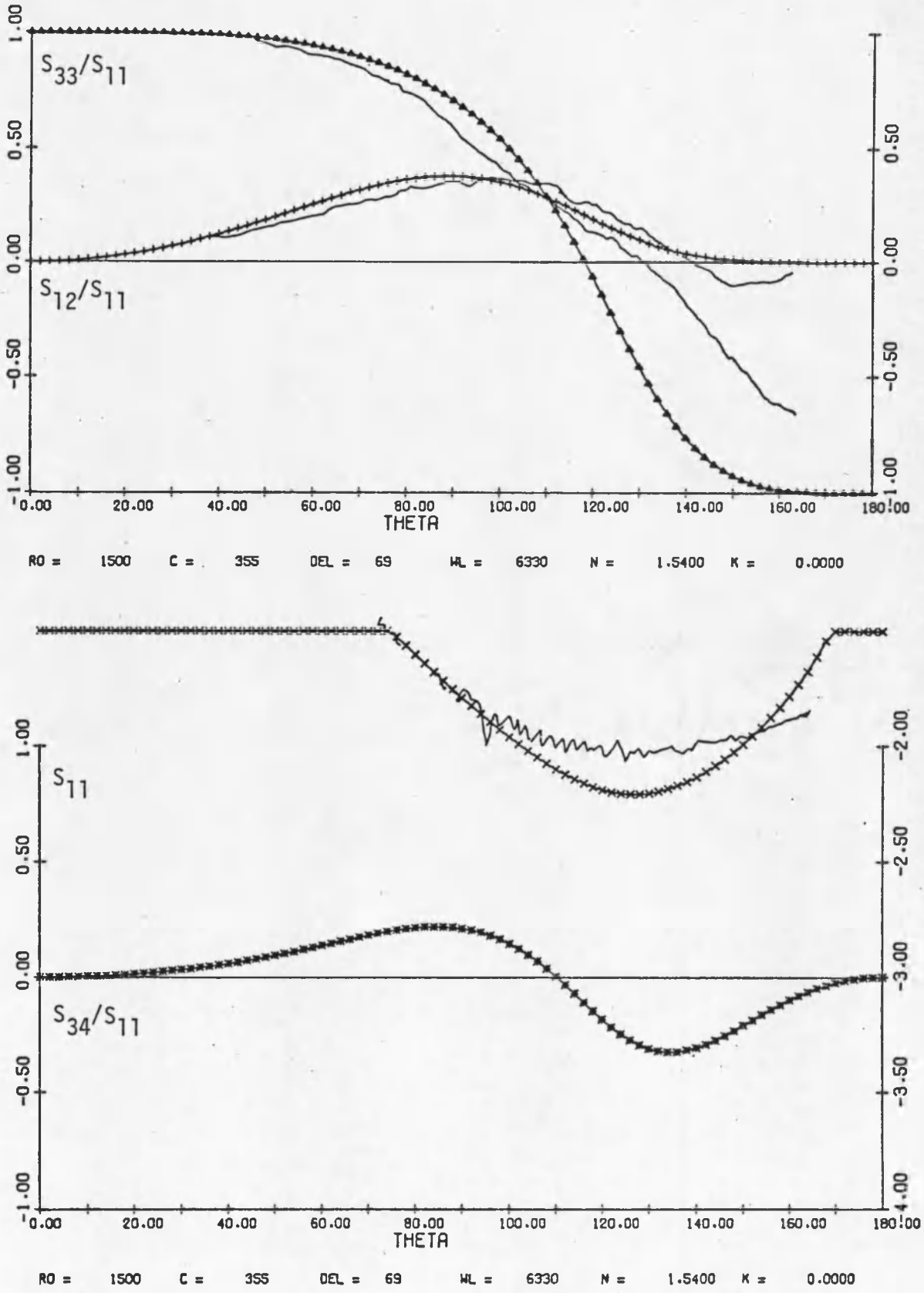

Fig. B1. Scattering Measurements NaCl 1.25 gm/l a. x = 1.5

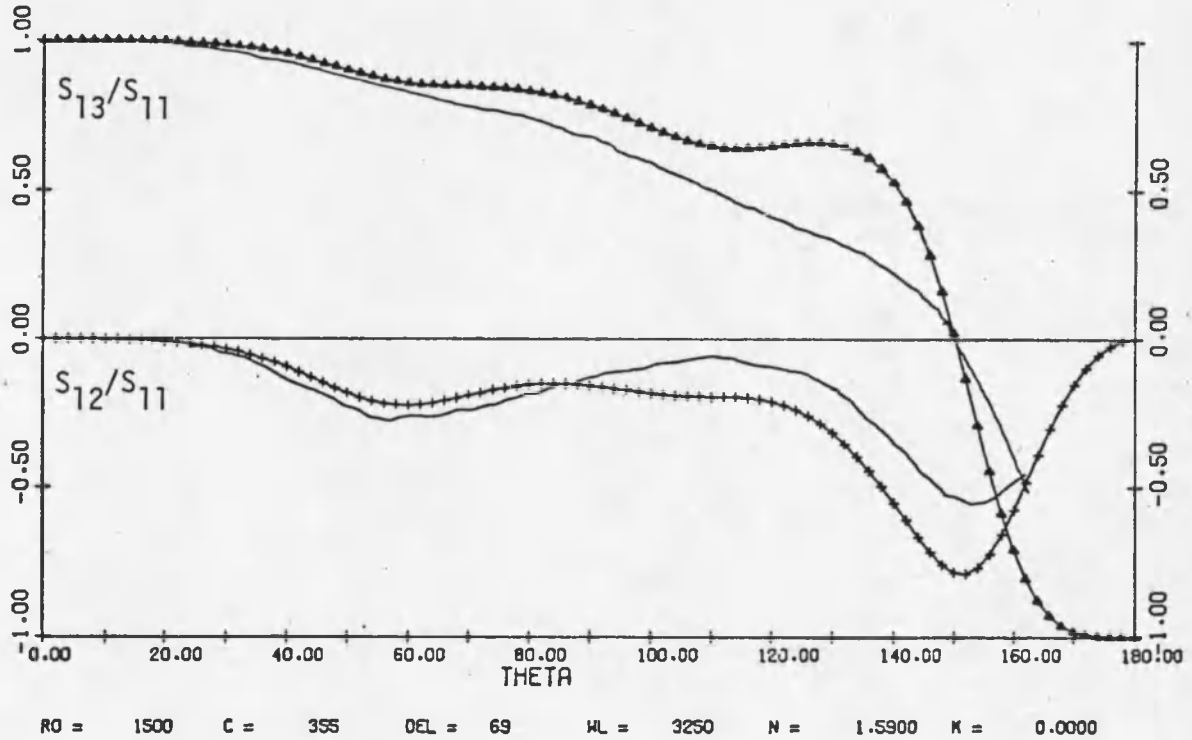

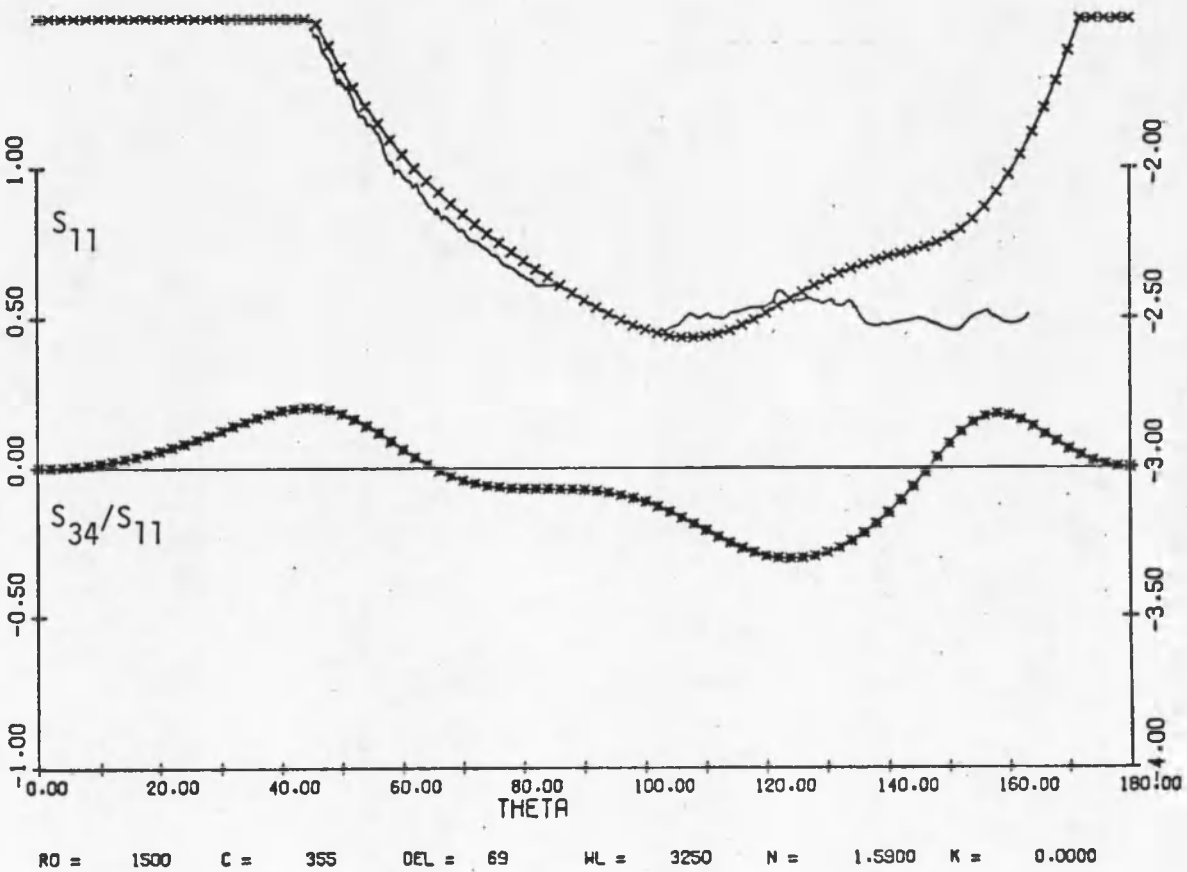

Fig. B1. continued. b. x= 2.9

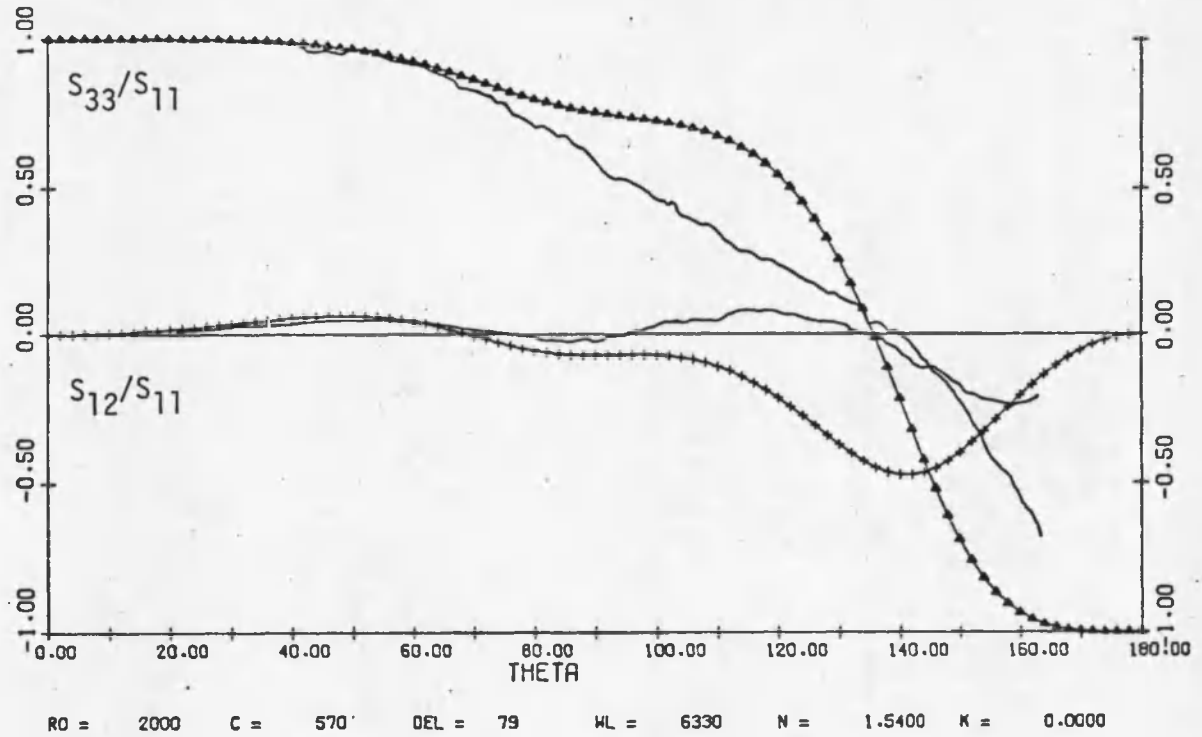

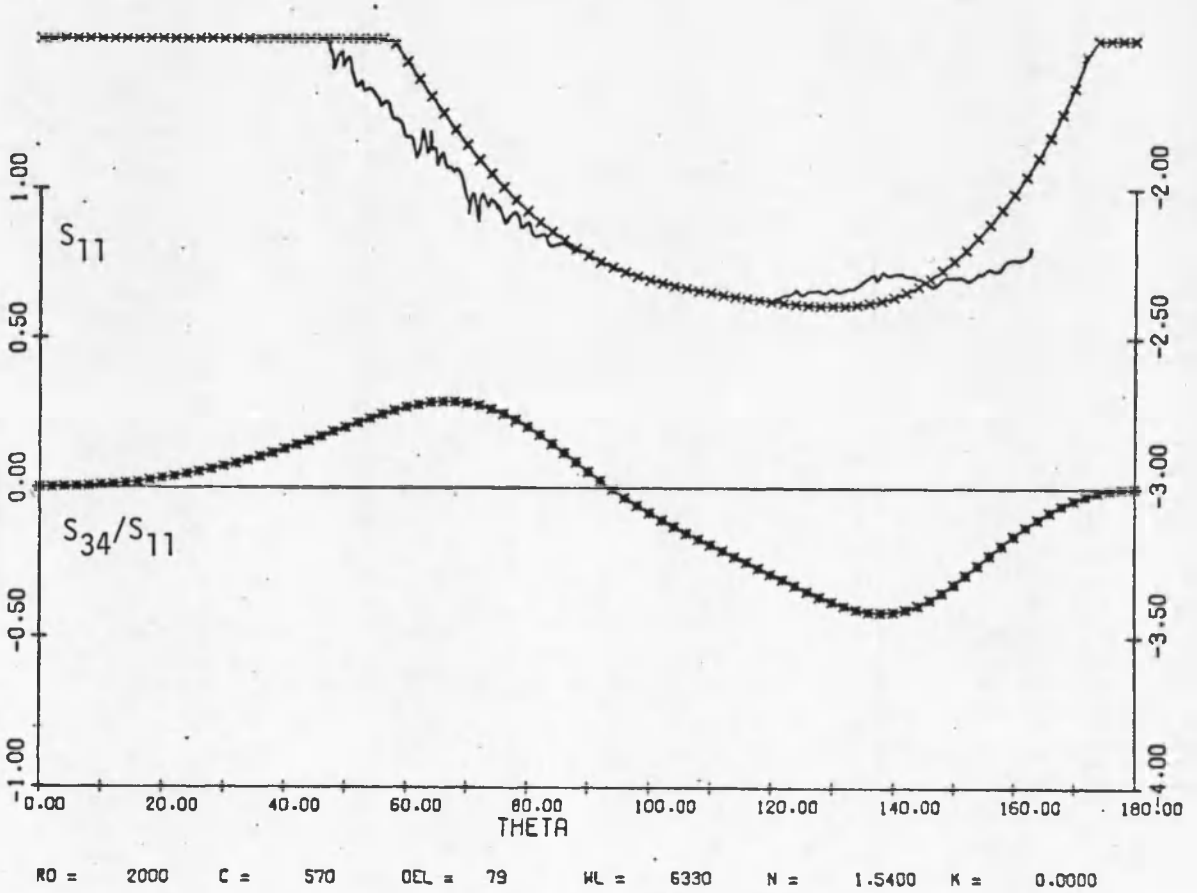

Fig. B2. Scattering Measurements NaCl 4.22 gm/l a. x = 2.0

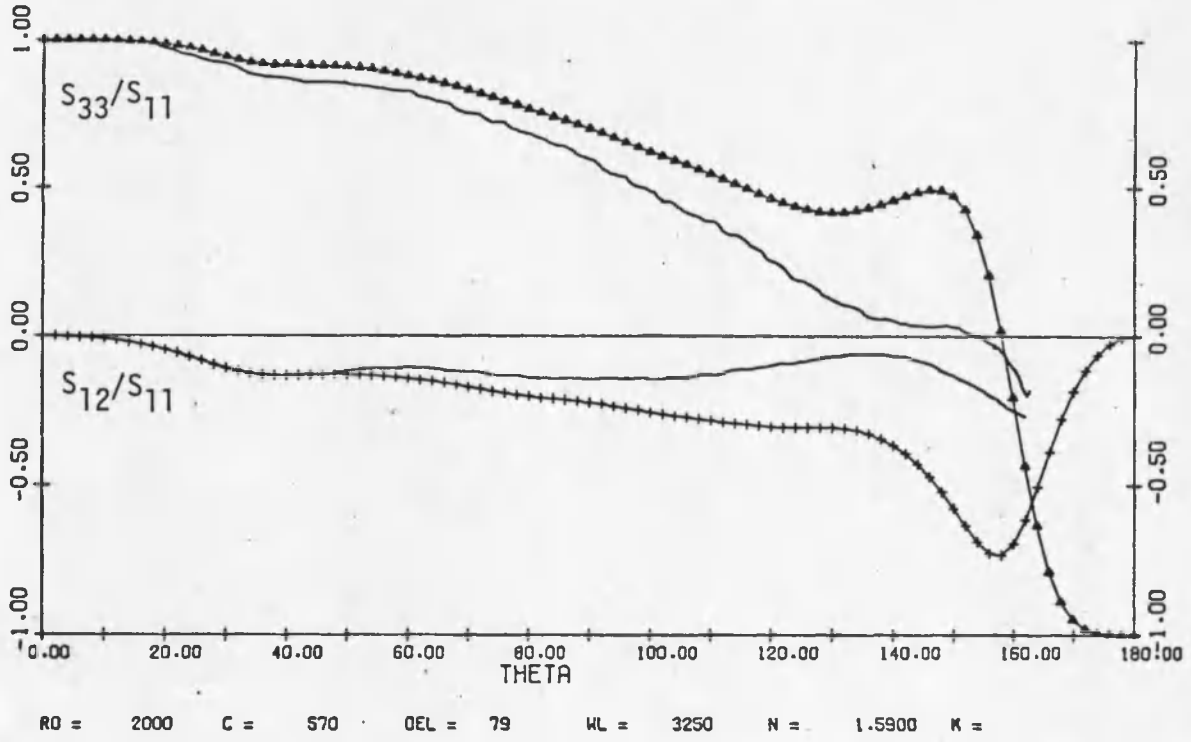

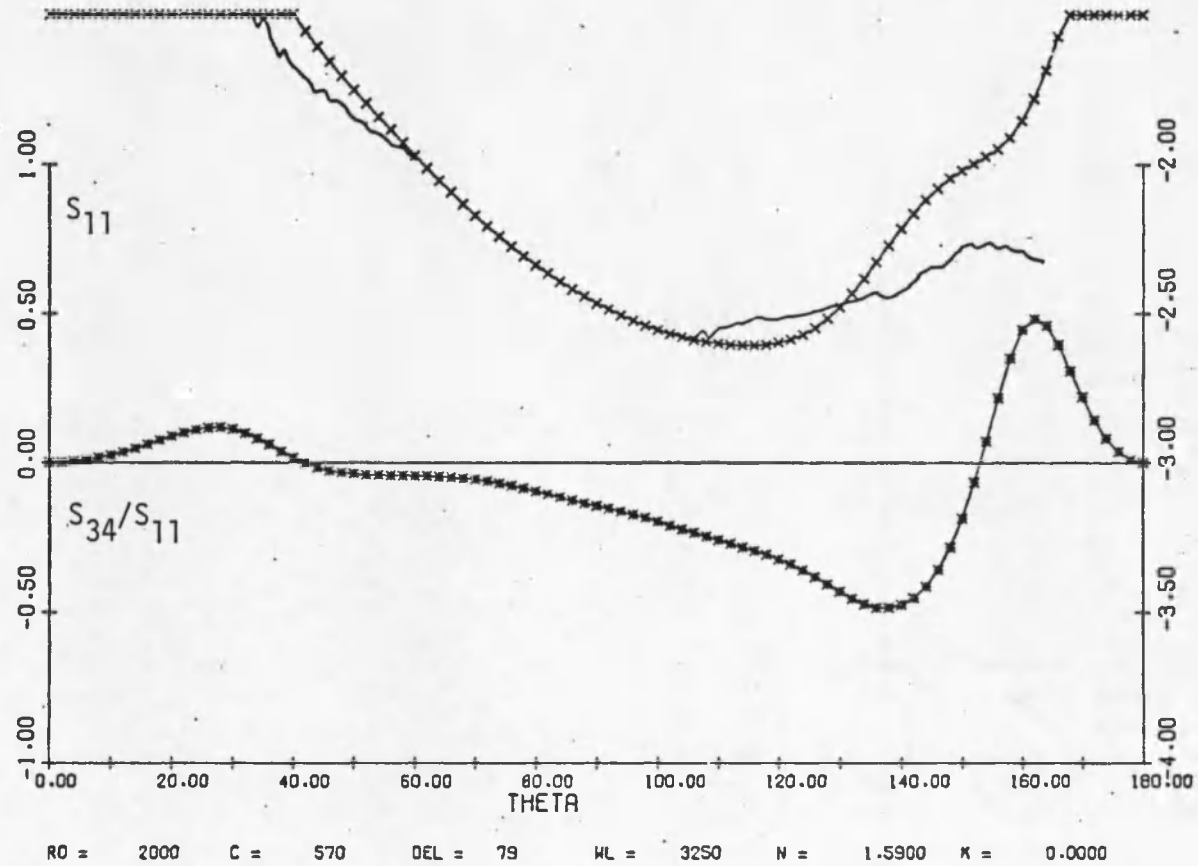

Fig. B2. continued. b. X= 3.9

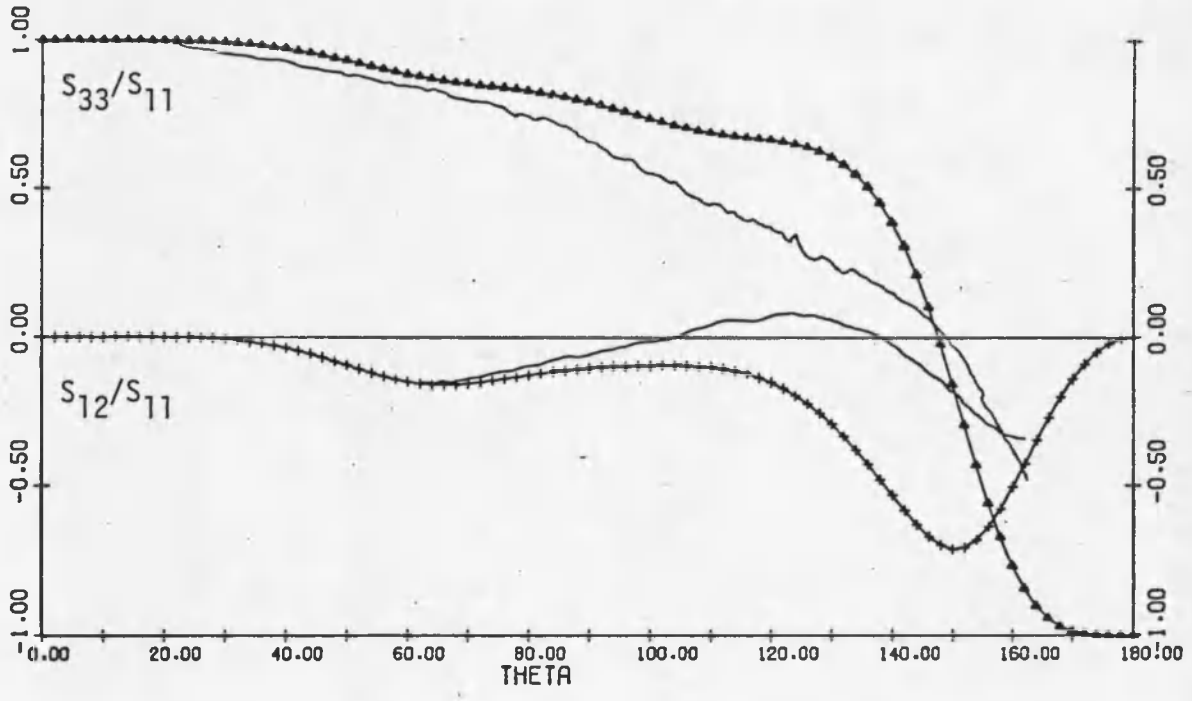

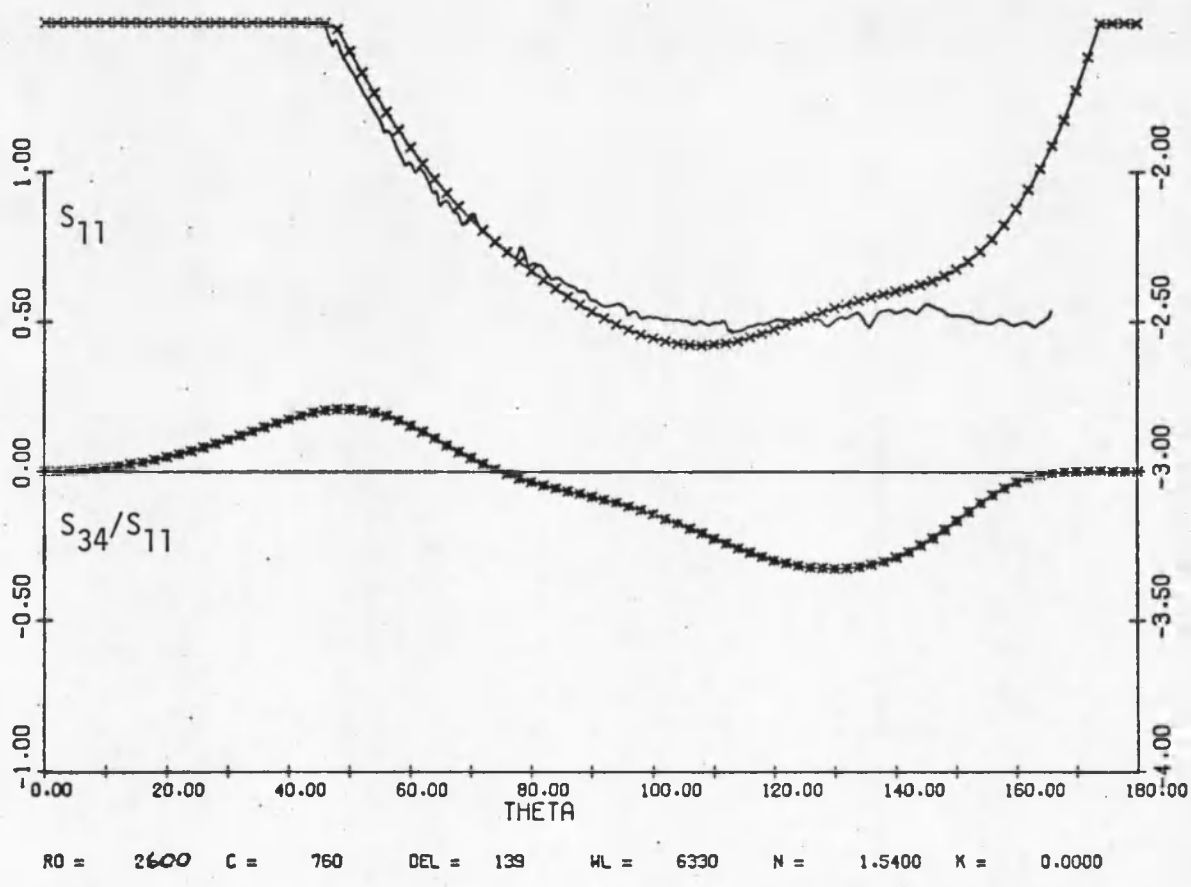

Fig. B3. Scattering Measurements NaCl 10.0 gm/l a. x = 2.6

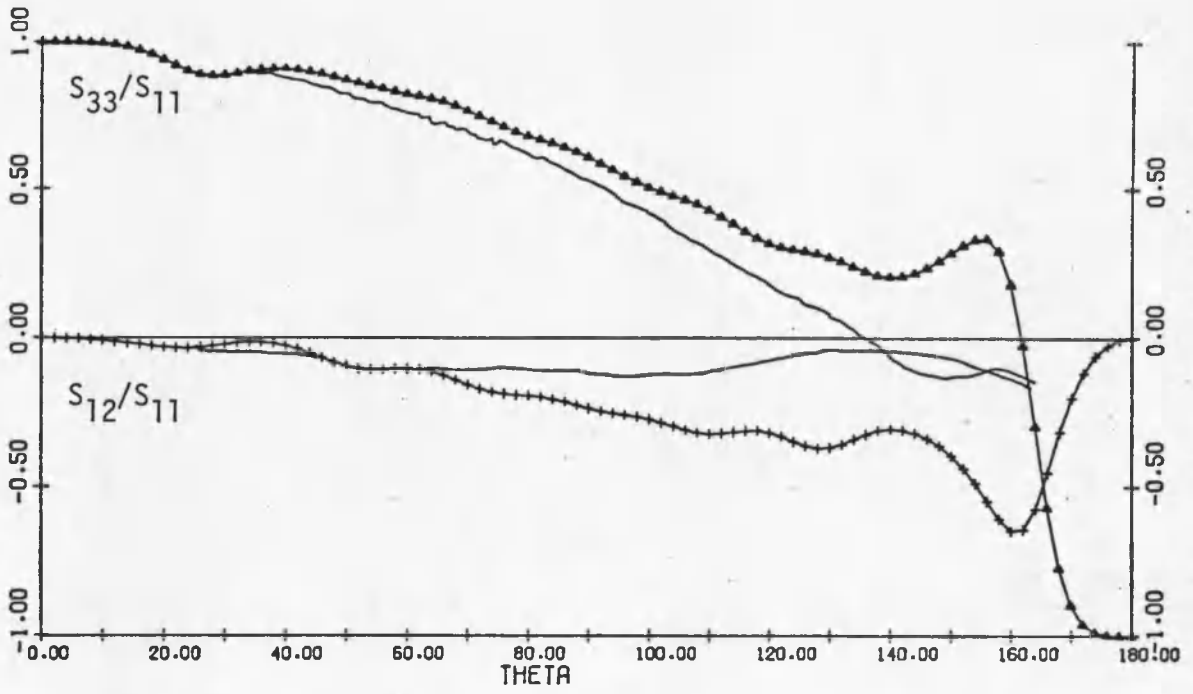

RO = 2600 C = 760 DEL = 139 WL = 3250 N = 1.5900 K = 0.0000

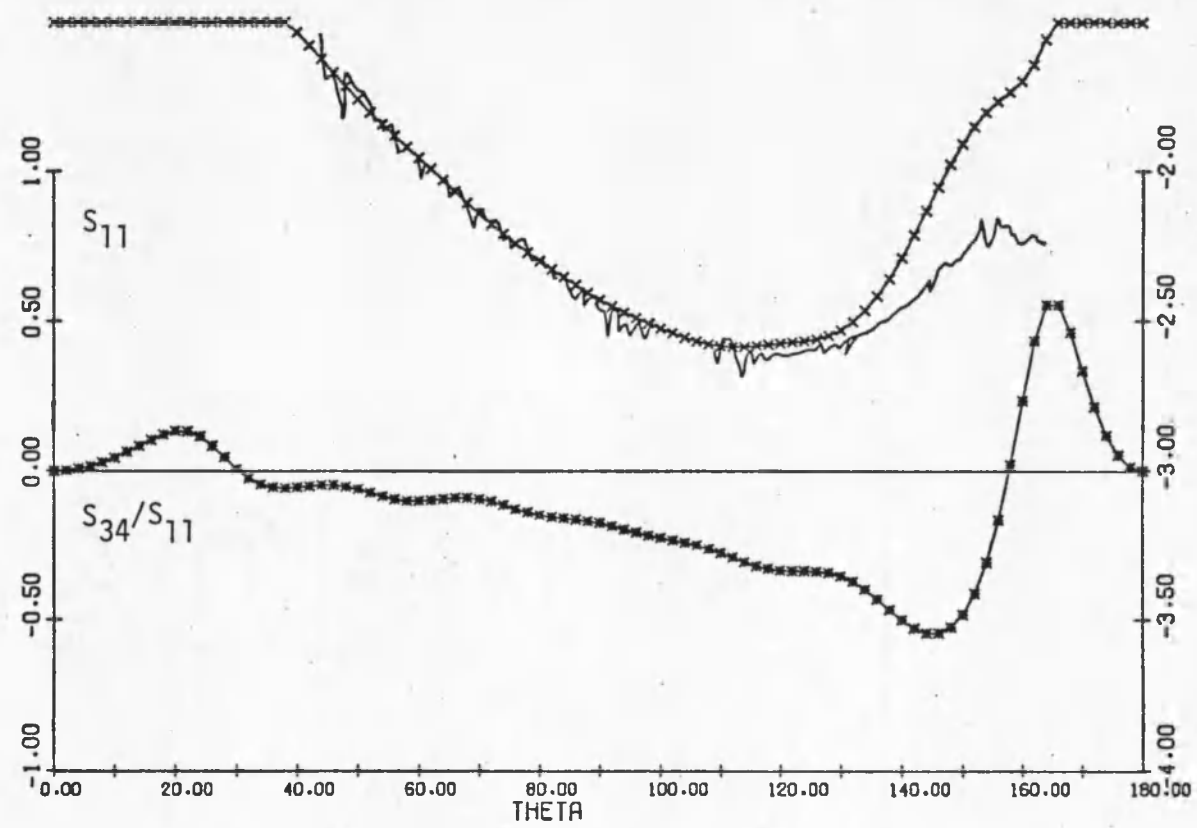

RO = 2600 C = 760 DEL = 139 WL = 3250 N = 1.5900 K = 0.0000

Fig. B3. continued. b. x= 5.0

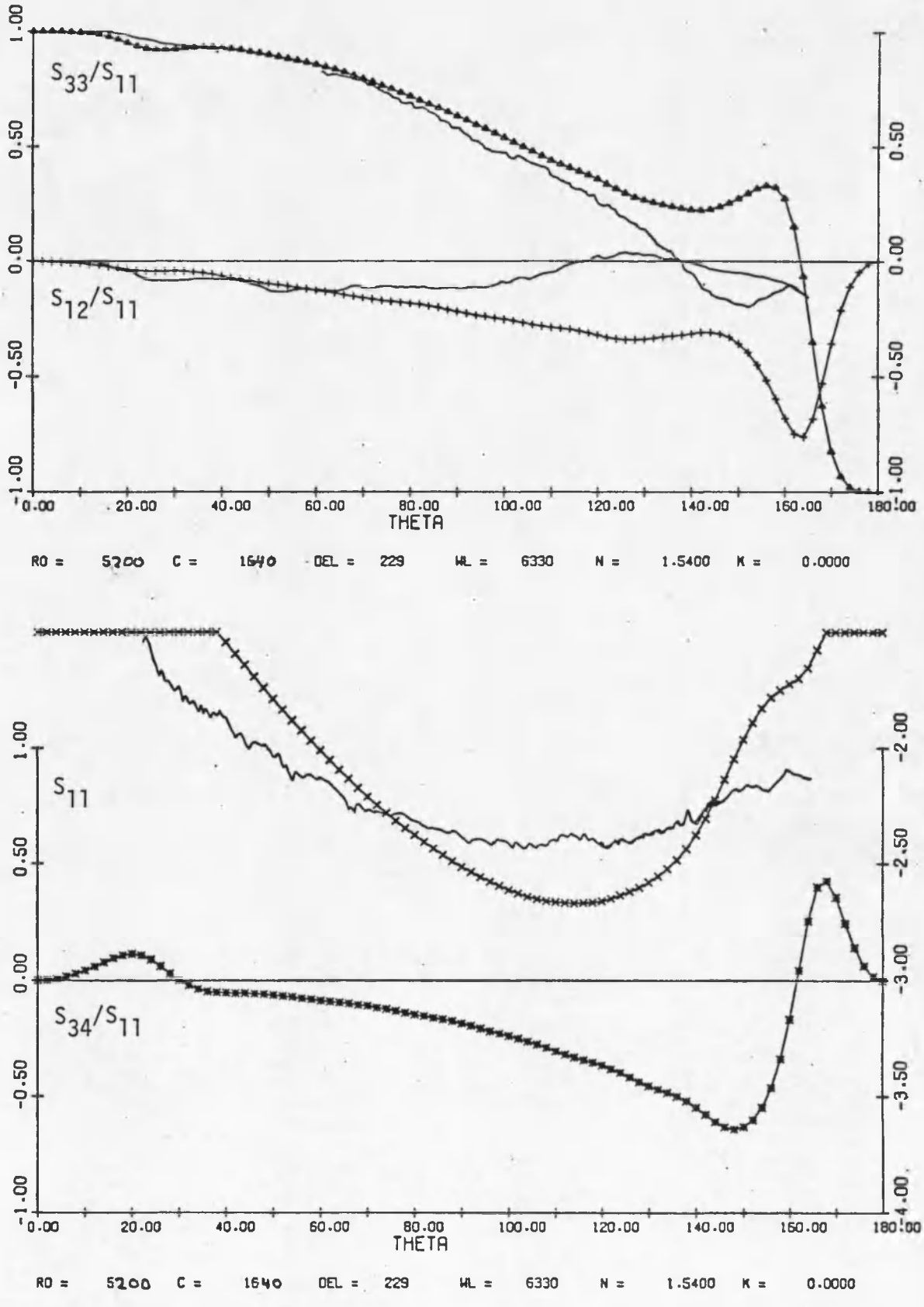

Fig. B4. Scattering Measurements NaCl 80.2 gm/l a. x = 5.2

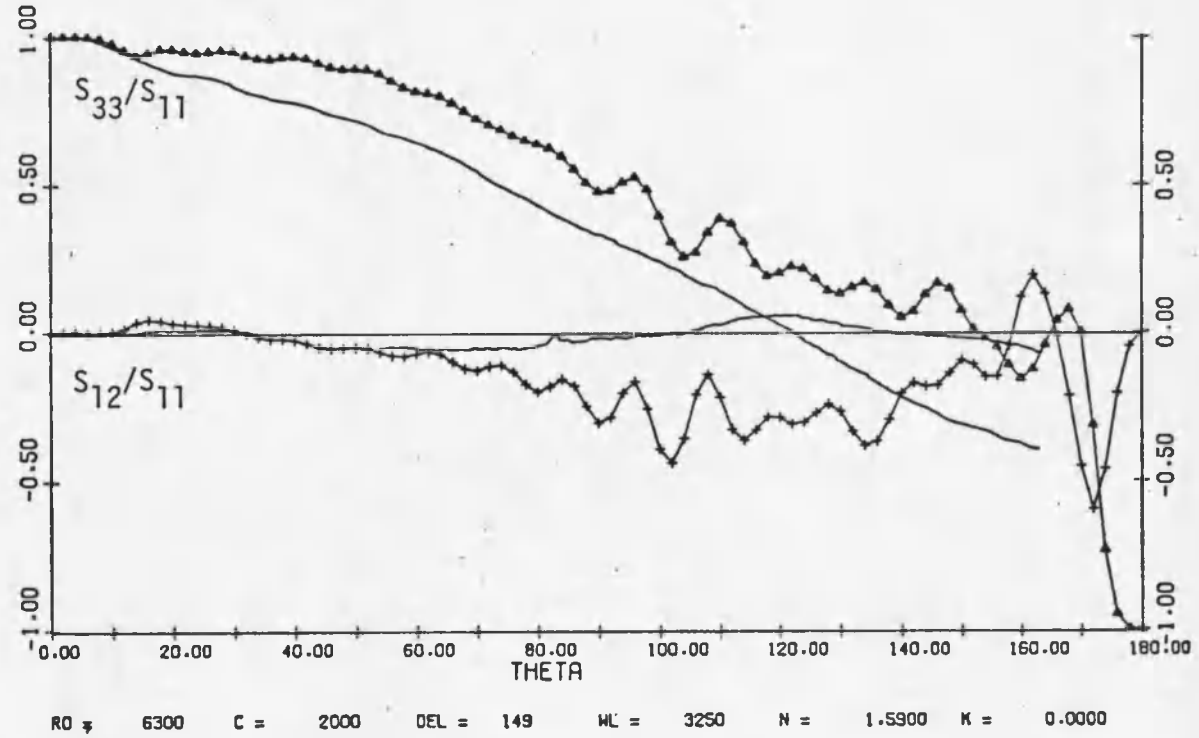

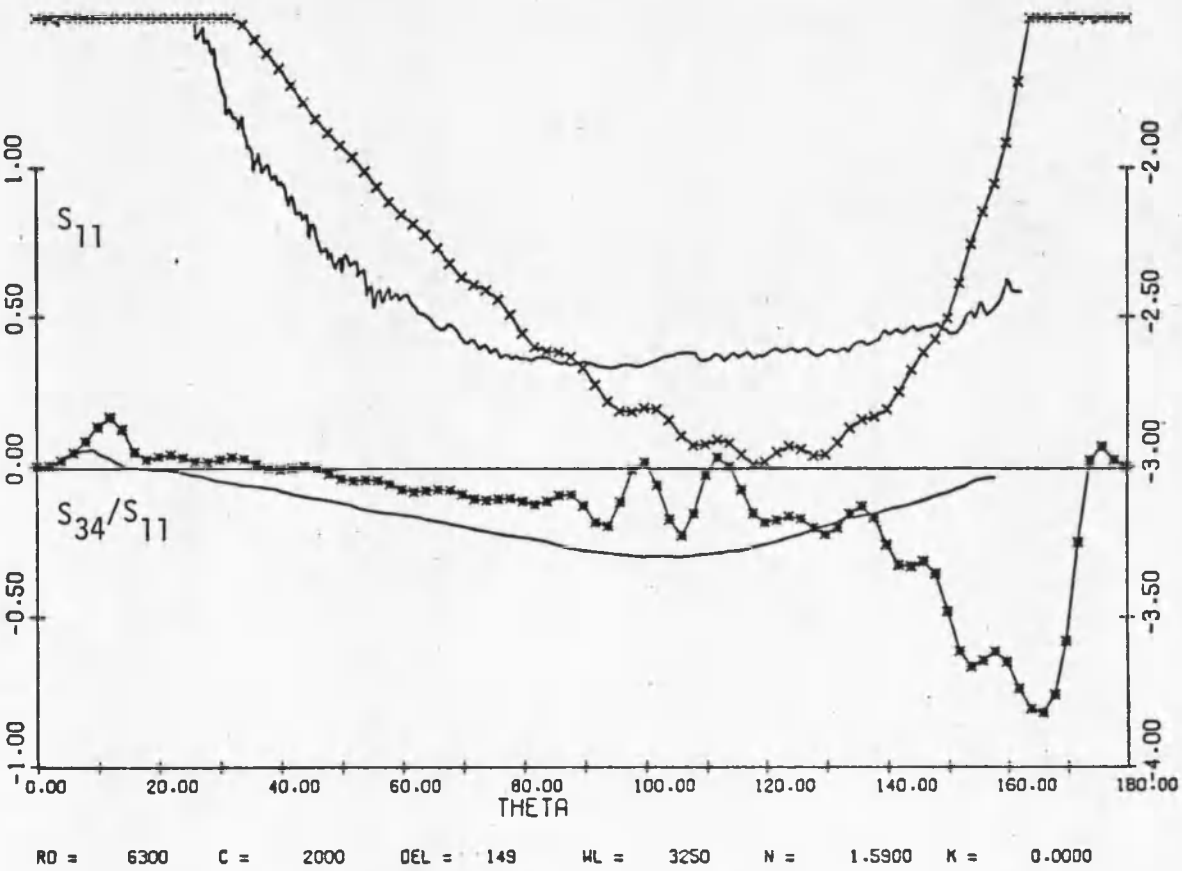

Fig. B4. continued. b. x = 12.2

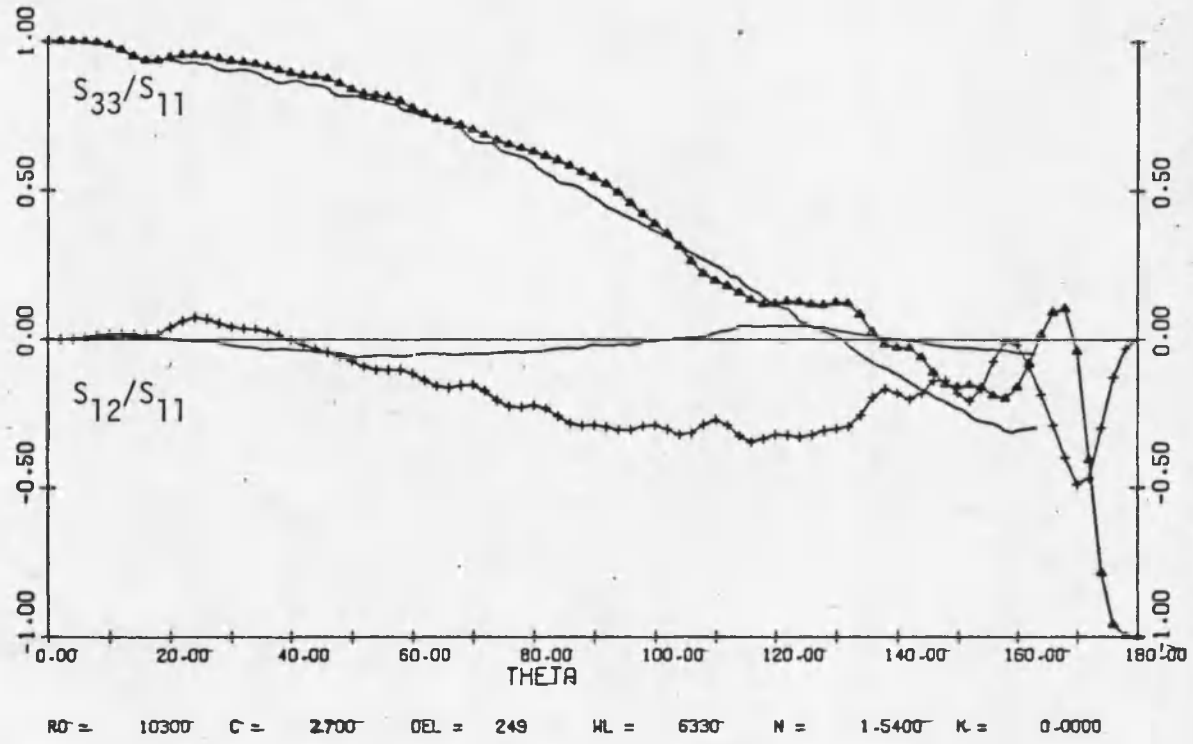

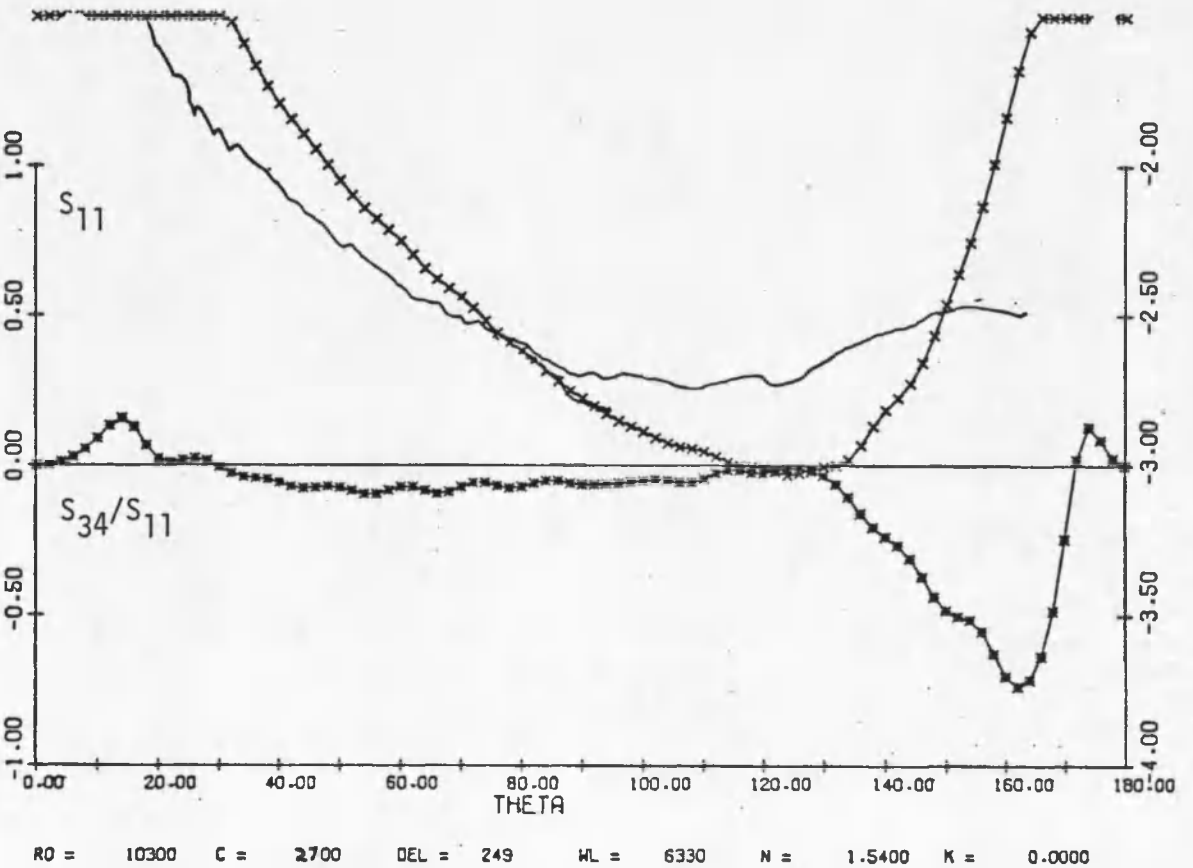

Fig. B5. Scattering Measurements NaCl 320 gm/l a. x = 10.2

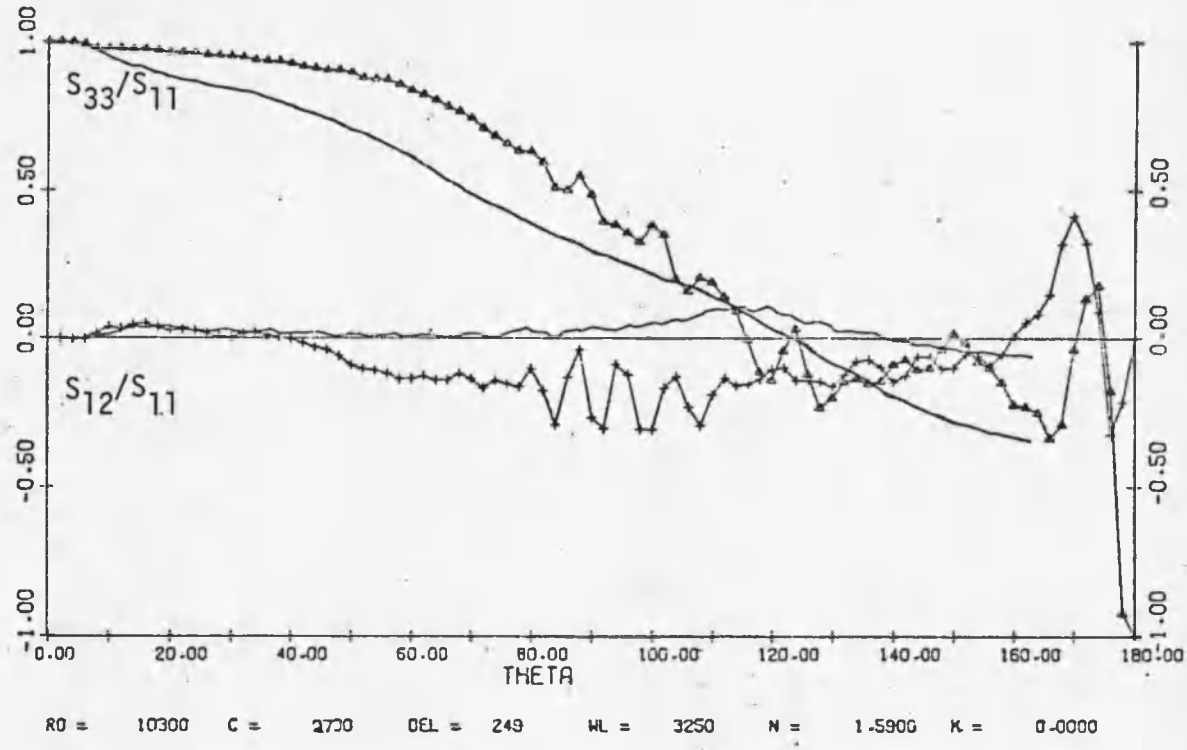

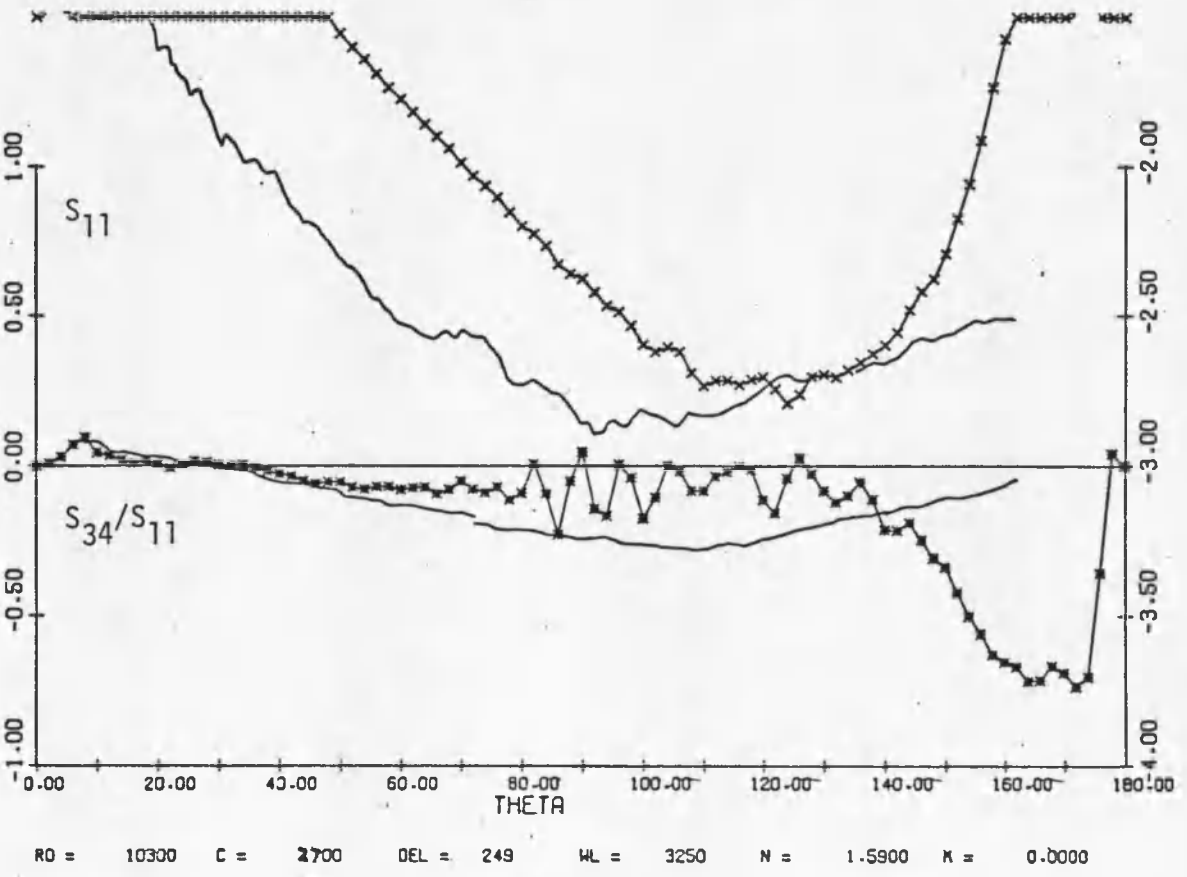

Fig. B5. continued. b. x = 19.9

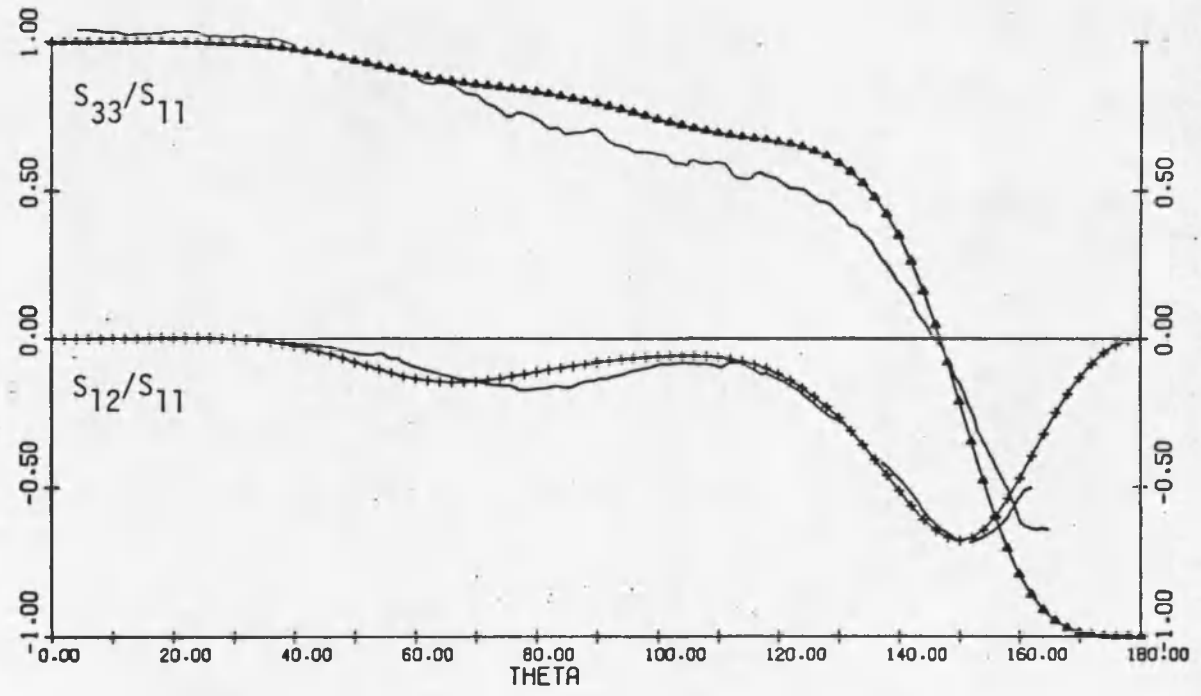

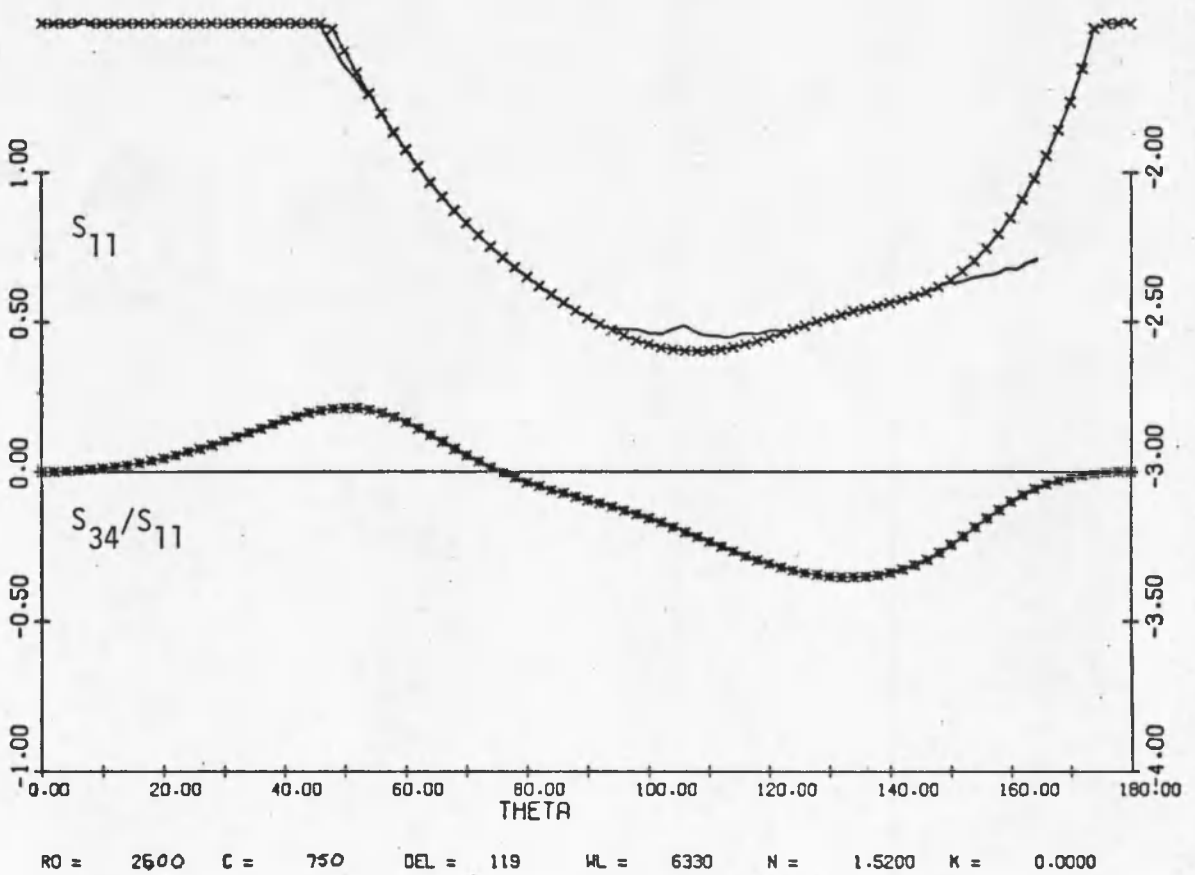

Fig. B6. Scattering Measurements $(NH_4)_2SO_4$ 5.00 gm/l a. x = 2.6

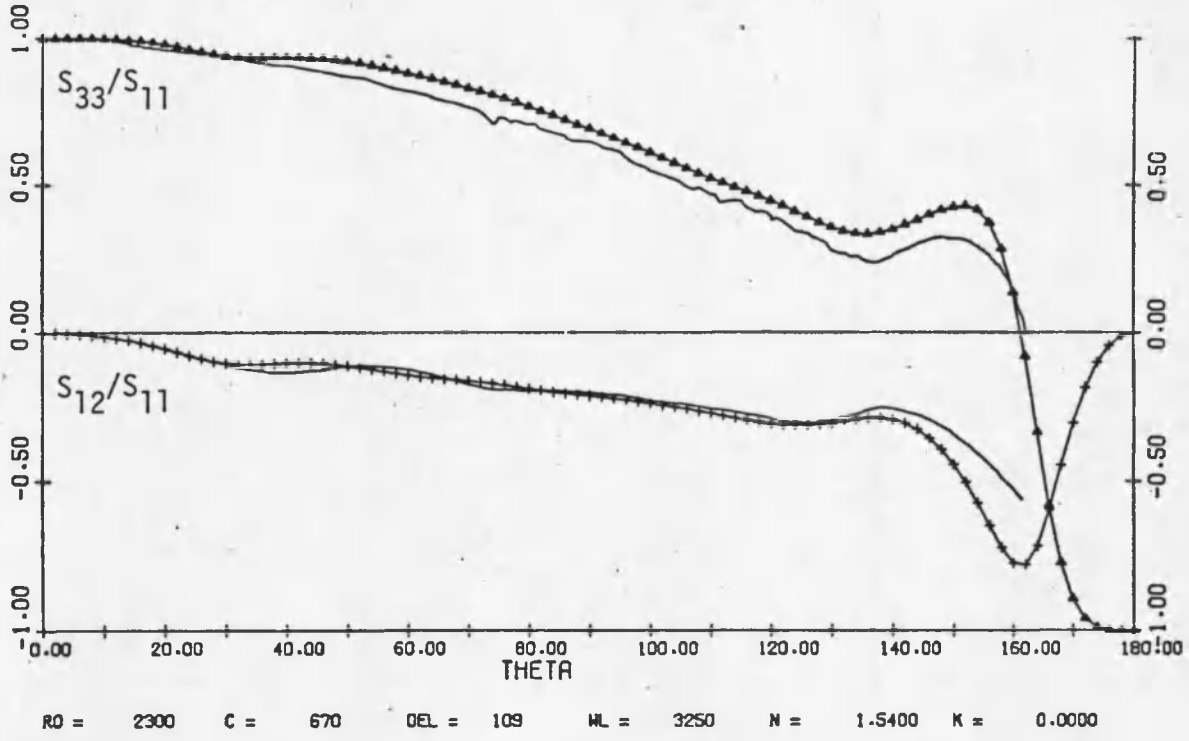

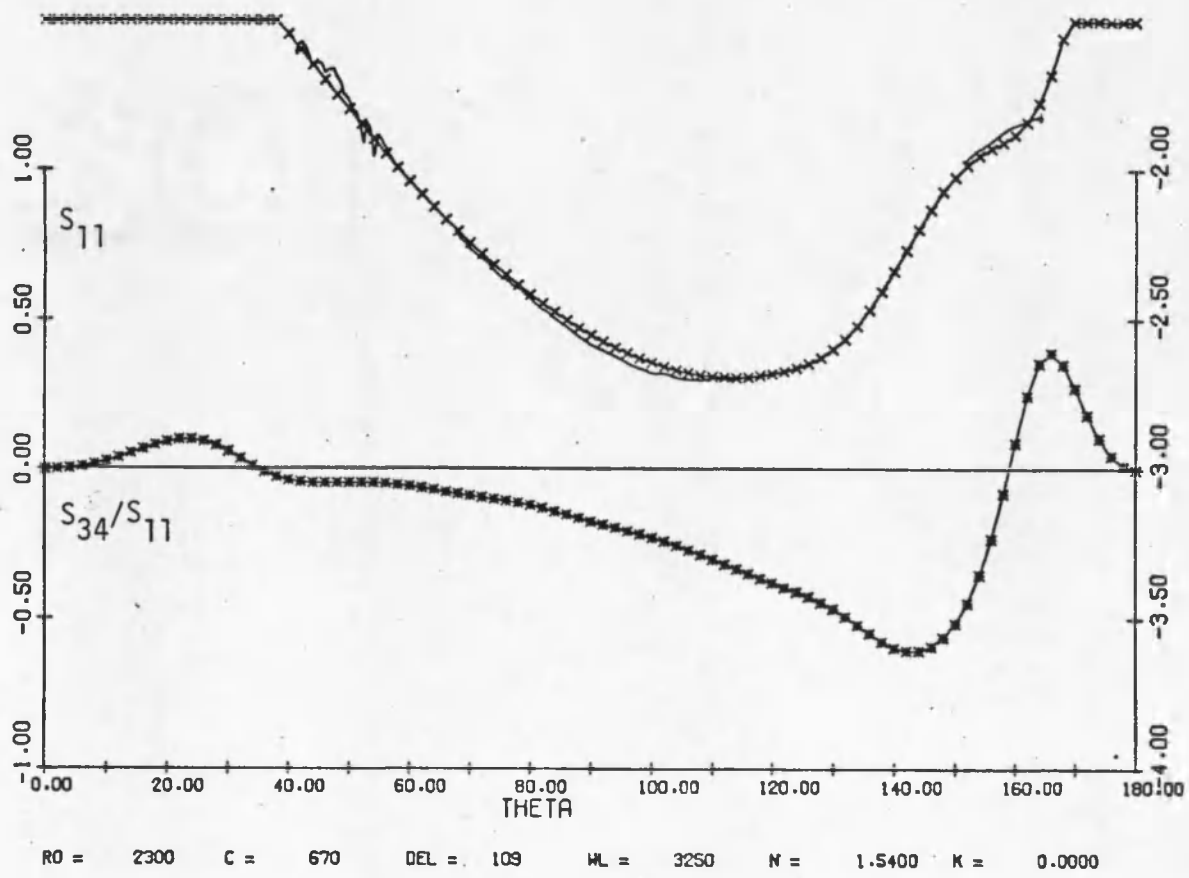

Fig. B6. continued. b. x = 4.4

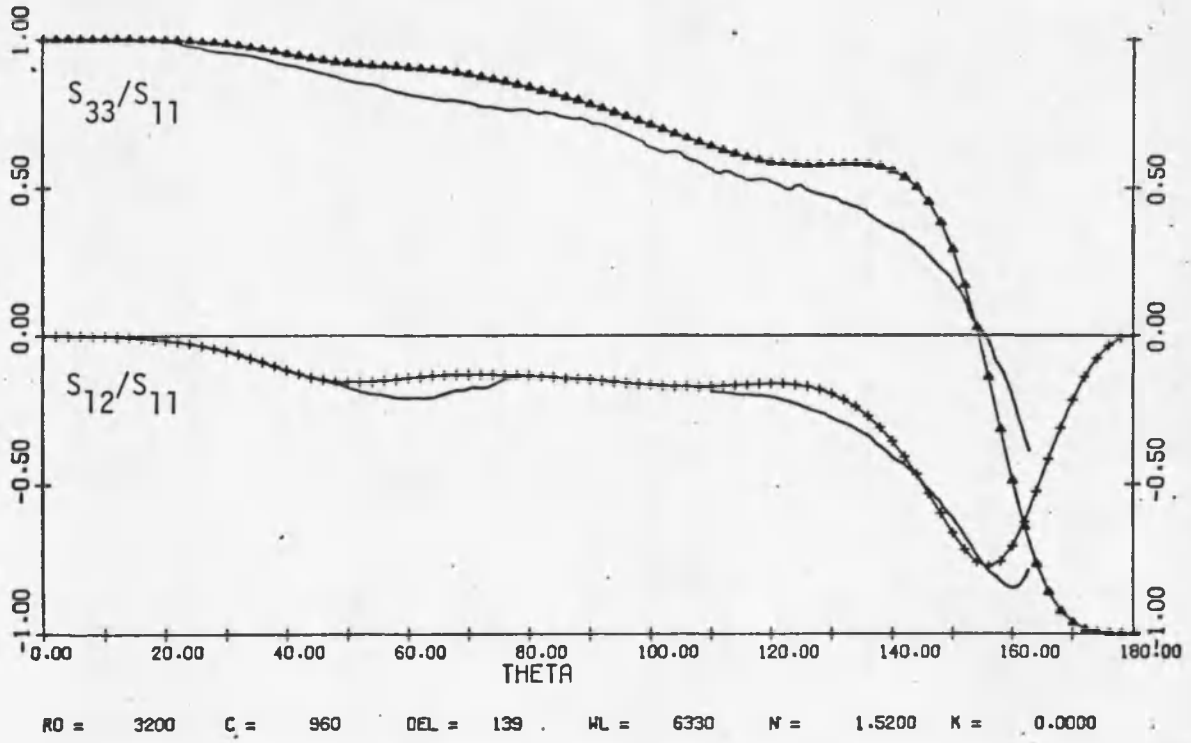

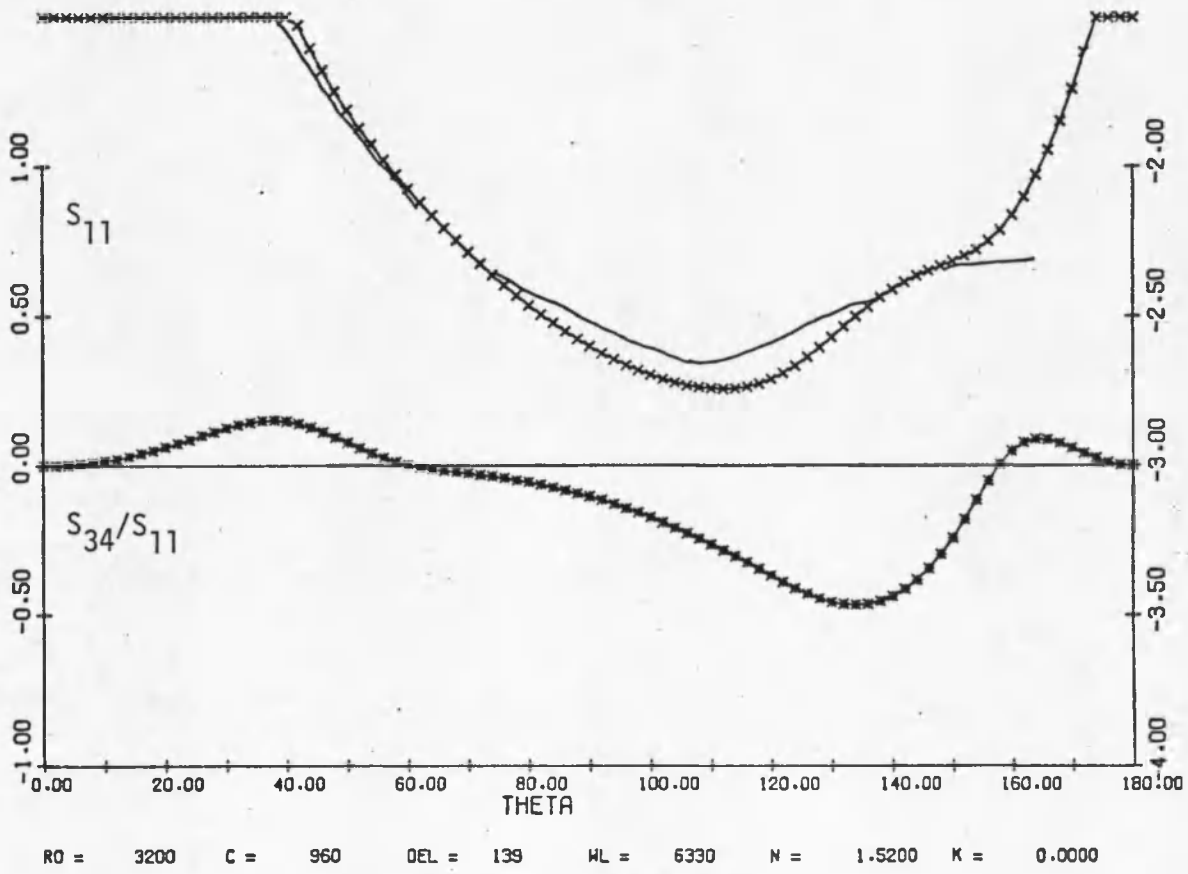

Fig. B7. Scattering Measurements $(NH_4)_2SO_4$ 10.0 gm/l a. x = 3.2

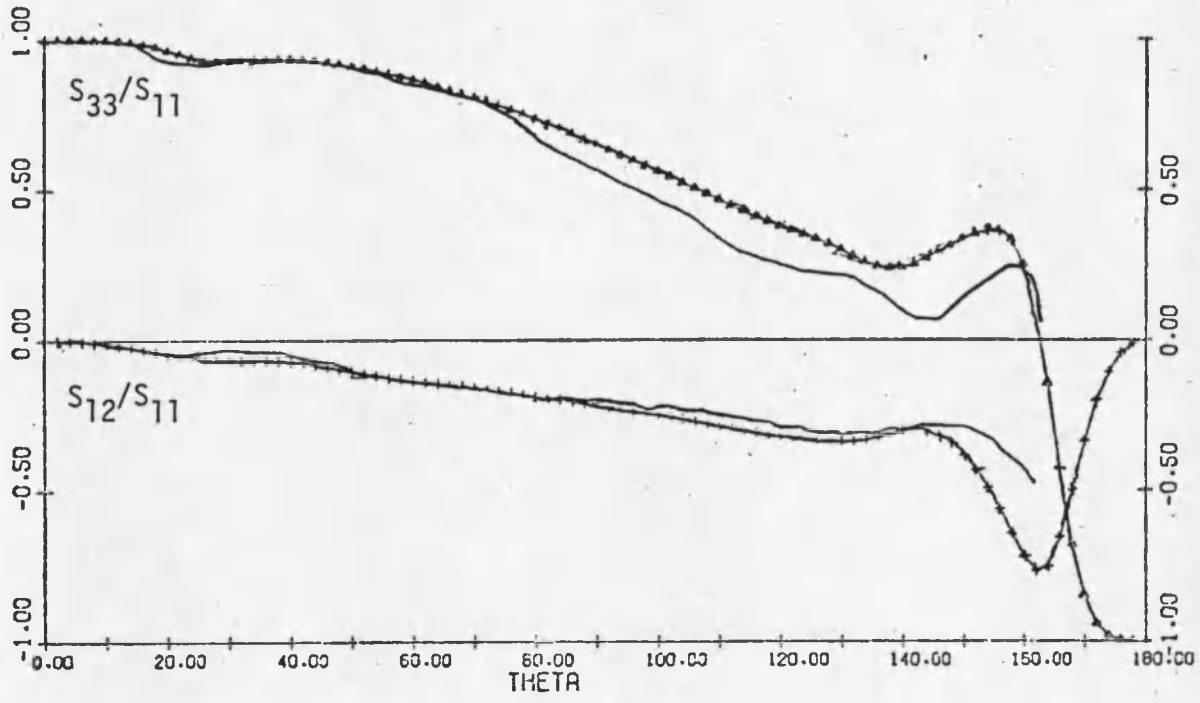

RO = 2600 C = 750 DEL = 119 WL = 3250 N = 1.5400 K = 0.0000

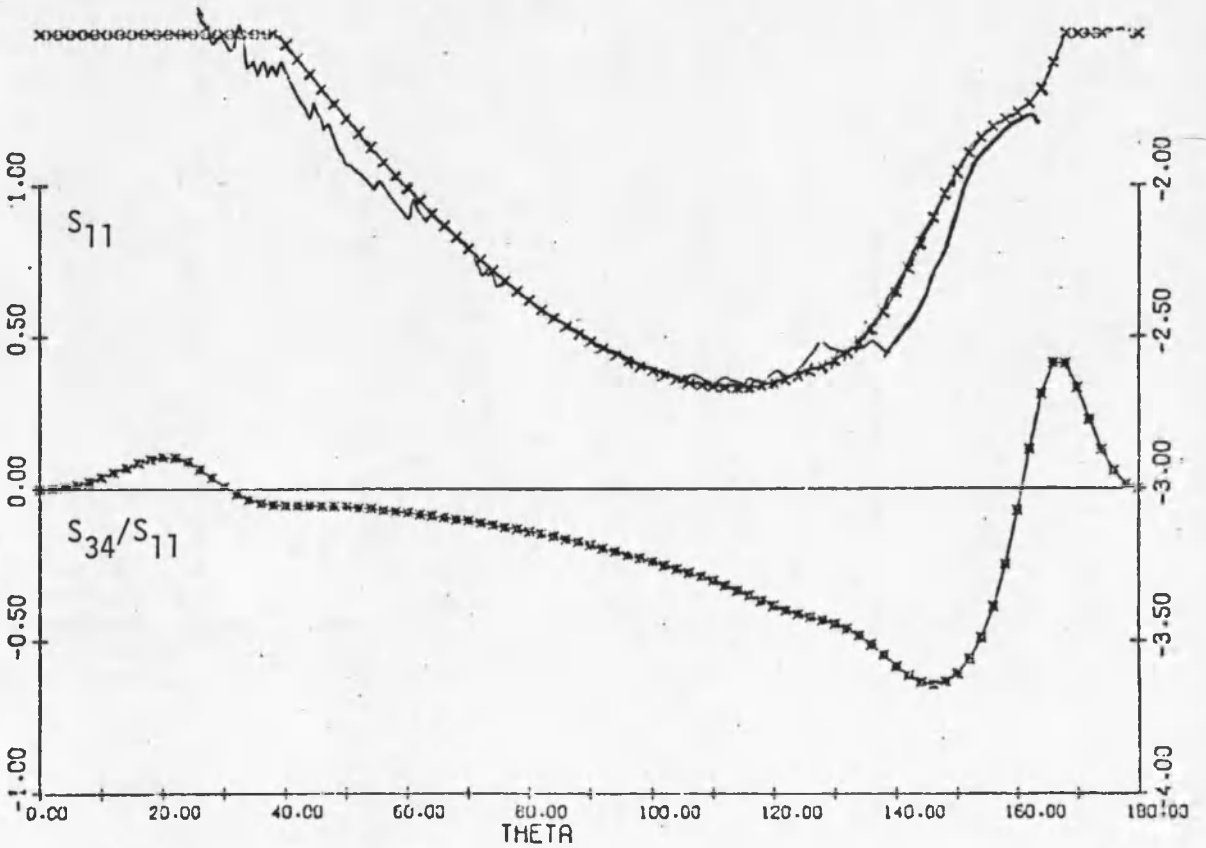

RO = 2600 C = 750 DEL = 119 WL = 3250 N = 1.5400 K = 0.0000

Fig. B7. continued. b. x = 5.0

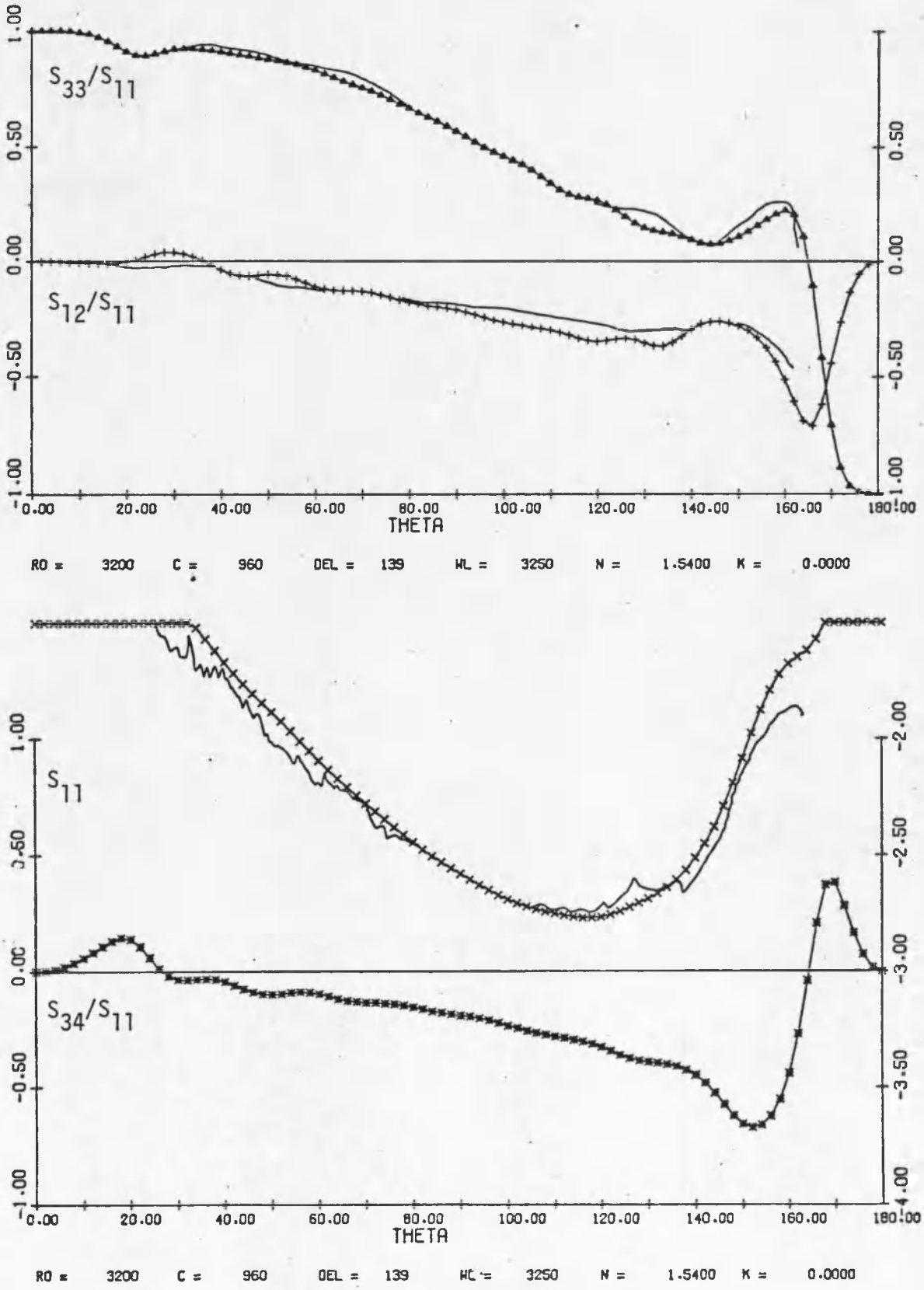

Fig. B7. continued. c. x = 6.2

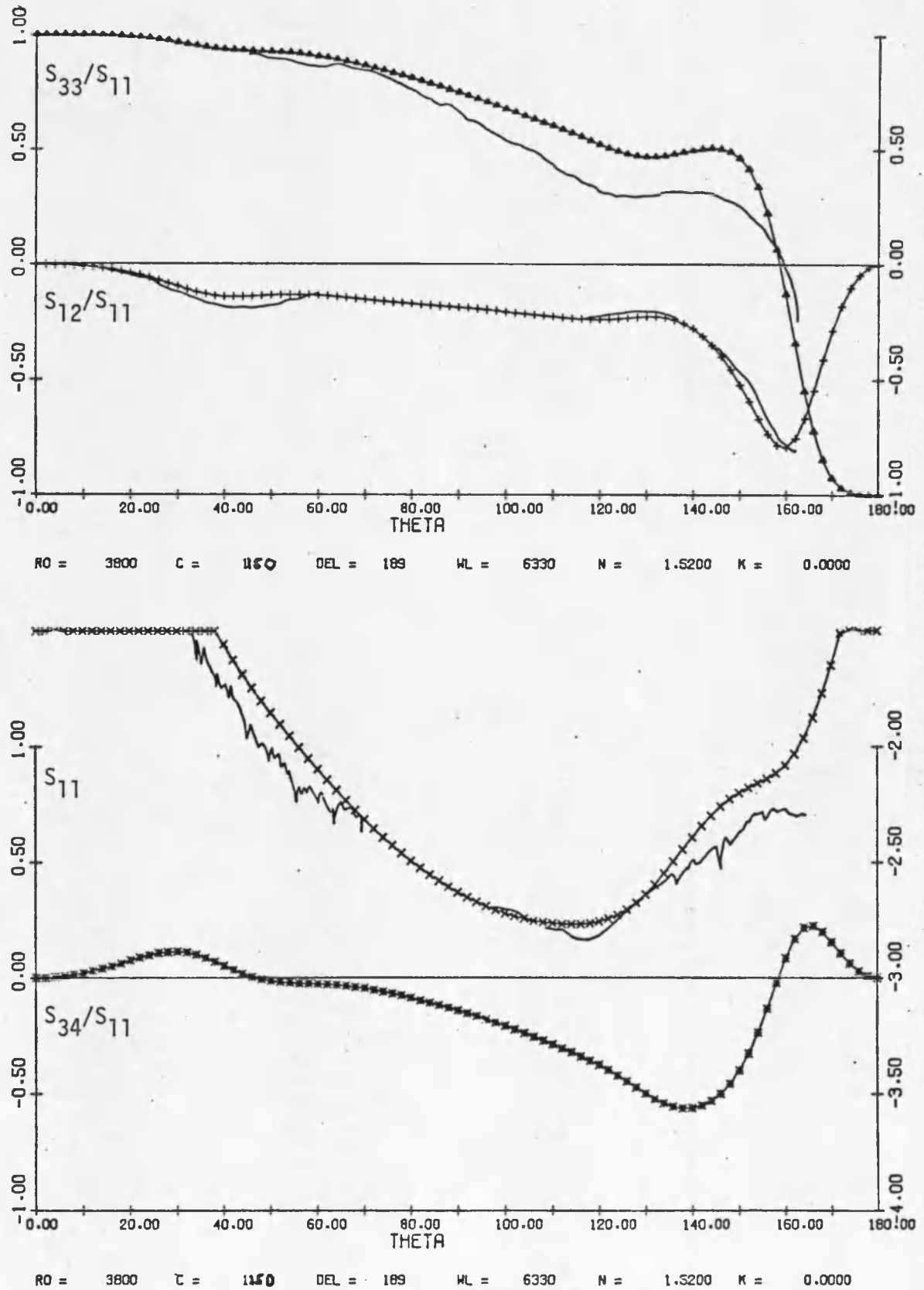

Fig. B8. Scattering Measurements $(NH_4)_2SO_4$ 20.2 gm/l a. x = 3.8

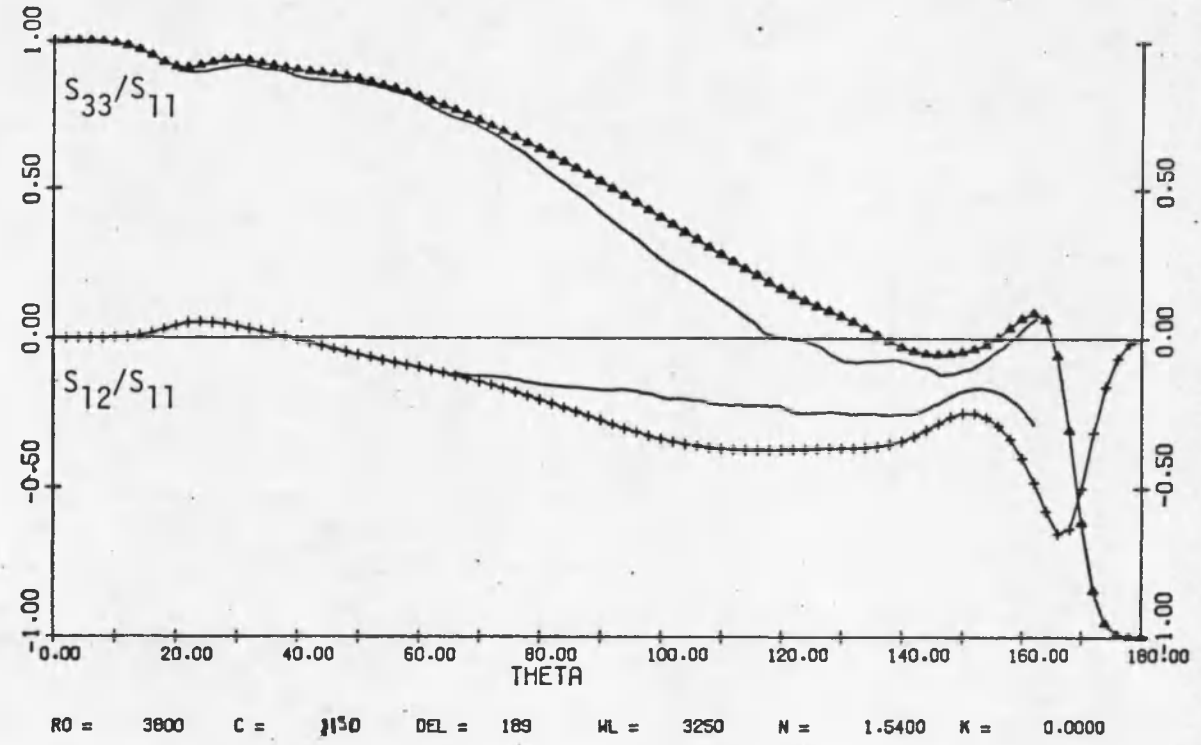

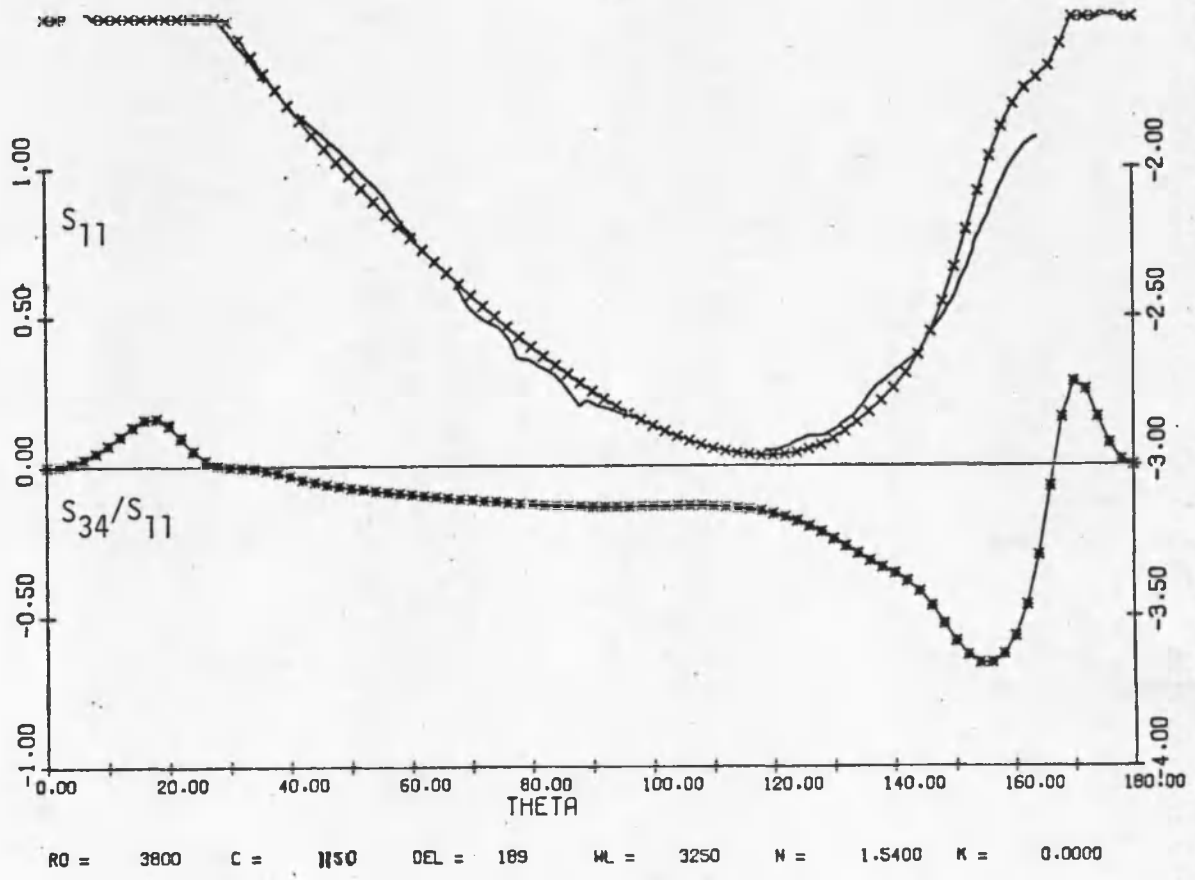

Fig. B8. continued. b. x = 7.3

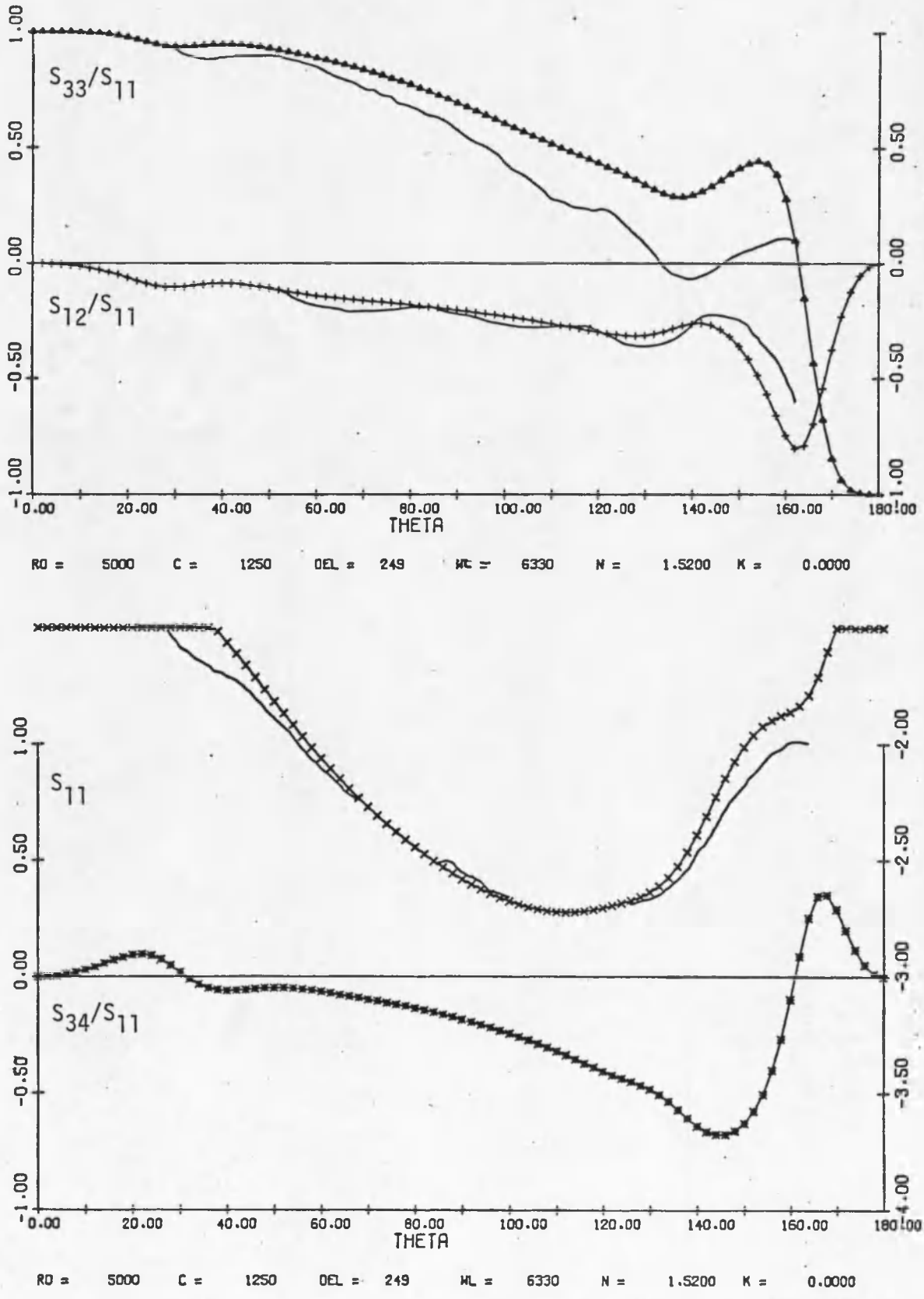

Fig. B9. Scattering Measurements $(NH_4)_2SO_4$ 51.4 gm/l a. x = 5.0

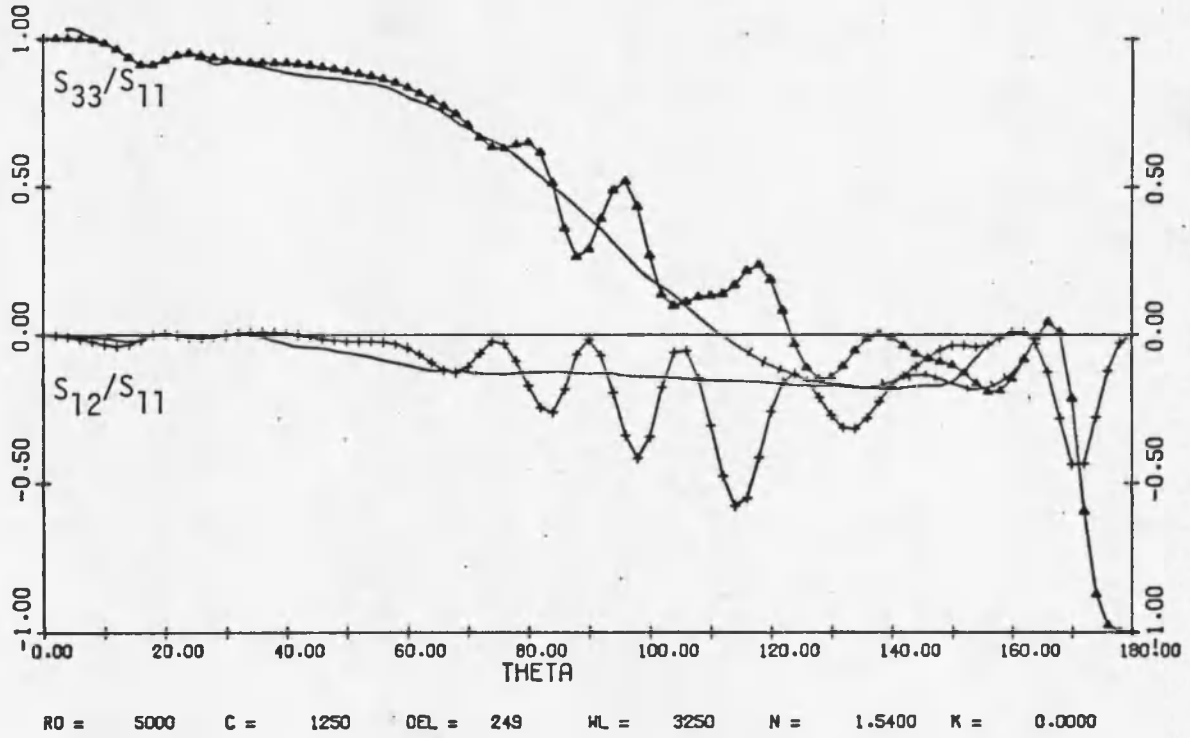

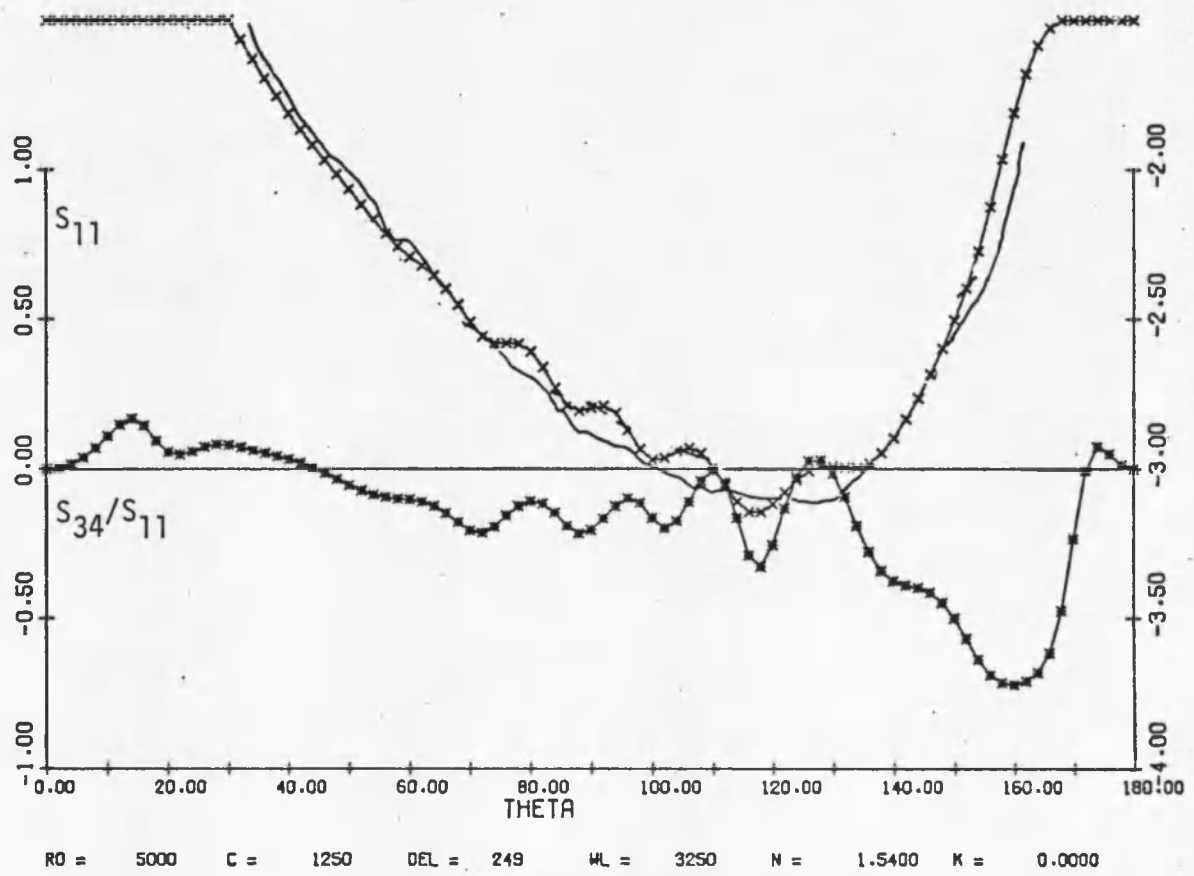

Fig. B9. continued. b. x = 9.7

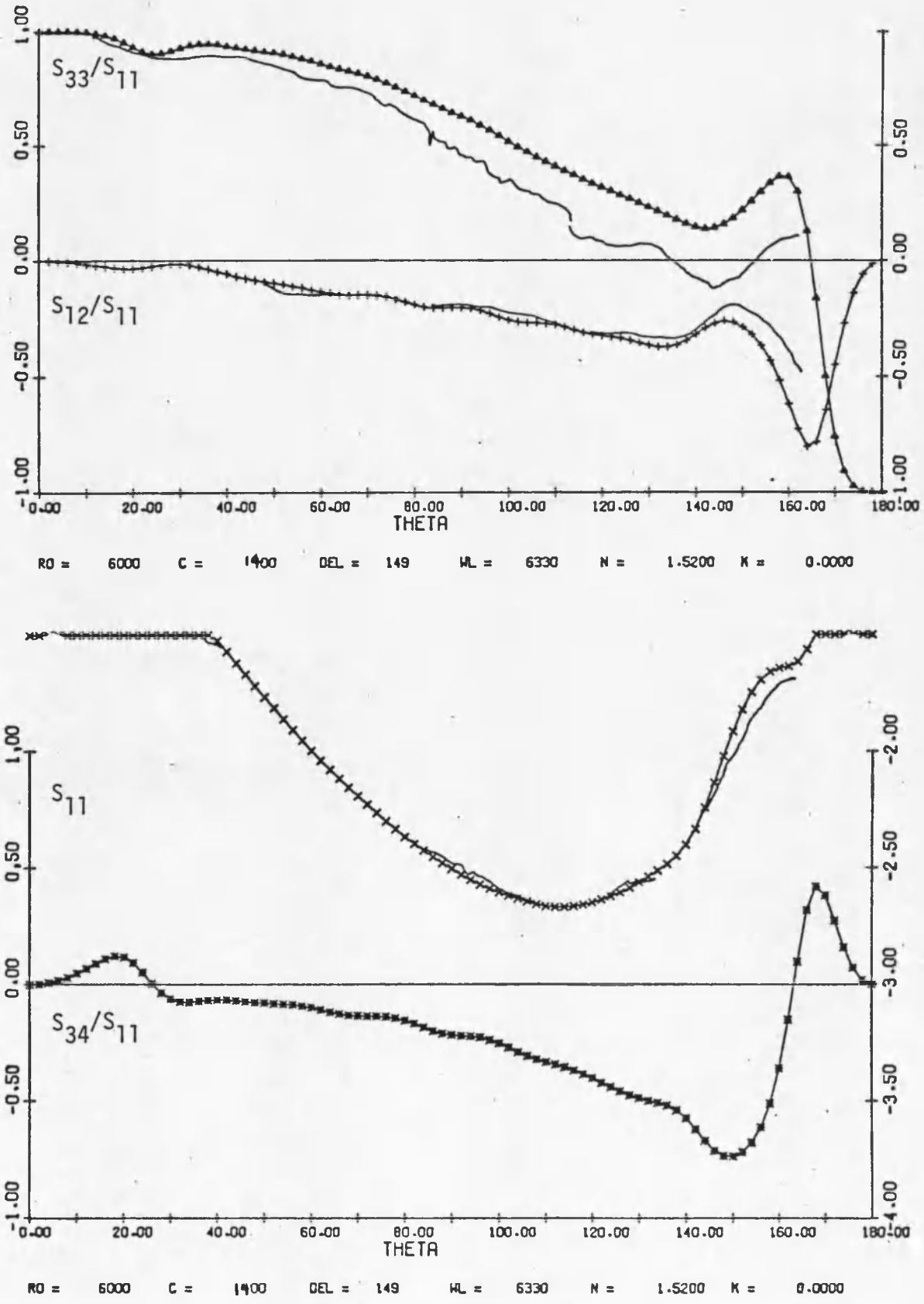

Fig. B10. Scattering Measurements $(NH_4)_2SO_4$ 78.2 gm/l a. x = 6.0

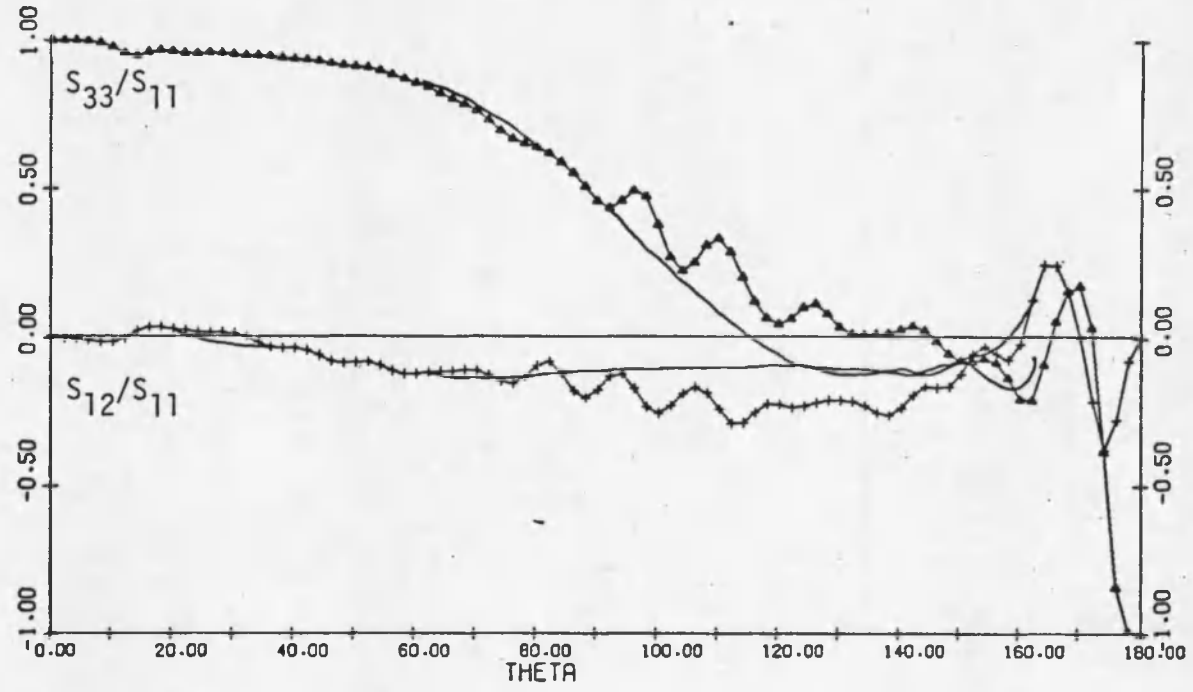

RO = 6600 C = 2100 DEL = 149 WL = 3250 N = 1.5400 K = 0.0000

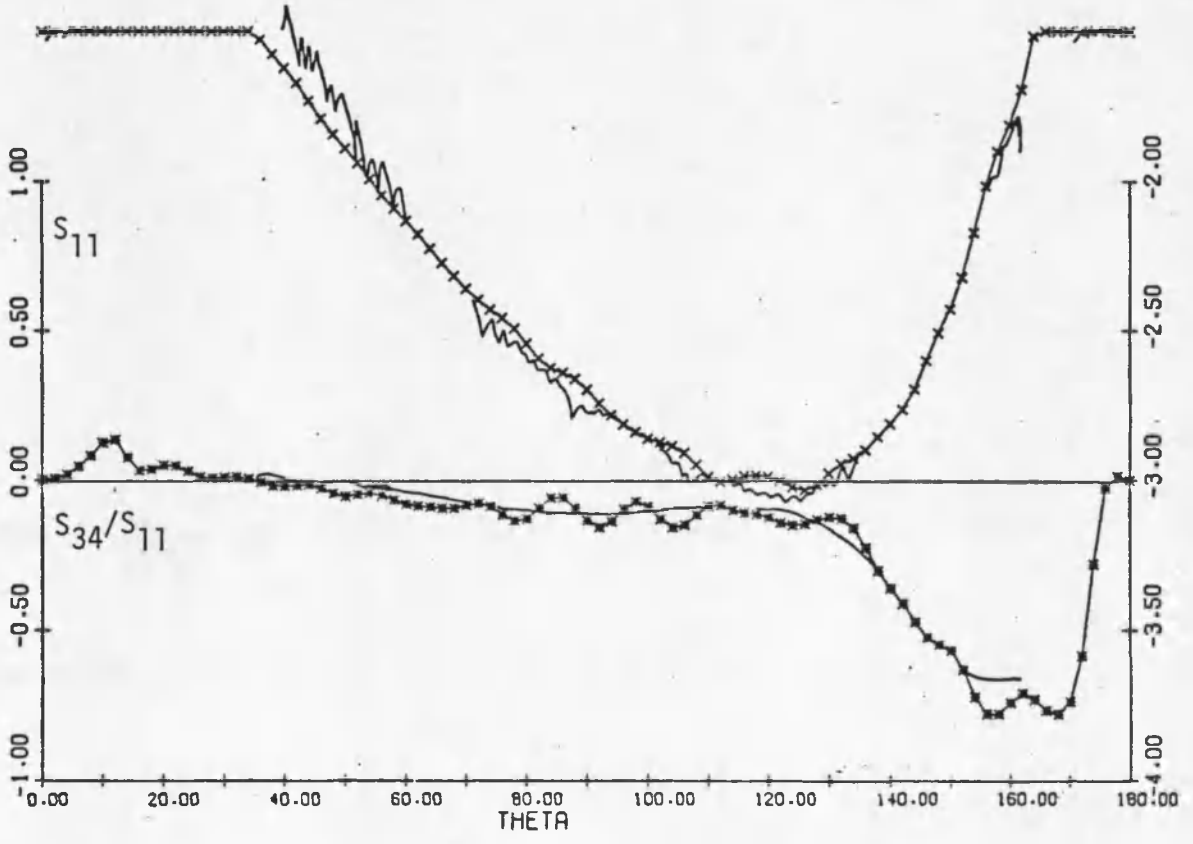

RO = 6600 C = 2100 DEL = 149 WL = 3250 N = 1.5400 K = 0.0000

Fig. B10. continued. b. x = 12.8

APPENDIX C

AEROSOL PARTICLE SIZES AND DISTRIBUTIONS

```
NACL   1.25 GM/L
MAGNIFICATION  20000      TOTAL NUMBER COUNTED 249 SCALING FACTOR  1.680E-08
ALL PARTICLE SIZES IN MICRONS
MEAN SIZE  3.001E-01      STD  7.088E-02           MEAN VARIATION  5.395E-02
FRACTIONAL STD 2.362E-01 SKEWNESS  7.078E-01      EXCESS  1.173E+00
MOMENTS ABOUT ORIGIN
U2= 9.507E-02             U3= 3.179E-02           U4= 1.122E-02
MOMENTS ABOUT MEAN
M2= 5.004E-03             M3= 2.506E-04           M4= 1.045E-04
PERCENT FREQUENCY
        0.00     .40   0.00   3.61  16.47  31.33  24.10  15.66   4.42   1.61
        2.41    0.00   0.00   0.00   0.00   0.00   0.00   0.00   0.00   0.00
        0.00    0.00   0.00   0.00   0.00   0.00   0.00   0.00   0.00   0.00
LOWER LIMIT  0.           UPPER LIMIT  1.50E+00    NUMBER OF INTERVALS   30
MINIMUM SIZE  8.398E-02  MAXIMUM SIZE  5.375E-01
            PERCENT FREQUENCY
        0    5   10   15   20   25   30   35   40   45
  0.00 *....*....*....*....*....*....*....*....*....*
       .
       .
P      .
A      .XXXX
R 0.25 .XXXXXXXXXXXXXXX
T      .XXXXXXXXXXXXXXXXXXXXXXXXXXXXXX
I      .XXXXXXXXXXXXXXXXXXXXXXXX
C      .XXXXXXXXXXXXXXX
L      .XXXX
E 0.50 .XX
       .XX
       .
S      .
I      .
Z 0.75 .
E      .
       .
       .
       .
  1.00 .
       .
       .
       .
       .
  1.25 .
       .
       .
       .
       .
  1.50 .
```

NACL 4.22 GM/L
MAGNIFICATION 20000 TOTAL NUMBER COUNTED 119 SCALING FACTOR 1.775E-08
ALL PARTICLE SIZES IN MICRONS
MEAN SIZE 4.561E-01 STD 1.152E-01 MEAN VARIATION 9.147E-02
FRACTIONAL STD 2.525E-01 SKEWNESS 4.86CE-01 EXCESS -1.472E-01
MOMENTS ABOUT ORIGIN
U2= 2.212E-01 U3= 1.136E-01 U4= 6.152E-02
MOMENTS ABOUT MEAN
M2= 1.315E-02 M3= 7.333E-04 M4= 4.936E-04
PERCENT FREQUENCY

0.00	0.00	0.00	0.00	1.68	3.36	10.92	16.81	21.01	16.81
7.56	8.40	6.72	1.68	5.04	0.00	0.00	0.00	0.00	0.00
0.00	0.00	0.00	0.00	0.00	0.00	0.00	0.00	0.00	0.00

LOWER LIMIT 0. UPPER LIMIT 1.50E+00 NUMBER OF INTERVALS 30
MINIMUM SIZE 2.130E-01 MAXIMUM SIZE 7.277E-01

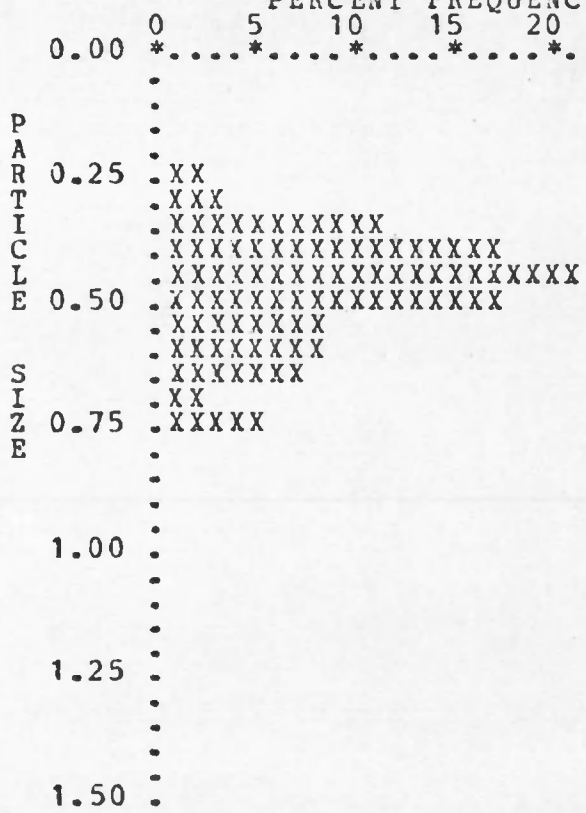

NACL 10.00 GM/L
MAGNIFICATION 10000 TOTAL NUMBER COUNTED 314 SCALING FACTOR 3.570E-08
ALL PARTICLE SIZES IN MICRONS
MEAN SIZE 5.009E-01 STD 1.451E-01 MEAN VARIATION 1.096E-01
FRACTIONAL STD 2.898E-01 SKEWNESS 3.682E-01 EXCESS 9.509E-01
MOMENTS ABOUT ORIGIN
U2= 2.719E-01 U3= 1.583E-01 U4= 9.852E-02
MOMENTS ABOUT MEAN
M2= 2.100E-02 M3= 1.120E-03 M4= 1.742E-03
PERCENT FREQUENCY

0.00	2.23	6.05	17.83	27.71	21.97	16.88	4.14	2.23	.64
.32	0.00	0.00	0.00	0.00	0.00	0.00	0.00	0.00	0.00
0.00	0.00	0.00	0.00	0.00	0.00	0.00	0.00	0.00	0.00

LOWER LIMIT 0. UPPER LIMIT 3.00E+00 NUMBER OF INTERVALS 30
MINIMUM SIZE 1.428E-01 MAXIMUM SIZE 1.071E+00

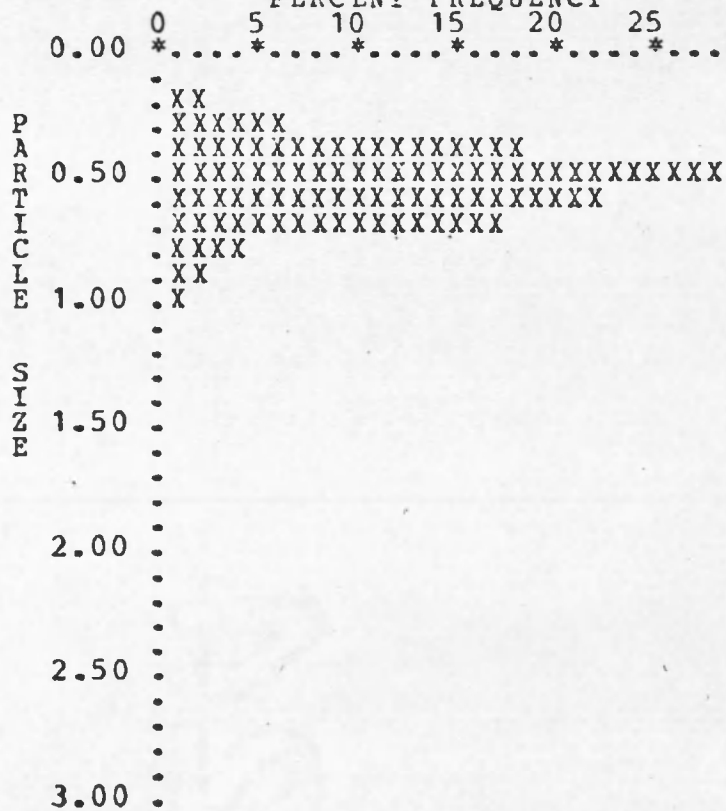

```
NACL  10.00 GM/L
MAGNIFICATION  20000      TOTAL NUMBER COUNTED  88 SCALING FACTOR  1.769E-08
ALL PARTICLE SIZES IN MICRONS
MEAN SIZE  5.464E-01      STD  1.677E-01            MEAN VARIATION  1.317E-01
FRACTIONAL STD 3.069E-01 SKEWNESS  5.862E-01       EXCESS  5.711E-01
MOMENTS ABOUT ORIGIN
U2= 3.263E-01             U3= 2.114E-01            U4= 1.476E-01
MOMENTS ABOUT MEAN
M2= 2.779E-02             M3= 2.716E-03            M4= 2.758E-03
PERCENT FREQUENCY
         0.00    0.00    2.27   18.18   21.59   22.73   15.91   14.77    1.14    2.27
         0.00    1.14    0.00    0.00    0.00    0.00    0.00    0.00    0.00    0.00
         0.00    0.00    0.00    0.00    0.00    0.00    0.00    0.00    0.00    0.00
LOWER LIMIT  0.           UPPER LIMIT  3.00E+00     NUMBER OF INTERVALS   30
MINIMUM SIZE  2.123E-01  MAXIMUM SIZE  1.114E+00
              PERCENT FREQUENCY
        0     5    10    15    20    25    30    35    40    45
  0.00 *....*....*....*....*....*....*....*....*....*....*
       .
       .
P      .XX
A      .XXXXXXXXXXXXXXXXX
R 0.50 .XXXXXXXXXXXXXXXXXXXXXX
T      .XXXXXXXXXXXXXXXXXXXXXXX
I      .XXXXXXXXXXXXXXXX
C      .XXXXXXXXXXXXXXX
L      .X
E 1.00 .XX
       .
       .X
S      .
I      .
Z 1.50 .
E      .
       .
       .
       .
  2.00 .
       .
       .
       .
       .
  2.50 .
       .
       .
       .
  3.00 .
```

NACL 80.20 GM/L
MAGNIFICATION 5000 TOTAL NUMBER COUNTED 335 SCALING FACTOR 7.310E-08
ALL PARTICLE SIZES IN MICRONS
MEAN SIZE 1.007E+00 STD 3.185E-01 MEAN VARIATION 2.561E-01
FRACTIONAL STD 3.164E-01 SKEWNESS -1.857E-02 EXCESS -4.069E-01
MOMENTS ABOUT ORIGIN
U2= 1.114E+00 U3= 1.325E+00 U4= 1.665E+00
MOMENTS ABOUT MEAN
M2= 1.011E-01 M3=-5.972E-04 M4= 2.653E-02
PERCENT FREQUENCY

0.00	0.00	.60	3.28	2.39	6.27	2.39	8.96	13.13	9.85
18.51	7.76	7.76	9.25	3.58	1.19	4.48	.60	0.00	0.00
0.00	0.00	0.00	0.00	0.00	0.00	0.00	0.00	0.00	0.00

LOWER LIMIT 0. UPPER LIMIT 3.00E+00 NUMBER OF INTERVALS 30
MINIMUM SIZE 2.924E-01 MAXIMUM SIZE 1.754E+00

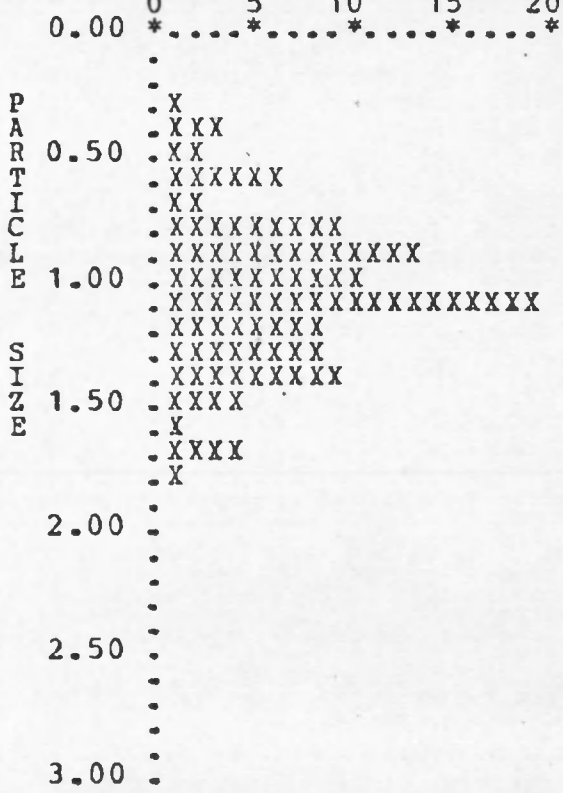

```
NACL  80.20 GM/L
MAGNIFICATION  10000      TOTAL NUMBER COUNTED  79 SCALING FACTOR  3.624E-08
ALL PARTICLE SIZES IN MICRONS
MEAN SIZE  1.065E+00      STD  3.456E-01          MEAN VARIATION  2.755E-01
FRACTIONAL STD 3.245E-01 SKEWNESS  5.351E-01      EXCESS  2.268E-01
MOMENTS ABOUT ORIGIN
U2= 1.253E+00             U3= 1.607E+00          U4= 2.228E+00
MOMENTS ABOUT MEAN
M2= 1.180E-01             M3= 2.168E-02          M4= 4.490E-02
PERCENT FREQUENCY
        0.00   0.00   0.00   0.00   2.53   3.80  10.13   8.86   8.86  11.39
       12.66  10.13   5.06  13.92   2.53   3.80   2.53   0.00   1.27   1.27
        0.00   1.27   0.00   0.00   0.00   0.00   0.00   0.00   0.00   0.00
LOWER LIMIT  0.          UPPER LIMIT  3.00E+00    NUMBER OF INTERVALS   30
MINIMUM SIZE  4.349E-01  MAXIMUM SIZE  2.138E+00
                PERCENT FREQUENCY
          0    5    10   15   20   25   30   35   40   45
  0.00   *....*....*....*....*....*....*....*....*....*
         .
         .
P        .
A        .
R  0.50  .XXX
T        .XXXX
I        .XXXXXXXXXX
C        .XXXXXXXXX
L        .XXXXXXXXX
E  1.00  .XXXXXXXXXXX
         .XXXXXXXXXXXXX
         .XXXXXXXXXX
S        .XXXXX
I        .XXXXXXXXXXXXX
Z  1.50  .XXX
E        .XXXX
         .XXX
         .
         .X
  2.00   .X
         .
         .X
         .
  2.50   .
         .
         .
         .
  3.00   .
```

NACL 320.00 GM/L
MAGNIFICATION 5000 TOTAL NUMBER COUNTED 132 SCALING FACTOR 7.129E-08
ALL PARTICLE SIZES IN MICRONS
MEAN SIZE 1.661E+00 STD 4.365E-01 MEAN VARIATION 3.522E-01
FRACTIONAL STD 2.628E-01 SKEWNESS -2.821E-01 EXCESS -2.104E-01
MOMENTS ABOUT ORIGIN
U2= 2.947E+00 U3= 5.499E+00 U4= 1.068E+01
MOMENTS ABOUT MEAN
M2= 1.891E-01 M3=-2.320E-02 M4= 9.974E-02
PERCENT FREQUENCY

0.00	0.00	0.00	0.00	.76	.76	0.00	2.27	2.27	1.52
5.30	.76	6.82	3.03	12.88	10.61	4.55	9.09	5.30	13.64
3.03	6.82	6.06	0.00	3.03	.76	0.00	.76	0.00	0.00

LOWER LIMIT 0. UPPER LIMIT 3.00E+00 NUMBER OF INTERVALS 30
MINIMUM SIZE 4.990E-01 MAXIMUM SIZE 2.709E+00

PERCENT FREQUENCY

```
        0    5   10   15   20   25   30   35   40   45
  0.00 *....*....*....*....*....*....*....*....*....*
       .
       .
P      .
A      .
R 0.50 .X
T      .X
I      .
C      .XX
L      .XX
E 1.00 .XX
       .XXXXX
       .X
S      .XXXXXXX
I      .XXX
Z 1.50 .XXXXXXXXXXXXX
E      .XXXXXXXXXXX
       .XXXXX
       .XXXXXXXXX
       .XXXXX
  2.00 .XXXXXXXXXXXXX
       .XXX
       .XXXXXXX
       .XXXXXX
       .
  2.50 .XXX
       .X
       .
       .X
       .
  3.00 .
```

(NH4)2SO4 5.00 GM/L
MAGNIFICATION 10000 TOTAL NUMBER COUNTED 329 SCALING FACTOR 3.303E-08
ALL PARTICLE SIZES IN MICRONS
MEAN SIZE 5.155E-01 STD 1.498E-01 MEAN VARIATION 1.177E-01
FRACTIONAL STD 2.906E-01 SKEWNESS 8.386E-01 EXCESS 6.299E-01
MOMENTS ABOUT ORIGIN
U2= 2.881E-01 U3= 1.744E-01 U4= 1.139E-01
MOMENTS ABOUT MEAN
M2= 2.237E-02 M3= 2.806E-03 M4= 1.817E-03
PERCENT FREQUENCY

0.00	0.00	4.26	23.10	30.40	18.24	13.37	5.17	3.65	1.52
.30	0.00	0.00	0.00	0.00	0.00	0.00	0.00	0.00	0.00
0.00	0.00	0.00	0.00	0.00	0.00	0.00	0.00	0.00	0.00

LOWER LIMIT 0. UPPER LIMIT 3.00E+00 NUMBER OF INTERVALS 30
MINIMUM SIZE 2.312E-01 MAXIMUM SIZE 1.024E+00

```
(NH4)2SO4  10.00 GM/L
MAGNIFICATION  10000      TOTAL NUMBER COUNTED 167 SCALING FACTOR  3.238E-08
ALL PARTICLE SIZES IN MICRONS
MEAN SIZE  6.939E-01      STD  2.095E-01          MEAN VARIATION  1.662E-01
FRACTIONAL STD 3.019E-01 SKEWNESS  6.421E-01      EXCESS  3.650E-01
MOMENTS ABOUT ORIGIN
U2= 5.252E-01             U3= 4.308E-01          U4= 3.805E-01
MOMENTS ABOUT MEAN
M2= 4.361E-02             M3= 5.849E-03          M4= 6.401E-03
PERCENT FREQUENCY
        0.00   0.00   0.00   6.59  13.17  15.57  15.57  22.16  10.18   8.38
        2.99   2.99   1.20   1.20   0.00   0.00   0.00   0.00   0.00   0.00
        0.00   0.00   0.00   0.00   0.00   0.00   0.00   0.00   0.00   0.00
LOWER LIMIT  0.          UPPER LIMIT  3.00E+00    NUMBER OF INTERVALS   30
MINIMUM SIZE  3.562E-01  MAXIMUM SIZE  1.392E+00
              PERCENT FREQUENCY
         0    5    10   15   20   25   30   35   40   45
  0.00  *....*....*....*....*....*....*....*....*....*
        .
        .
P       .
A       .XXXXXXX
R 0.50  .XXXXXXXXXXXXX
T       .XXXXXXXXXXXXXXXXX
I       .XXXXXXXXXXXXXXXXX
C       .XXXXXXXXXXXXXXXXXXXXXXX
L       .XXXXXXXXXX
E 1.00  .XXXXXXXX
        .XXX
        .XXX
S       .X
I       .X
Z 1.50  .
E       .
        .
        .
        .
  2.00  .
        .
        .
        .
        .
  2.50  .
        .
        .
        .
        .
  3.00  .
```

(NH4)2SO4 20.20 GM/L
MAGNIFICATION 5000 TOTAL NUMBER COUNTED 392 SCALING FACTOR 6.428E-08
ALL PARTICLE SIZES IN MICRONS
MEAN SIZE 8.597E-01 STD 2.858E-01 MEAN VARIATION 2.237E-01
FRACTIONAL STD 3.325E-01 SKEWNESS 8.431E-01 EXCESS 7.316E-01
MOMENTS ABOUT ORIGIN
U2= 8.205E-01 U3= 8.651E-01 U4= 9.997E-01
MOMENTS ABOUT MEAN
M2= 8.149E-02 M3= 1.961E-02 M4= 2.478E-02
PERCENT FREQUENCY

0.00	.26	0.00	1.79	3.06	12.50	9.95	20.66	17.35	7.14
11.22	3.06	5.87	1.02	3.06	.77	1.79	0.00	0.00	.51
0.00	0.00	0.00	0.00	0.00	0.00	0.00	0.00	0.00	0.00

LOWER LIMIT 0. UPPER LIMIT 3.00E+00 NUMBER OF INTERVALS 30
MINIMUM SIZE 1.928E-01 MAXIMUM SIZE 1.928E+00

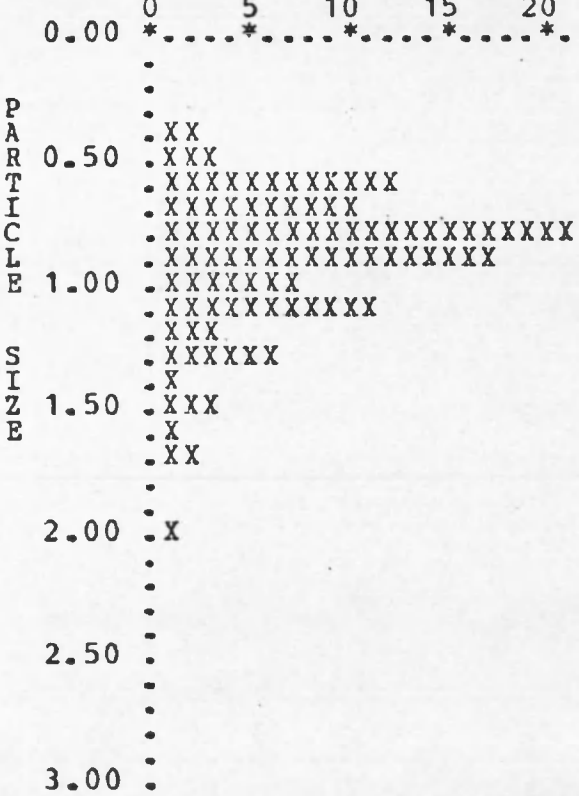

(NH4)2SO4 51.40 GM/L
MAGNIFICATION 5000 TOTAL NUMBER COUNTED 295 SCALING FACTOR 6.565E-08
ALL PARTICLE SIZES IN MICRONS
MEAN SIZE 1.150E+00 STD 3.565E-01 MEAN VARIATION 2.689E-01
FRACTIONAL STD 3.101E-01 SKEWNESS 1.125E+00 EXCESS 1.654E+00
MOMENTS ABOUT ORIGIN
U2= 1.449E+00 U3= 2.008E+00 U4= 3.061E+00
MOMENTS ABOUT MEAN
M2= 1.267E-01 M3= 5.075E-02 M4= 7.470E-02
PERCENT FREQUENCY

0.00	0.00	0.00	.34	0.00	2.03	2.71	8.81	7.12	18.64
9.83	16.61	5.08	10.17	3.05	5.08	3.05	1.36	.68	2.03
.34	1.36	.68	.68	0.00	.34	0.00	0.00	0.00	0.00

LOWER LIMIT 0. UPPER LIMIT 3.00E+00 NUMBER OF INTERVALS 30
MINIMUM SIZE 3.939E-01 MAXIMUM SIZE 2.560E+00

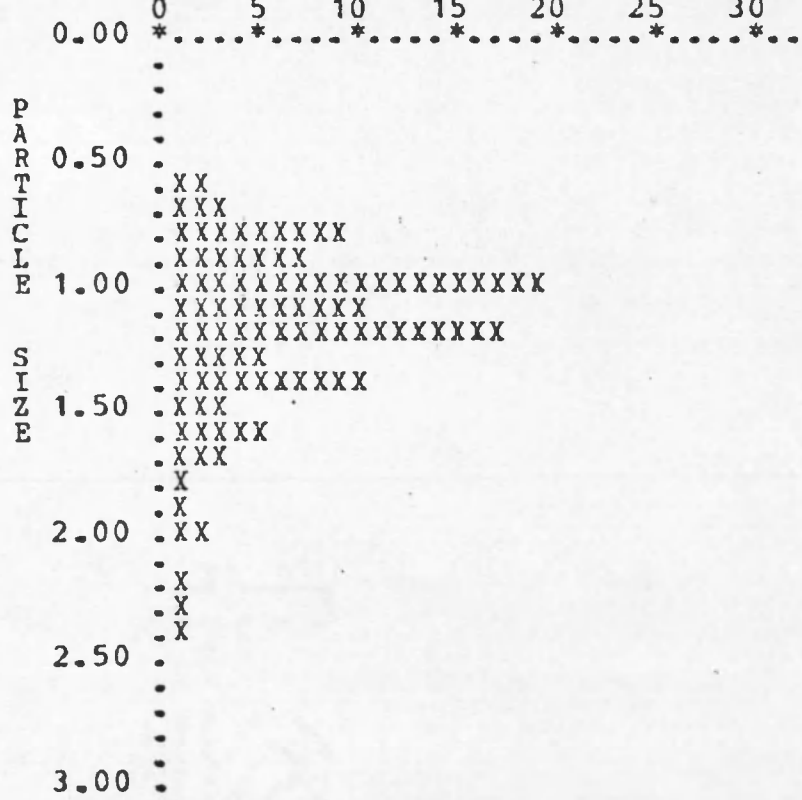

(NH4)2SO4 78.20 GM/L
MAGNIFICATION 5000 TOTAL NUMBER COUNTED 183 SCALING FACTOR 7.248E-08
ALL PARTICLE SIZES IN MICRONS
MEAN SIZE 1.280E+00 STD 4.212E-01 MEAN VARIATION 3.133E-01
FRACTIONAL STD 3.291E-01 SKEWNESS 1.258E+00 EXCESS 2.012E+00
MOMENTS ABOUT ORIGIN
U2= 1.814E+00 U3= 2.866E+00 U4= 5.049E+00
MOMENTS ABOUT MEAN
M2= 1.764E-01 M3= 9.322E-02 M4= 1.560E-01
PERCENT FREQUENCY

0.00	0.00	0.00	0.00	0.00	1.64	0.00	5.46	10.93	6.56
15.30	9.29	10.38	9.84	9.29	6.56	2.19	1.09	2.19	1.09
1.64	1.64	1.09	2.73	0.00	0.00	0.00	0.00	1.09	0.00

LOWER LIMIT 0. UPPER LIMIT 3.00E+00 NUMBER OF INTERVALS 30
MINIMUM SIZE 5.074E-01 MAXIMUM SIZE 2.899E+00

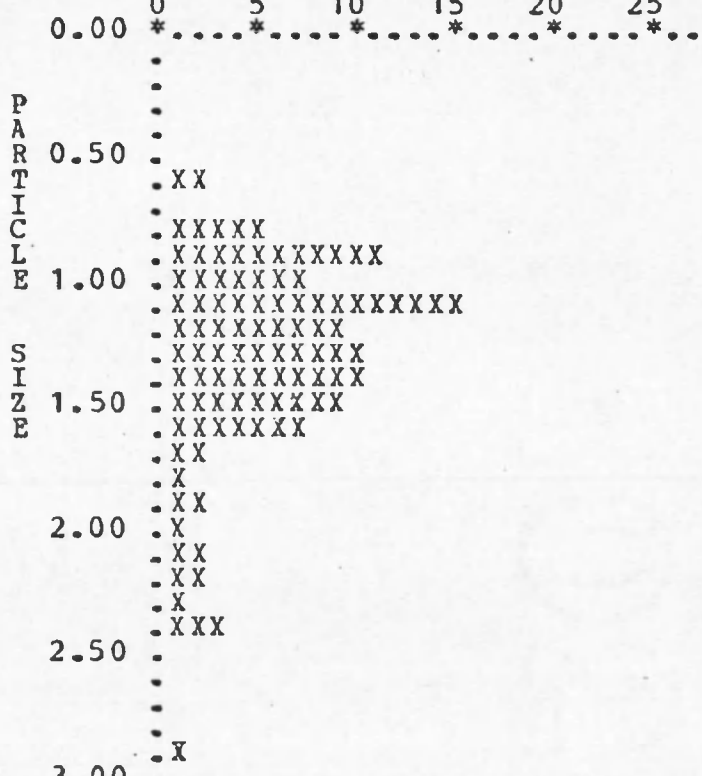

REFERENCES

Abramowitz, Milton and Irene A. Stegun, eds., 1972: Handbook of Mathematical Functions. National Bureau of Standards, Washington D. C., p. 409 and pp. 927-930.

Dave, J. V., 1968: Subroutines for Computing the Parameters of the Electromagnetic Radiation Scattered by a Sphere, IBM Scientific Center, Palo Alto, California, Report #320-3236.

Deirmendjian, D.,1964: Scattering and Polarization Properties of Water Clouds and Hazes in the Visible and Infrared, Applied Optics 3, p.187.

Denton, M. B. and D. B. Swartz, 1974: An Improved Ultrasonic Nebulizer System for the Generation of High Density Aerosol Dispersions, Review of Scientific Instruments 45, pp. 81-83.

Elderton, W. Palin, 1917: Frequency-Curves and Correlation. Institute of Actuaries Publication, London, pp. 36-91.

Frank, Evelyn R., James P. Lodge and Alexander Goetz, 1972: Experimental Sea Salt Profiles, Journal of Geophysical Research 77, p. 5147.

Gray, Dwight E., ed., 1972: American Institute of Physics Handbook. McGraw-Hill, New York, New York, p.6--43.

Hanson, James E. and J. W. Hovenier, 1974: Interpretation of the Polarization of Venus, manuscript. Published 1974 in the Journal of the Atmospheric Sciences 31, pp. 1137-1160.

Herzenberg, L. A., R. G. Sweet and L. A. Herzenberg, 1976: Flurescence-Activated Cell Sorting, Scientific American 234, p. 108.

Holland, A. C. and G. Gagne, 1970: The Scattering of Polarized Light by Polydisperse Systems of Irregular Particles, Applied Optics 9, pp. 1113-1121.

Holland, A. C. and G. Gagne, 1971: Letters to the Editor, Applied Optics 10, p. 1173.

Huffman, Paul J., 1970: Polarization of Light Scattered by Ice Crystals, Journal of Atmospheric Sciences 27, p. 1207.

Huffman, Paul J. and William R. Thursby, 1969: Light Scattering by Ice Crystals, Journal of Atmospheric Sciences 26, pp. 1073-1077.

Hunt, Arlon J., 1974: An Experimental Investigation of the Angular Dependence of Polarization of Light Scattered from Small Particles, Doctoral Dissertation, University of Arizona.

Hunt, Arlon J. and Donald R. Huffman, 1973: A New Polarization-Modulated Light Scattering Instrument, Review of Scientific Instruments 44, pp. 1753-1762.

Junge, C. E., 1972: Our Knowledge of the Physico-chemistry of Aerosols in the Undistrubed Marine Environment, Journal of Geophysical Research 77, pp. 5183-5200.

Kerker, Milton, 1965: Scattering from Spheres and Cylinders, Electromagnetic Scattering. Robert L. Rowell and Richard S. Stein, editors, Gordon and Breach Science Publishers,

Kerker, Milton, 1972: Some Optical and Dynamic Properties of Aerosols, Aerosols and Atmospheric Chemistry. G. M. Hidy, editor, Academic Press, New York, New York, pp. 7-11.

Lang, Robert J., 1962: Ultrasonic Atomization of Liquids, Journal of the American Acoustical Society 34, pp.6-8.

Lobdell, Donn D., 1968: Particle Size-Amplitude Relation for the Ultrasonic Atomizer, Journal of the American Acoustical Society 43, pp. 229-231.

Mie, G., 1908: Beiträge zur optik trüber medien, speziell kolloidaler met allösungen, Ann. Physik 25, pp. 377-445.

Perrin, Francis, 1942: Polarization of Light Scattered by Isotropic Opalescent Media, Journal of Chemical Physics 10, p. 415.

Pinnick, R. G., D. E. Carrol and D. J. Hofmann, 1976: Polarized Light Scattered from Monodisperse Randomly Oriented Nonspherical Aerosol Particles Measurements, Applied Optics 15, pp. 384-393.

Plass, G. N. and G. W. Kattawar, 1971: Letters to the Editor, Applied Optics 10, p. 1172.

Pritchard, B. S. and W. G. Elliott, 1960: Two Instruments for Atmospheric Optics Measurements, Journal of the American Optical Society 50, p.191.

Shurcliff, William, A., 1962: Polarized Light. Harvard University Press, Cambridge, Massachusetts.

Stupar, J. and J. B. Dawson, 1968: Theoretical and Experimental Aspects of the Production of Aerosols for Use in Atomic Absorption Spectroscopy, Applied Optics 7, pp. 1351-1358.

van de Hulst, H. C., 1957: Light Scattering by Small Particles. John Wiley and Sons, New York, New York.

Vouk, V., 1948: Projected Area of Convex Bodies, Nature 162. p.330.

Weast, Robert C., ed., 1970: Handbook of Chemistry and Physics. 51st ed. The Chemical Rubber Co., Cleveland, Ohio.